

GEOPHYSICAL STUDIES OF ANZA GRABEN N.E. KENYA

EDWIN WANDUBI DINDI

UNIVERSITY OF NAIROBI LIBRARIES

**A thesis submitted in fulfilment for the degree
of Doctor of Philosophy in the
University of Nairobi**

**THIS THESIS HAS BEEN ACCEPTED FOR
THE DEGREE OF...*Ph.D. (1992)*...
AND A COPY MAY BE PLACED IN THE
UNIVERSITY LIBRARY.**

1992

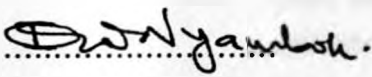
DECLARATION

I, Edwin Wandubi Dindi, hereby declare that this thesis is my original work and has not been presented for a degree in any other University.

.....

E.W. Dindi (B.Sc., M.Sc.)

We hereby declare that this thesis has been submitted for examination with our knowledge as University Supervisors.

.....

Prof. I.O. Nyambok

.....

Prof. J.P. Patel

CONTENTS

	Pg
Abstract	IX
Acknowledgements	XI
1 GENERAL INTRODUCTION	1
1.1 Location and importance of the area	1
1.2 A review of the geophysical activities in the area and in other parts of Eastern Kenya	5
1.3 Aims of the present study and scope	9
2 REGIONAL GEOLOGY	11
2.1 Geological correlation using deep boreholes	12
2.2 Sedimentary rocks	13
2.2.1 Permo - Triassic	14
2.2.2 Jurassic	15
2.2.3 Cretaceous	16
2.2.4 Tertiary	18
2.3 Metamorphic rocks	20
2.4 Igneous rocks	21
2.5 Major structures and structural trends	22
2.6 Past and present views on the sedimentation and tectonic history of the region	24
2.7 Conclusions to be drawn from existing works	27
3 SEISMICS	29
3.1 Reflection Seismics	29
3.1.1 Importance of the data and quality	29
3.1.2 Interpretations and results	30
3.2 Refraction Seismics	35
3.2.1 Data quality	35

3.2.2	Basic travel-time curves and correlations	37
3.3	Modelling techniques	43
3.4	Modelling and results	46
3.5	Discussion of the model	48
3.6	Conclusions	52
4	REDUCTION, ANALYSIS AND QUALITATIVE INTERPRETATION OF THE GRAVITY DATA	54
4.1	Data sources and quality	56
4.1.1	Leicester University Data	56
4.1.2	British Petroleum Data	57
4.1.3	Chevron Data	58
4.1.4	Burmah Data	58
4.1.5	Data from survey during the present study	59
4.2	Computation of Bouguer anomalies	61
4.3	General features of the Bouguer anomaly map	63
4.3.1	Matasade High	65
4.3.2	Mochesa High	66
4.3.3	Garissa High	67
4.4	Techniques of processing and analysis	67
4.4.1	Polynomial fitting	69
4.4.2	Wavelength filtering	69
4.4.3	Vertical gradient of gravity	73
4.5	Filtered gravity maps	74
5	MODELLING OF THE GRAVITY DATA	83
5.1	Choice between 2D and 3D modelling	83
5.2	Techniques used in modelling	85
5.2.1	The method of plane distribution of mass	85
5.2.2	The 3D interactive modelling technique	88

5.3	Inversion of the gravity data	118
	by the method of plane distribution of mass	92
5.4	3D Interactive modelling	95
	5.4.1 Basis for the selection of the start model	95
	5.4.1.1 Start model based on the structural map of Kenya	96
	5.4.1.2 Start model based on inverted data	98
	5.4.2 Problem of the determination of the model parameters	99
	5.4.2.1 Basement depth	99
	5.4.2.2 Rock densities	100
	5.4.2.3 Margins of the structure	105
	5.4.3 Model data preparation	106
	5.4.4 Tentative models	106
	5.4.5 The final model	109
6	MAGNETICS	115
	6.1 The basis of the magnetic method	115
	6.2 Techniques used in data analysis	120
	6.2.1 Upward continuation	121
	6.2.2 Reduction to the pole	122
	6.3 Preparation of a unified map of the aeromagnetic data	124
	6.4 Features of the magnetic maps	126
	6.5 Features of the filtered aeromagnetic data	131
	6.5.1 Low pass filtered maps	132
	6.5.2 Reduced to the pole maps	135
	6.6 Modelling technique	140
	6.7 Modelling and results	142
	6.8 Conclusions	146

7	GEOLOGICAL SYNTHESIS	148
7.1	Shallow structure	148
7.1.1	Geometry of the graben	148
7.1.2	Graben fill	150
7.1.3	Graben shoulders	152
7.2	Deep structure	153
7.3	Tectonic and structural evolution models	154
8	DISCUSSIONS AND CONCLUSIONS	161
8.1	Comparison of some rifts with Anza Graben	163
8.1.1	The Kenya Rift Valley	163
8.1.2	The rifts of the Central and Southern Sudan	164
8.1.3	The Benue Trough	167
8.1.4	The Baikal Rift	168
8.1.5	The Rhine Graben	169
8.1.6	The Godavari Rift of India	170
8.2	Some deductions from the comparative study	171
8.3	Conclusions	172
	REFERENCES	175
	APPENDIX	A1
	BEAM87	A1
	Frequency Domain Filtering Program Package	A3
	IGAS	A3
	MAG2D	A4

LIST OF FIGURES

Fig.		Pg
1.0	Location of the study area	2
2.1	The distribution of deep boreholes in Eastern Kenya	12
2.2	A simplified regional geological map of Eastern Kenya	14
2.3	A simplified structural map of Kenya	23
3.1	Location of the seismic reflection lines	31
3.2a	Reflection line REFL1.	32
3.2b	Reflection line REFL2.	33
3.2c	Reflection line REFL3.	34
3.3	KRISP90 Location map	35
3.4	Correlated record section, synthetic seismograms and ray diagram for S-P LTS	39
3.5	Correlated record section, synthetic seismograms and ray diagram for S-P ILA.	40
3.6	Correlated record section, synthetic seismograms and ray diagram for S-P LAI.	41
3.7	Correlated record section, synthetic seismograms and ray diagram for S-P CHF.	42
3.8	P-Wave velocity depth model for KRISP90 Profile E	47
4.1	Elevation map of the study area and the surrounding areas.	62
4.2	Bouguer anomaly map of the Anza Graben	64
4.3	Filter characteristics of ideal low pass and high pass filters.	72
4.4	Filter characteristics of a vertical gradient filter.	74
4.5	The residual gravity field using a polynomial of the second order	76
4.6a	Regional gravity field with wavelength = 190 km.; effective cut-off wavelength = 180 km	77

4.6b	Regional gravity field with wavelength= 130 km.; effective cut-off wavelength = 120 km	78
4.6c	Regional gravity field with wavelength = 65 km.; effective cut-off wavelength = 65 km	79
4.6d	Regional gravity field with wavelength = 32 km.; effective cut-off wavelength = 30 km	80
5.1	The representation of a mass plane at depth and the undulation of the interface	85
5.2	Presentation of an arbitrary structured polygon	89
5.3	Presentation of polyeder surface	91
5.4	Presentation of a simple two layer substructure	92
5.5	Undulation boundary with D=35 km, D-RHO = -350 kg/m^3	93
5.6	Undulation boundary with D= 8 km, D-RHO = -300 kg/m^3	94
5.7	The structural map of the study area	97
5.8	The section through the model along plane 7 in the southern part of Anza Graben	110
5.9	The section through the model along plane 12 in the northern part of Anza Graben	111
5.10	A 3D perspective picture of the model	112
6.1	The filter characteristics of the upward continuation filter	122
6.2	Real and imaginary parts of the 2D transfer to the magnetic pole	123
6.3	The unified aeromagnetic map of Anza Graben	127
6.4	Ground magnetic map of the southern part of Anza Graben	129
6.5a	Filtered aeromagnetic map of NW Anza Graben	133
6.5b	Filtered aeromagnetic map of SE Anza Graben	134
6.6a	Pole- reduced map of the NW Anza Graben	136
6.6b	Pole- reduced map of the SE Anza Graben	137
6.7a	Vertical gradient of the gravity of NW Anza Graben	138

6.7b	Vertical gradient of the gravity of SE Anza Graben	139
6.8a-b	Magnetic models along planes 7, and 11	144
6.8c-d	Magnetic models along planes 14, and 17	145
A	flow chart for the ray tracing package BEAM87	A2

LIST OF TABLES

Table	Pg
1	Geophysical activities and drilling activities in Eastern Kenya 7
2	Thickness estimates from boreholes and from stratigraphic correlation 17
3	Data about the shot points LTS, ILA, LAI, CHF 36
4	Sources of the gravity data and their distribution 55
5.1	Shale densities in Duma 100
5.2	Shale densities in Ndovu 101
5.3	Density measurements in Sirius 102
5.4	Densities of Permo-Triassic rocks at coastal Kenya 104

ABSTRACT

Anza Graben is situated in the north and northeastern Kenya. It is about 120 km wide and approximately 600 km long. The area of the present study is located mainly in NE Kenya and constitutes a strike length of about 300 km. The graben is almost entirely sediment filled and is estimated to be of Cretaceous age. It is characterized by a prominent negative Bouguer anomaly reaching -40 mGal.

Several studies were made in an effort to determine its subsurface structure. These involved interpretation of a number of seismic reflection profiles, 3D interactive gravity modelling using fixed density contrasts between the sediment infill and the basement, and the analysis by filtering and modelling of the aeromagnetic data over the graben. A crustal modelling of refraction data along the western shoulder of the Anza graben using 2D ray tracing was also performed.

Two major basins are recognizable from the results of the studies, namely the southern basin which has a northeasterly dip and the northern basin having a southwesterly one. This alternating asymmetry is also indicated for an adjoining smaller basin located to the west of the graben. The density contrast used for the final gravity model is -300 kg/m^3 which indicates a maximum sediment thickness of about 8 km. The modelling of aeromagnetic data however favour a maximum thickness of at least 10 km. A 2D refraction crustal P wave model of the western shoulder indicates that the crust thins northwestwards with the Moho depth

decreasing from 35 km under Chanler's Falls to approximately 29 km under the southeastern shores of Lake Turkana. The abrupt shallowing of the Moho in the Lake Turkana area is attributed to the effects of the Kenya Rift Valley. However the gentle variation in the Moho depth along the remaining section of the shoulder of Anza Graben appears to depict a regional phenomenon also attributable to the formation of the Kenya Rift Valley. It is proposed from the study that sections of the graben shoulder are underlain by slightly denser rocks and that the crustal thinning associated with Anza Graben is not significant.

ACKNOWLEDGEMENTS

I am greatly indebted to my supervisors Prof. I.O. Nyambok and Prof. J.P. Patel of the University of Nairobi and Prof. Dr. G. Jentsch and Dr. R. Veas of the Technical University (TU) Clausthal, Germany, for their encouragement and support through discussions at the various stages of the study.

I would like to thank Prof. Dr. J. Wohlenberg, Dr. C.J. Swain, Dr. A. Khan and Dr. C. Prodehl for useful discussions and encouragement at the initial stages of the study.

My appreciation goes to Dr. M. Wagener and Dr. T. Jahr of the Gravity Working Group of the TU Clausthal for their support.

I am thankful to Dr. D. Gajewski for useful discussions and interest in my work.

I thank Mr. J. Melzer and Miss R. E. Weber for reading through the draft of this thesis.

I am very grateful to the KRISP90 Working Group headed by Dr. C. Prodehl for enabling me to participate in the KRISP90 Experiment and the subsequent Workshops and for kindly providing part of the KRISP90 data for my work.

The equipment used for the gravity and ground magnetic fieldwork was kindly provided by the Departments of Geology, Physics, and Surveying and Photogrammetry of the University of Nairobi, the Meteorological Department of the Ministry of Transport and Communication, Kenya and

the Department of Geology, University of Leicester. To all these institutions I acknowledge their kindness.

I am grateful to the National Council for Science and Technology (N.C.S.T) for supporting the project and the Deutscher Akademischer Austauschdienst (D.A.A.D) for enabling me to carry out the analysis of my data in Germany.

I am grateful to Prof. Dr. R.K. Bortfeld for making the necessary arrangements for me to use the research facilities of Geophysics Institute of the Technical University Clausthal.

I wish to express my sincere gratitudes to the Staff of the Foreign Students' Office of the TU Clausthal and the D.A.A.D Offices in Nairobi and Bonn for their encouragement and support.

I would like to thank the Staff of the Department of Geology, University of Nairobi headed by Prof. J. S. Gaciri for their support and encouragement throughout the study period.

Finally, I would like to thank my wife and children for their patience and support.

This study constitutes project No. N.C.S.T/5/003/D/46 of the Kenya National Council for Science and Technology.

CHAPTER ONE

GENERAL INTRODUCTION

1.1 Location and importance of the area

The area on which this study is based is situated in the northern and northeastern Kenya (Fig. 1). It lies between longitudes 37°E and 41°E and stretches from about the equator to 3°N . As the orientation of Anza Graben is NW-SE, the coordinates mentioned above merely enclose but do not define its margins. Anza Graben belongs to those structures classified as bearing the Anzan trend (N.O.C.K., 1986). Structures with this trend can be traced all the way from off-shore Kenya through Sudan up to southern Chad. This has caused some differing opinions on the extent of Anza Graben. Some authors have used the term Lamu Embayment to define the entire sedimentary section from Lake Turkana to Lamu and beyond (e.g. Patrut, 1977) while others have reserved the term embayment only for the section between Garissa and Lamu. Still others define the Anza Graben as extending from Garissa to Lake Turkana (e.g. Reeves et al., 1987). The area of this study extends from the region between Garissa and Hagadera to the latitude of Marsabit town (Fig. 1). This constitutes a length extent of about 300 km. The imposition of this limit was based on the fact that this stretch constitutes the most well defined and probably best developed sector of the Graben. Furthermore, it was only on this section that a reasonable quantity of data with good coverage was available for the support of this study.

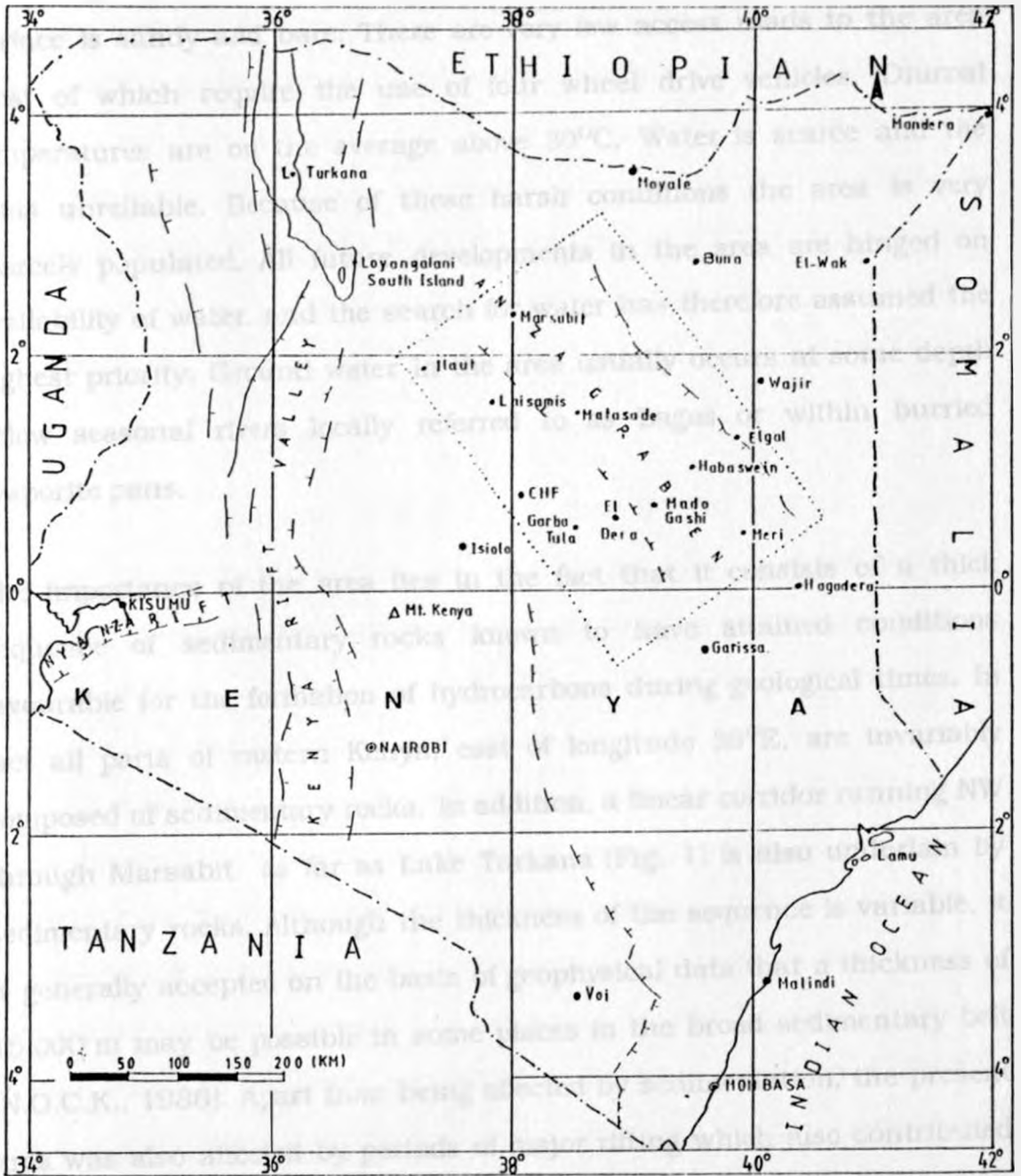


Fig. 1: Location of the study area (In the dotted rectangle; map after Mines and Geological Department, 1967).

The area is almost flat with an average elevation of about 300 m above sea level. Climatically, it can be classified under deserts. Vegetation is scarce consisting of scattered shrubs and small leaved thorny trees. Most of the surface is sandy and bare. There are very few access roads to the area most of which require the use of four wheel drive vehicles. Diurnal temperatures are on the average above 30°C. Water is scarce and the rains unreliable. Because of these harsh conditions the area is very scarcely populated. All future developments in the area are hinged on availability of water, and the search for water has therefore assumed the highest priority. Ground water in the area usually occurs at some depth below seasonal rivers locally referred to as Lagas or within buried evaporite pans.

The importance of the area lies in the fact that it consists of a thick sequence of sedimentary rocks known to have attained conditions favourable for the formation of hydrocarbons during geological times. In fact all parts of eastern Kenya, east of longitude 39°E, are invariably composed of sedimentary rocks. In addition, a linear corridor running NW through Marsabit as far as Lake Turkana (Fig. 1) is also underlain by sedimentary rocks. Although the thickness of the sequence is variable, it is generally accepted on the basis of geophysical data that a thickness of 15,000 m may be possible in some places in the broad sedimentary belt (N.O.C.K., 1986). Apart from being affected by sedimentation, the present area was also affected by periods of major rifting which also contributed towards the deep burial of older sediments. These phenomena are considered to have been rapid enough to enable oil generation to occur. Despite the absence of oil findings to date, studies on rock samples from

the area have shown the existence of source, reservoir as well as caprocks in places (Patrut, 1977).

In a recent work (Reeves et al., 1987), views have been expressed that Anza Graben constitutes a failed arm of a triple junction. Aulacogens elsewhere are known to hold rich reserves of petroleum deposits. Burke (1977) gives examples of these as Benue Trough of West Africa, Oklahoma Aulacogen of U.S.A, and the North Sea Graben of NE Scotland. Further, the discovery of oil in the Abu Gabra Rift of Sudan (Schull, 1988) which falls within the Anzan trend has lent more weight to the interest in the area.

Apart from the economic potential, the area is also of great academic interest. The fragmentation of the East African coast and the generally accepted breakdown of Gondwana and the drifting of Madagascar from Africa is estimated to have occurred within the same time span as the evolution of Anza Graben (Reeves et al., 1987). If this view is true as evidence indicates, a detailed study of the structure of Anza Graben and of its evolution history should improve our understanding of the regional tectonics that resulted in the present East African continental margin. In this respect it is also important to compare and contrast the two rifts, Anza Graben and the Kenya Rift Valley which are geographically very close to each other. In the Lake Turkana area, trends of the Kenya Rift Valley running approximately N-S and those belonging to the Anzan trend intersect. However, because of the age difference between the two trends the continuity of the Anza Graben in the region of overlap is not clearly discernible. Measured along the equator the two rifts are situated about 400 km apart. It is therefore of interest to investigate the forces that resulted in changes of the regional stresses from the ceasing of the rifting

of Anza Graben to the onset of the development of the Kenya Rift Valley. An understanding of the relationships between Anza Graben, the continental margin and the Kenya Rift Valley doming and development should lead to a new tectonic model of the region. Many presentations have already been made on the geology, structure and evolution of the coastal margin (Kent, 1974; Kent et al., 1971) and on the Kenya Rift Valley (Baker and Wohlenberg, 1971; Baker et al., 1972). Up to the time of this study however, not much in the form of presentations can be cited for Anza Graben.

1.2 A review of geophysical activities in the area and in other parts of Eastern Kenya

Geophysical activities in eastern Kenya started in 1955. Nearly all activities recorded to date were geared towards the search for oil. The exploration activities were conducted on ad hoc basis being concentrated in areas considered most promising. A systematic continuous coverage of the area was not a priority. Typically, exploration tended to lag for long periods after the drilling as in all past cases negative results were obtained. Revival of activities depended on whether another company was willing to come in or whether a new technique or system warranted a resurvey. Overall there was a general lack of continuity in ground coverage.

Nearly all geophysical activities carried out in eastern Kenya between 1955 and 1972 were conducted by British Petroleum (BP) Shell Oil company. Most of these activities were centred in the area between Garissa and Lamu (Fig. 1). The beginning of the seventies saw a growth in the interest in eastern Kenya with companies like Burmah Oil, Wainaco,

and Chevron stepping in. The area of activities correspondingly broadened to include the marine area of Kenya. During this period the Government of Kenya played a major role in the acquisition of aeromagnetic data over the region. Teams from Leicester improved the gravity coverage. The geophysical methods employed during the seventies were gravity, aeromagnetism, and seismic reflection. By 1977 a fairly good coverage of the region through geophysical surveys had been achieved. Twenty three wells had been drilled, half of them over 1500 m deep and eight going beyond 3600 m depth. All these wells were dry. The following five years saw a total lag in geophysical activities. Active fieldwork was not picked up until after 1982 when several new companies came in. These included Amoco of U.S.A, Petrofina of Canada and Total of France. Some of these companies are, to date, still actively involved in the area. A summary of the geophysical activities up to 1986 is shown in Table 1.

Although a fair amount of geophysical data has been collected over the last three decades, very little in the form of publications or presentations on the area has been forthcoming. This can partly be attributed to the secrecy with which the data has been handled over the years. Thus only activity reports with little technical information were available. As the little information that could be accessed covered varying parts of the sedimentary belt and were by different oil companies, there was an urgent need to correlate the findings to try to construct a regional picture of the subsurface geology. A first attempt was carried out by Patrut (1977). He used information from various sources such as geophysical measurements, borehole and geological data to formulate models for the sedimentation history of the area. Swain (1979) pointed out that the

	1955	1956	1957	1958	1959	1960	1961	1962	1963	1964	1965	1966	1967	1968	1969	1970
Gravity surveys	xxxx	xxxx			xxxx	xxxx		xxxx			xxxx	xxxx	xxxx	xxxx	xxxx	
Airborne magnetics						xxxx						xxxx				
Ground magnetics																
Seismic surveys					xxxx	xxxx	xxxx	xxxx	xxxx			xxxx	xxxx	xxxx	xxxx	xxxx
Stratigraphical/ Exploratory drilling					xxxx	xxxx	xxxx	xxxx	xxxx			xxxx	xxxx	xxxx	xxxx	xxxx
	1971	1972	1973	1974	1975	1976	1977	1978	1979	1980	1981	1982	1983	1984	1985	1986
Gravity surveys		xxxx	xxxx		xxxx							xxxx	xxxx	xxxx	xxxx	xxxx
Airborne magnetics												xxxx				
Ground magnetics												xxxx	xxxx	xxxx	xxxx	xxxx
Seismic surveys				xxxx	xxxx	xxxx	xxxx					xxxx	xxxx	xxxx	xxxx	xxxx
Stratigraphical/ Exploratory drilling	xxxx				xxxx	xxxx						xxxx				xxxx

Table. 1: Geophysical and drilling activities in Eastern Kenya (1955-1986)

gravity anomaly over Anza as well as two other anomalies located at 40.5°E , 1.0°N and at 40.9°E , 2.9°N were the most significant in the region.

In the early eighties, the Government of Kenya initiated a program to compile all the previous findings in the form of a technical report. This was coupled with the creation of a data bank mainly for the purpose serving those interested in doing further exploration in the area. The exercise involved collection of all existing data and compilation of an accompanying report outlining the important findings made from the various data sets. This exercise covered not only NE Kenya but also parts of Kenya Rift Valley. These efforts resulted in the compilation of an up to date report on the Kenyan Rift Valley (N.O.C.K., 1986) and in the production of a revised geological map of Kenya, a structural contour map and a Bouguer anomaly map (N.O.C.K., 1987).

The first attempt to model the gravity and magnetic data over the sedimentary belt is that by Reeves et al. (1987). Their study however stretched over a very large area extending from Lamu to Lake Turkana (Fig. 1) and comprised two profiles over Anza Graben. Their modelling was based on 2D and 2.5D methods. They estimate the basement to have a maximum depth of 8 to 10 km from gravity and magnetic data, respectively. The positive shoulder anomalies are attributed to thinning of the crust. A crustal extension of 60 km has been suggested. The authors proposed a triple junction in the region and pointed out the close resemblance of the structural characteristics with those of the Benue Trough, a well known arm of a triple junction. The centre of the triple junction in this case is estimated to be located around Garissa (Fig. 1).

They proposed that Anza Graben constitutes the failed arm of the triple junction.

Simiyu (1989) has carried out studies involving gravity and seismic reflection in the Lamu area of coastal Kenya. It is indicated from the study that the major tectonic disturbances in the Lamu area were caused by basement complex block faulting. A major fault trend running NNW - SSE and a minor one running NE - SW was confirmed from the study.

1.3 Aims of the present study and scope

It is clear from the previous section that before this study no detailed structural studies involving modelling of gravity and magnetic data were conducted over Anza Graben. This is in great contrast with the main Kenya Rift Valley where a lot of research work was carried out and earlier models have been refined over the years in pace with the improvement in measuring, analysis, modelling and interpretation techniques. The present study is aimed at determining the structural characteristics of Anza Graben through detailed analysis, modelling and interpretation of gravity data supported by magnetic, seismic, borehole and geological data. Gravity constitutes the main body of the study. The rest of the data served the purpose of supplementing gravity through providing boundary conditions control at the modelling as well as geological synthesis stages.

Since the basin is not uniform in character over the 300 km length, 3D modelling of gravity data was considered most appropriate for use. The main advantages of this approach are that there is an unquestionable increase in the amount of information one can derive and a reduction in the amount of freedom of the vertices defining the model thus resulting in

reduced ambiguity. The choice of 3D modelling was therefore aimed not only at having a realistic representation of subsurface structures but also at maximizing on the amount of information that could be obtained.

Having presented the best fit models for the various data sets, the next step was to carry out a geological synthesis of the models and to determine the present structural and geological relationships both for the shallow and deep structures. Eventually, structural evolution models for the Graben were to be worked out and their fit into the tectonic framework of the region evaluated. This involves taking into consideration the East African continental margin as well as the Kenyan Rift Valley which are the major structural features in the region. Finally, a comparative study involving Anza Graben and other well known grabens was conducted. This part of the study was considered important in helping to define the aspects that should be given high priority in future studies of the area. In summary, the objectives of the present study can be listed as follows:

1. to delineate the subsurface structure of the Graben through modelling of the gravity data supported by other data including seismic and magnetic data;
2. to work out models for the geological and structural evolution;
3. to attempt to reconstruct the tectonic history of the region taking into account the structural patterns depicted from the modelling of potential field data;
4. to compare Anza Graben with other well known grabens.

CHAPTER TWO

REGIONAL GEOLOGY

The broad region within which the present area lies is underlain by rocks of sedimentary origin. They range in age from Permian to Recent (Patrut, 1977). Metamorphic rocks although present occupy only a small portion of the area. Volcanic rocks occur only in the northern part of the area. On the other hand, intrusive rocks have very limited exposure and are restricted to the western shoulder of the Graben.

The older consolidated sedimentary sequence is in most places covered by unconsolidated sediments and lava flows of Quaternary age. Thus, most of what is known about the older rocks has been obtained mainly through correlation with adjacent areas where these older sequences are exposed supplemented by borehole data. Pioneering geological works in the sedimentary region are contained in the reports by Ayer (1952), Miller (1952), Caswell and Baker (1953), Caswell (1956), Thompson (1954), Sanders (1956), Saggerson and Müller (1957), Baker and Saggerson (1958), Williams (1958), Kent et al. (1971) and Walsh (1972). Later works include those by K.A.M.E. (1975), Patrut (1977), Cannon et al. (1981), Key et al. (1987), and Hackman et al. (1990). These works have mainly dwelt on geological mapping of the various parts of the belt. In most of the cases, thickness estimates for the various sedimentary units were also made. In nearly all the cases, the authors also attempted to reconstruct the geological histories of their respective study areas.

2.1 Geological correlation using deep boreholes

A limited number of deep boreholes has been drilled into the sedimentary formation of eastern Kenya since 1959. Most of these boreholes are situated in the region between Garissa and Lamu. Up to the time of this



Fig. 2.1: The distribution of deep boreholes in Eastern Kenya

study only a few boreholes existed between Garissa and Lake Turkana (Fig. 2.1). Boreholes drilled in the sedimentary belt (Fig. 2.1) were intended for testing suspected structural traps or for stratigraphic correlations. Because the entire region is covered by young sediments, these boreholes

have proved to be very useful for studies related to the subsurface geology, correlation, depositional environment, sedimentation and hydrocarbons potential.

Tab. 2 gives the thicknesses and the geological correlation results of some of the boreholes. Generally the boreholes predict a very thick sequence of sediments to comprise the belt. So far no borehole has reached the underlying metamorphic rocks. In most places the Mesozoic sequence has hardly been penetrated. Thus, existing informations concerning the formation directly overlying the basement and the basement geometry are still conjectural. Only in the area to the north of Marsabit was the basement reached at a surprisingly shallow depth (about 2600 m). This however occurs in an area affected by block faulting and hence does not represent the general order of magnitudes of depths expected to the underlying metamorphic rocks.

2.2 Sedimentary rocks

Sedimentary rocks are considered to have been deposited in several basins which developed in eastern Kenya from the Carboniferous times (N.O.C.K., 1982). The evolution of these basins is usually attributed to the breakup of Gondwanaland and the eventual development of the Indian Ocean. Most of these basins are located east of longitude 39.0°E. Because the region was affected by various phases of transgression, regression and erosion (Patrut, 1977), the sedimentary formations are not uniformly developed. It is therefore difficult to make generalizations about their thicknesses.

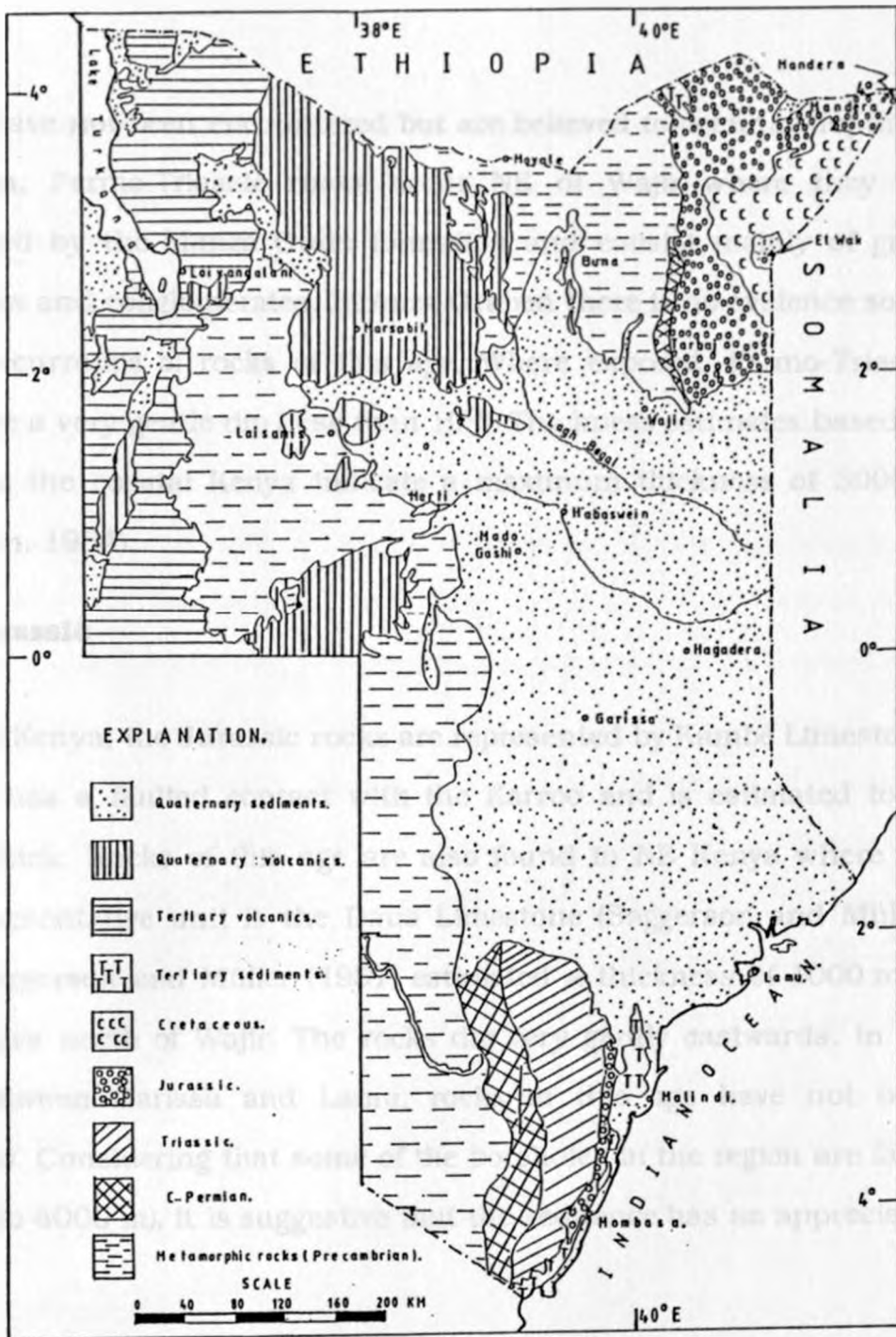


Fig. 2.2: A simplified regional geological map of Eastern Kenya (After, Mines and Geological Dept., Kenya., 1967).

2.2.1 Permo-Triassic

The Permo-Triassic, which are generally referred to as the Karroo (after the type area where the sequence was first mapped in southern Africa) are best exposed at the coastal Kenya (Fig. 2.2) where they consist of grits, shales, and sandstones. In the area between Garissa and Lamu, rocks of

this age have not been encountered but are believed to occur at depth. In NE Kenya, Permo-Triassic rocks occur NE of Wajir where they are represented by the Manza Guda formation and consist mainly of grits, sandstones and conglomerates. In Anza Graben there is no evidence so far for the occurrence of rocks of this age. Where exposed, Permo-Triassic rocks have a very gentle dip (less than 10°). Thickness estimates based on studies at the coastal Kenya indicate a maximum thickness of 3000 m (Thompson, 1954).

2.2.2 Jurassic

In coastal Kenya, the Jurassic rocks are represented by Kambe Limestone. The unit has a faulted contact with the Karroo and is estimated to be 1700 m thick. Rocks of this age are also found in NE Kenya where the most representative unit is the Daua Limestone (Saggerson and Müller, 1957). Saggerson and Müller (1957) estimated a thickness of 1000 m in Tabaka area north of Wajir. The rocks dip very gently eastwards. In the region between Garissa and Lamu, rocks of this age have not been penetrated. Considering that some of the boreholes in the region are fairly deep (up to 4000 m), it is suggestive that the sequence has an appreciable depth.

Around Garissa, two wells have encountered but not penetrated a Jurassic sequence. In the well designated as Garissa 1, 205 m of Jurassic was entered. The sequence consists of mudstones and shales interbedded with siltstones and compact sandstones. In the well Kencan, 2712 m of the unit were penetrated. However, it is not certain whether the unit below is still Jurassic or the beginning of the Triassic. The Upper Jurassic here consists of sandstones, siltstones, shales, mudstones and limestones.

Inliers of Jurassic occur at Merti on the western shoulder of Anza Graben. They consist of oolitic limestones (100 m), grading into siltstones (30 m) and fine grained sandstone and quartzites. Farther north in the region around Lake Turkana grits occur considered to stretch from late Mesozoic to Tertiary (Morley et al., 1991). They are considered to represent reworkings of the basement rocks. Their exact ages are however still unconfirmed although there are views that they are of late Jurassic to early Cretaceous (N.O.C.K., 1986). They occur in an unconformable contact with the Precambrian basement rocks and are considered to represent the onset of rifting within the Turkana region (Williamson and Savage, 1986). The well Sirius drilled some 50 km NW of Marsabit may have encountered Jurassic before hitting the basement at 2600 m. However, there is no definite proof that the rocks are of Jurassic or Cretaceous age. The isolated occurrences of rocks showing Jurassic characteristics suggest the existence of rocks of equivalent age at depth in Anza Graben. Although fairly deep boreholes (up to 4000 m) have been sunk in the graben, a distinct Jurassic sequence has not been reached. A typical Jurassic sequence in the region is essentially a marine facies consisting predominantly of shale and limestone (Patrut, 1977).

2.2.3 Cretaceous

Outcrops of Cretaceous at the coast occur near Mombasa (Fig. 2.2). The maximum thickness is estimated to be 4000 m (R.R.I.L., 1986). In northern Kenya these rocks are exposed only around El Wak. They consist mainly of sandstones referred to as the Marehan Sandstones (Baker and

WELL	PLIO- QUAR.	TERTIARY			CRETACEOUS				JUR.	PERMO- TRIAS	BASEMENT DEPTH	TOTAL DEPTH
		MIO	EO-OL	PAL	CE-SE	ALB	APT	NE				
Kipini	177	1705	1274	-	510	-	-	-	-	-	-	3664
Pate	174	1042	2974	10	-	-	-	-	-	-	-	4190
Dodori	287	927	2324	775	-	-	-	-	-	-	-	4313
Pandangua	50	1058	927	-	-	-	-	-	-	-	-	1981
Mararani	184	982	826	-	-	-	-	-	-	-	-	1992
Walu	-	600	850	-	1000	1174	110	-	-	-	-	3730
Hargaso	132	489	218	-	800	1476	-	-	-	-	-	3093
Walmerir	244	635	595	-	-	500	250	1446	-	-	-	3796
Garissa	100	472	463	-	-	-	-	-	205	-	-	1240
Kencan	201	-	314°	-	-	59°	-	-	2712	-	-	3863
Meri	305	530	1107	-	-	-	-	-	-	-	-	1942
Bahati												1042
Anza			2050°									3662
Hothori			3353°									4390
Ndovu			1335°		280	2507						4267
Duma			3063									3333
Sirius	200				1426	300					2597	2597
Maximum thicknesses based on a generalized stratigraphic column for Kenya. (from Patrut, 1977)												
			5700°			2300°		1700		5000-7700°		

Table 2. Thickness estimates from borehole and from stratigraphic correlations estimates in meters (from N.O.C.K., 1990). (PLIO-QUAR - Pliocene-Quaternary, JUR- Jurassic, PERM-TRIAS- Permo-Triassic, MIO- Miocene, EO-OL- Eocene-Oligocene, PAL- Paleocene, CE- Cenomanian, AL- Albian, APT- Aptian, NE- Neocomian ° combined thicknesses).

Saggerson, 1958). A thickness of 100 m was estimated in the Mandera area. Along the Lamu Embayment-Anza Graben axis, rocks of the Cretaceous age have however not been penetrated so that the maximum thickness is uncertain. Where penetrated the thicknesses are variable possibly due to varying levels of erosion. In Tab. 2. the boreholes are arranged according to the increasing distance towards the Anza Graben.

The variation in the thickness of the Cretaceous is remarkable. Starting from Lamu area, Tertiary is very thick so that Cretaceous is hardly reached. As one moves farther interior, it shallows has been penetrated around Garissa. Here the Jurassic has been encountered. Farther NW Cretaceous again shows an apparent increase in thickness as indicated in Hothori, Ndovu, and Duma. In general, the area to the south of Garissa is dominated by shallow marine type deposition. NW of Garissa not much description has been made mainly due to almost complete absence of fossils of correlative value (Patrut, 1977). It is therefore quite difficult to identify age boundaries. The absence of fossils suggests a predominance of a non-marine environment of deposition in this region.

2.2.4 Tertiary

Tertiary deposits are the most developed in NE Kenya as recorded from drilling logs (Patrut, 1977). These overlie different stratigraphic members unconformably. At the coastal Kenya, these sediments are mainly marine but become continental inland. In NE Kenya outcrops of Pliocene sediments occur in the southern section of Anza Graben and in the area to the east of Wajir. These consist of sandstones and sands. Older Tertiary sediments have only been encountered in boreholes. Like in the case of the Cretaceous the trend is for the sequence to thicken from the area around Garissa towards the sea and also in the NW direction. Thus, in the Garissa area thicknesses of less than 1000 m are registered but in the middle of Anza Graben they increase to about 3000 m. In the extreme north of the Graben, the sequence may be very thin or lacking. There is again the problem of distinguishing the units due to the absence of fossils.

The oldest Tertiary sediments are considered to be of Paleocene age and were recorded in Dodori well (Fig. 2.1). They consist of sandstones, shales and limestones. They seem to be confined to the coastal region as they have not been encountered in the wells inland and are considered to represent a marine regression phase.

Eocene and Oligocene deposits are developed in a dominant marine environment along the coastal Kenya and in a deltaic-continental one inland. The marine facies was penetrated in Dodori, Pate, Kipini and partially in Mararani. The facies is generally very fossiliferous.

The Lower Eocene unit consists of limestones, sandstones and shales. The thickness increases from 825 m in Dodori to 1040 m in Pate well. These sediments are considered to have been laid down in a shelf marine and partly deep water environment. The Middle Eocene unit was penetrated in Kipini, Pate and partially by Mararani. It consists of limestones, shales, and sandstones. The thickness varies from 1070 m to 1700 m, the maximum having been registered in Pate. The Upper Eocene unit consists of sands and sandstones. The thickness increases from 60 m at Mararani up to 320 m at Kipini. The Oligocene unit is considered lithologically to be very similar to Upper Eocene. The two are considered to have been laid down in a fluvial and deltaic environment. The sands are feldspathic suggesting that in the adjoining western land area, during this time, erosion began to act directly upon the basement.

The Lower Tertiary deposits become non-fossiliferous inland so that age determinations have not been precise. They are however overlain by Miocene deposits. They consist of mudstones, argillaceous sands and soft sandstones. This so called undated succession (Patrut, 1977) was entirely

penetrated in Walu, Hargaso, Garissa and Wal Merer wells. Its thickness has been recorded to vary from 200 m to over 1000 m. It is suspected to have been favoured by a deltaic and terrestrial environment of deposition.

The Miocene deposits are best developed along the coastal area consisting of limestones, mostly fossiliferous. Lower Miocene deposits extend towards the north but their thickness decreases and the limestones give way to argillaceous limestones, mudstones and sandstones. Deposition is considered to have occurred in a deltaic environment with intermittent marine invasion.

The Miocene deposits are overlain by a sequence of sands, clays, reef limestones and alluvial deposits. They mark the last sedimentary cycle in the region. They are thought to have been laid out under various conditions from marine along the present coastline to continental one. The thickness varies but is about 300 m.

Mutunguti (1988) carried out analyses of Kerogen of sediments from boreholes within the sedimentary formation. It was concluded from the study that the distribution of Kerogen in sediments is governed by both lithology and age and that there is more than the minimum percentage of Kerogen required to yield commercial hydrocarbon accumulations on maturation.

2.3 Metamorphic rocks

Metamorphic rocks (Fig. 2.2) occurring on the western edge of the vast sedimentary basin exhibit a faulted contact quite evident at the coast but less so in the hinterland. East of this contact, no metamorphic rocks are exposed except in the north eastern corner of Kenya where an 'island' of

metamorphic rocks outcrops. These rocks consist of gneisses and schists of the Mozambiquan system. They have neither been encountered in the boreholes in the Lamu Embayment nor within the Graben in the present area of study.

2.4 Igneous rocks

Both extrusive and intrusive igneous rocks occur in the region surrounding Anza Graben. Their occurrence is however limited to the northern part of the study area in the neighbourhood of Marsabit and Laisamis (Fig. 2.2). Parts of these areas were mapped geologically by Walsh (1972) and more recently by Key et al. (1987). Extrusive rocks occur as basaltic lavas resting in most sections on sedimentary sequences and forming conspicuous basalt plateaus. At Marsabit occurs the dome like shield volcano (Key et al., 1987). It has an oval plan with a NE-SW long axis about 115 km long and a SE-NW axis about 90 km long. The shield rises from about 600 m at the flank to 1700 m at its summit. Volcanic centres in the form of cinder cones and craters are concentrated in two belts about 15 km wide trending NE and NW through the summit of the shield. Key et al. (1987) suggest that the shield volcanism was controlled by the underlying fractures which may have been reactivated faults or contemporaneous structures. They further suggest that the NE structural trend may represent an important set of transcurrent fractures related to the Miocene development of the Kenya Rift System.

On account of their rareness in the area, intrusive rocks have not received much attention in past geological mappings. A noticeable concentration of intrusives occur in two areas on the western shoulder of the Anza Graben. These are to the west of Merti and to the south of Laisamis. They are basic

in character but their exact ages are not known. Within Anza Graben itself no evidence of large scale occurrence of intrusives has been adduced. Although igneous rocks have been encountered in some of the boreholes, they are usually of insignificant thicknesses.

2.5 Major structures and structural trends

In the sedimentary belt of northern and northeastern Kenya a number of major structural units apart from Anza Graben have been identified (N.O.C.K., 1986). These are the Lamu Embayment, the Mandera Basin, and the Turkana Trough in the north (Fig. 2.3). Lamu Embayment is here defined to represent the area between Garissa and the Kenya coast. It is bound to the west by the metamorphic rocks, and to the north by the onset of the Anza Graben. The region is characterized by complex block faulting and the accompanying anticlines and synclines. The Garissa High and the Lamu High are examples clearly depicted from gravity data. Unlike the Lamu High on which a fairly detailed study has been done (Simiyu, 1989), very little is known about the Garissa High. Off-shore the trend of the Lamu High (NW-SE) is depicted by the Davies Fracture which is believed to be the line of translation of Madagascar from Africa (Rabinowitz et al., 1982; Rabinowitz et al., 1983).

Mandera Basin trends in an approximately NE-SW direction and seems to terminate on the Anza Graben some 60 km south of Wajir. This basin extends into Somalia where it is reported to attain its maximum thickness. This axis is marked by the so called Tamola syncline (R.R.I.L., 1986) in Somalia. The basin is apparently faulted on the sides but not much data on the intensity of faulting has yet been presented. Occurring to the east of the Mandera Basin (in Somalia) is the Bur Acaba Uplift. The

two structures share a common trend. Two major structural trends are recognized in the study area. One is the NW-SE trend representing the Anza Graben and several anticlinal structures in the Lamu Embayment. It is the most important trend in the area and has been referred to as the Anzan trend (N.O.C.K., 1986). It extends from the off-shore Kenya where it aligns with the Davies Fracture (Rabinowitz et al., 1983) through Kenya, Sudan, terminating in Chad.

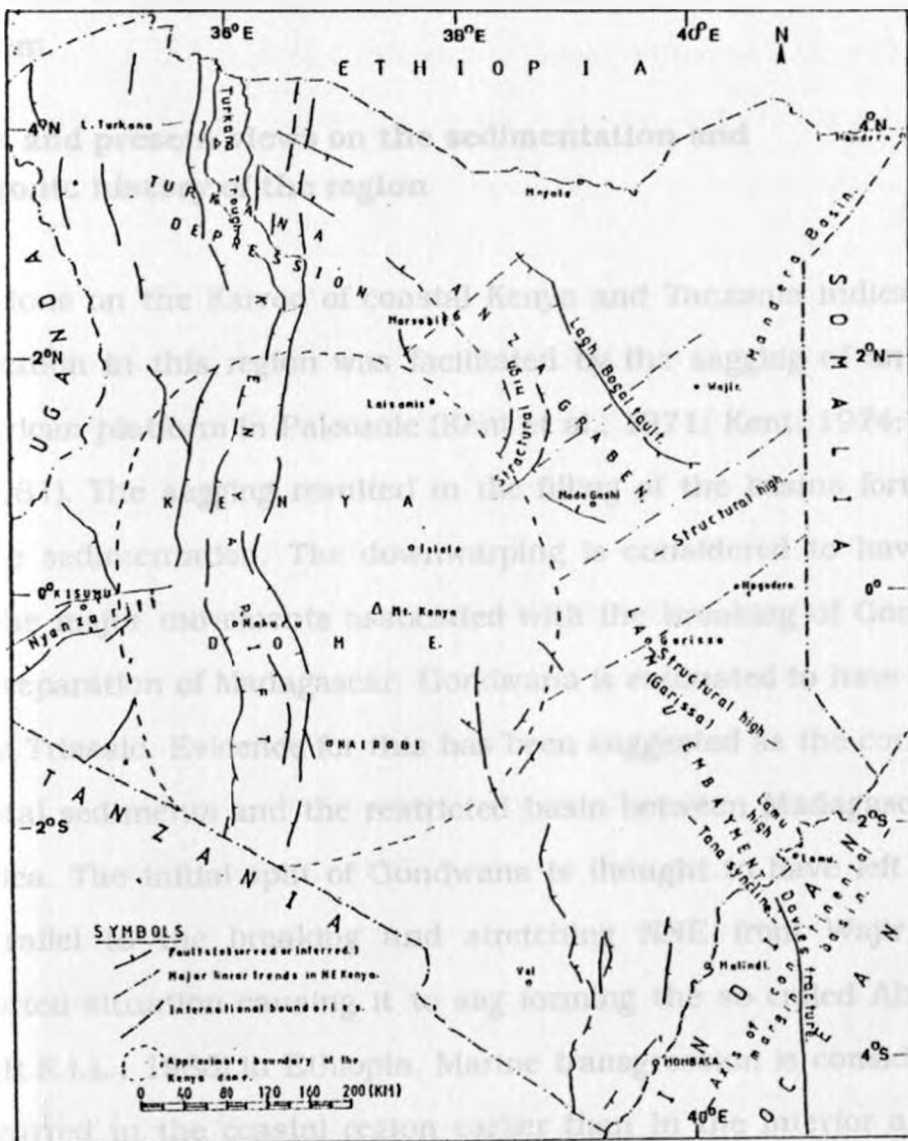


Fig. 2.3: A simplified structural map of Kenya (after, N.O.C.K., 1987).

The second trend runs NE-SW. This trend has been clearly confirmed from the geological mapping (Key et al., 1987). It is considered to have controlled the volcanism in Marsabit area. Similarly oriented lineaments occur at the southern termination of the present study area. Key et al. (1987) attribute the NW trend to the movements associated with the evolution of Anza Graben. They consider the NE trend to represent an important set of fractures related to the development of the Miocene Kenya Rift System.

2.6 Past and present views on the sedimentation and tectonic history of the region

Studies done on the Karroo of coastal Kenya and Tanzania indicate that sedimentation in this region was facilitated by the sagging of an earlier stable African platform in Paleozoic (Kent et al., 1971; Kent, 1974; Canon et al., 1981). The sagging resulted in the filling of the basins formed by lacustrine sedimentation. The downwarping is considered to have been part of the major movements associated with the breaking of Gondwana and the separation of Madagascar. Gondwana is estimated to have broken up in the Triassic. Evidence for this has been suggested as the correlative continental sediments and the restricted basin between Madagascar and East Africa. The initial split of Gondwana is thought to have left a zone lying parallel to the breaking and stretching NNE from Wajir in an unsupported situation causing it to sag forming the so called Abyssinia Trough (R.R.I.L., 1986) in Ethiopia. Marine transgression is considered to have occurred in the coastal region earlier than in the interior areas. It later spread into Abyssinia Trough possibly through Wajir in Jurassic. Rifting in the sedimentary basin of eastern Kenya is thought to have

developed in early to middle Jurassic. During the Jurassic, Cretaceous and Tertiary SE Kenya is thought to have been under tensional stress to which the formation of Anza Graben is attributed.

Patrut (1977) estimates an Upper Carboniferous age for the initiation of the Lamu Embayment. He recognizes three major transgression episodes characterized by increased sedimentation in Jurassic/Cretaceous, Eocene, and most of Miocene. Positive epeirogenic movements are estimated to have occurred at the end of Cretaceous, Lower Miocene and during the Recent. He attributes the formation of the Garissa High and a number of synclines in the region to the movements at the end of Cretaceous.

Rabinowitz et al. (1983) have attempted to explain the probable location of Madagascar before the break-up and the possible trend of motion. Their model places the axis of the breakup in the region along the Kenya and Somalia coasts. They suggest that the observed parallel diapiric salt structures at the continental margin of Kenya and Somalia were formed on a subsided continent and an embryonic ocean floor created during the separation of Madagascar from the mainland Africa. On the basis of the palaeomagnetic, and physiographic evidences as well as limited geophysical data the authors advance a strong case for movement of Madagascar from NE Kenya and SE Somalia. They argue that the margin bordering Kenya and Tanzania was created by transform motion of Madagascar along Africa.

Reeves et al. (1987) propose an existence of a paleo-triple junction of Jurassic age in eastern Kenya. They consider Kenya coast and Somalia coast to represent two arms and Anza Graben the third arm. In the region of Lamu Embayment, the authors suggest total absence of continental

crystalline rocks. The attenuated continental crust or oceanic crust which is suggested to underlie the region is expected to have uniform magnetization if it was emplaced during periods of stability in the geomagnetic field in the Jurassic. Alternatively, it may have no magnetization if it was depressed below the depth of the Curie temperature isotherm. The authors suggest existence of thinned crust below Anza Graben and consider the Matasade High as a compressional feature.

According to their model rifting was initiated along the Kenya coastline forming the first arm of the triple junction possibly at the beginning of Karroo (Late Carboniferous). Subsequently, there followed the deposition of continental sediments throughout the Permian, Triassic and early Jurassic with only minor marine conditions encroaching from the north in the middle to upper Jurassic. The second arm is the southern terminus of the exposed basement of north eastern Kenya. The arm is considered to have become active during the Jurassic, following the failure of an earlier parallel rift farther north now preserved as Manderu Lugh Basin. On both of these arms rifting is considered to have developed into ocean floor spreading. The third arm according to the authors is represented by what they refer to as Anza-Marsabit-Turkana Graben. This Graben is considered to have been subjected to extensive marine transgression during upper Jurassic. The initiation of the Kenya Rift Valley in Miocene is considered to have resulted in uplift and erosion of the Marsabit Turkana Trough in the present Lake Turkana area but also in reactivation of faulting in the Mesozoic grabens allowing them to receive sediments during Tertiary. Subsequent Quaternary deposition of sedimentary and volcanic rocks obscured the Anza Graben over its entire length.

2.7 Conclusions to be drawn from existing works

As the works cited show, great efforts have been expended in trying to obtain data and information about surface and subsurface geology of the sedimentary formation of eastern Kenya. The surface geological mapping has provided data for correlation purposes and also for thickness estimates. Most of the information on subsurface geology has come from boreholes mainly concentrated in the region between Garissa and the sea. The gravity, magnetic and seismic data have been used mainly in a qualitative sense in the past. Their capability as tools for yielding information about the subsurface structure were not exploited to the full. In summary, the present status of knowledge on basins and grabens in NE Kenya is still in the infancy stage. The models so far presented are still controversial. Several factors contribute to the slow growth of knowledge about the sedimentary belt of Kenya. The most crucial can be sighted as:

1. limited number and distribution of boreholes in the belt;
2. variation in the deposition, rapid facies change and erosional history resulting in problems in thickness estimates;
3. limited occurrence of fossils of correlative value especially in the inland sections;
4. scarce and varying quality and distribution of geophysical data;

5. immense thicknesses of sediments making it difficult to penetrate and study the entire sedimentary sections;

6. lack of representative well-developed type sections for correlation purposes.

While a few questions have been answered from previous studies, a number of questions concerning evolution of the sedimentary formation and the Anza Graben remain unanswered. The significance of the Garissa High is to date not fully explained. So far, not much is known about the geometry and set up of the basement surface beneath Anza Graben. The asymmetry in the geometry of the Graben is of interest but has not been fully investigated. It is also of interest to explain the role of the few intrusives dotted around the Graben in terms of its evolution. A more concerted effort at working on geophysical data in a quantitative sense, backed by additional deep boreholes should help in getting answers to some of these questions.

CHAPTER THREE

SEISMICS

The seismic reflection data used in this study were collected and processed by the Chevron Oil Company in 1974 and 1975 while the refraction data were collected by the Kenya Rift International Seismic Project in 1990 (KRISP90). Five refraction lines were shot during the latter project, the purpose of which was to investigate the variations in the crustal structure within and at the shoulders of the Kenya Rift Valley. The fifth profile runs along the north western shoulder of Anza Graben, almost parallel to it. The profile is thus equally relevant for studies related to Anza Graben.

Interpretation of the reflection data was done on the already processed data in the form of seismic sections while that of the refraction data involved the use of processed seismic sections as well as modelling by two dimensional (2D) ray tracing. The ray tracing was done using the program package BEAM87 by Cerveny (1985 , see appendix A1).

3.1 Reflection Seismics

3.1.1 Importance of the data and quality

Seismic reflection data were useful in this study mainly for the following purposes:

1. to study the structures of the sedimentary layers within the interpretable range;
2. to locate possible basement reflectors;

3. to identify major structural features such as faults, folds, intrusives, and unconformities;

Most of the reflection data available for this study are located in the SE section of the Graben around Habaswein (Fig. 3.1). A spacing of 200 m for the geophones with a 2500 m-200 m -0 m-200 m-2500 m systematic split spread configuration were used during the shooting. Most of the normal processing procedures had been applied to the data before the seismic sections used in this study were produced. They were however not migrated. Velocity analysis was done at selected points with sections being eventually presented as distance-depth sections. These sections were obtained uninterpreted. Attempts to reduce the record sections photographically resulted in substantial loss of detail and quality. They are therefore not included here. The original tapes were not available for this study.

3.1.2 Interpretations and results

There are several NW-SE and SW-NE trending seismic reflection lines concentrated in the southern portion of the present study area. These lines form a fan around Habaswein. Although all the lines were examined during the initial stages of the study, only the interpretations of the three most representative ones are presented. These lines are identified here as REFLL1, REFLL2 and REFLL3 and are shown in Fig. 3.1 together with the gravity modelling planes discussed in chapter five.

The interpretation of seismic sections was carried out using methods stated by McQuillin et al. (1984). This starts with reflection identification and correlation of misties leading to preparation of two way travel time (TWTT) to each horizon.

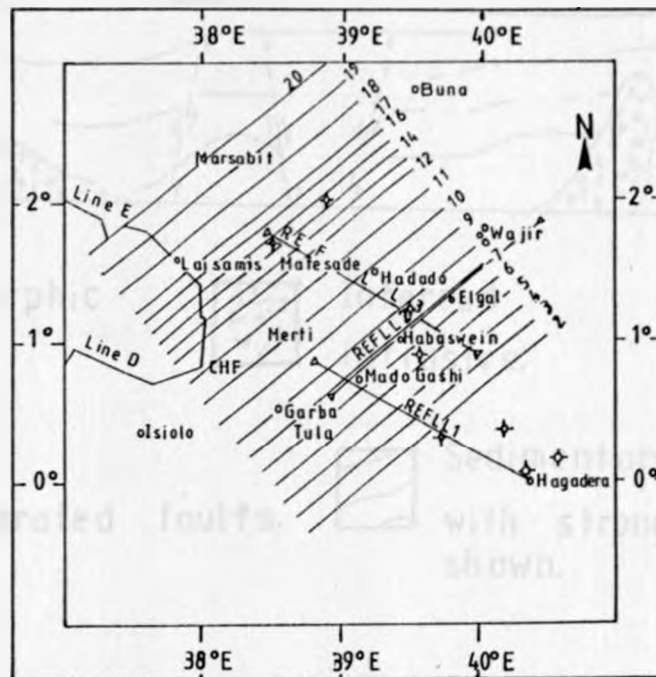


Fig. 3.1: Location of the seismic reflection lines REFLL1, REFLL2, and REFLL3. Also shown are parts of the KRISP90 refraction lines D and E and the planes used in the gravity modelling.

In the present case, the TWTT had already been converted to depths. The final steps involve geological interpretation which seeks to identify the structures.

Line REFLL1 (Fig. 3.2a) trends NW-SE and extends from NW of Mado Gashi to SE of Hagadera (Fig. 3.1), a distance of 340 km. The section around Mado Gashi characterised by absence of reflectors is interpreted to represent the crystalline basement. At this location faults apparently marking the western boundary of the Graben can be easily identified.

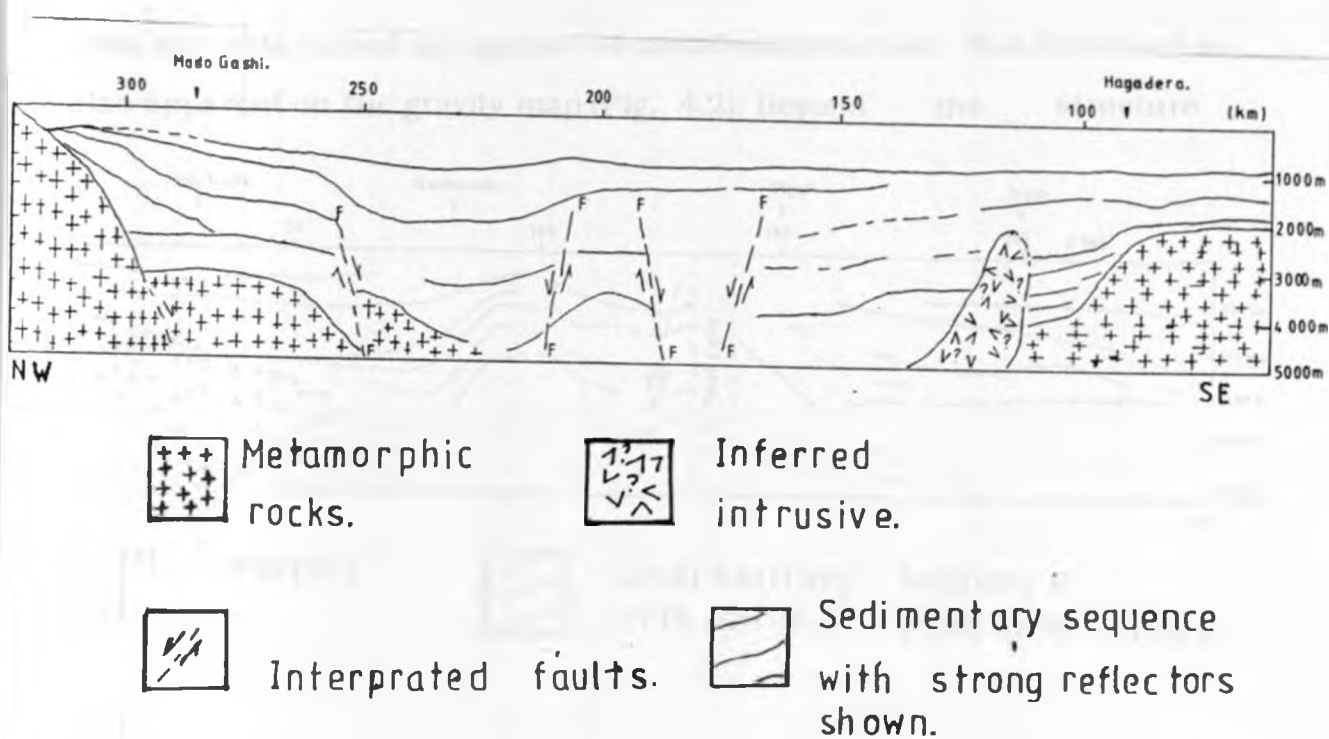


Fig. 3.2a: Reflection seismic line REFL1 (interpretation).

Generally the section indicates more faulting at depths over 1000 m mainly of normal type. Some uplifted horst features also occur. In the extreme south, a zone interpreted to represent a structural high occurs. No reflections occur in or below this uplifted feature which tends to suggest a fairly compact horst structure possibly involving basement rocks. Apart from the influence of faulting, the beds are gentle with no indications of extreme folding.

Line REFL2 (Fig. 3.2b) runs SW-NE from Mado Gashi through Habaswein to the area SE of Wajir. Its total length is 235 km. Basement reflections are prominent around Mado Gashi. The sedimentary beds show a gentle dip towards the east. But at Habaswein this trend is interrupted

with the beds raised up against an anticlinal structure. This structure is also apparent on the gravity map (Fig. 4.2). Beyond the structure

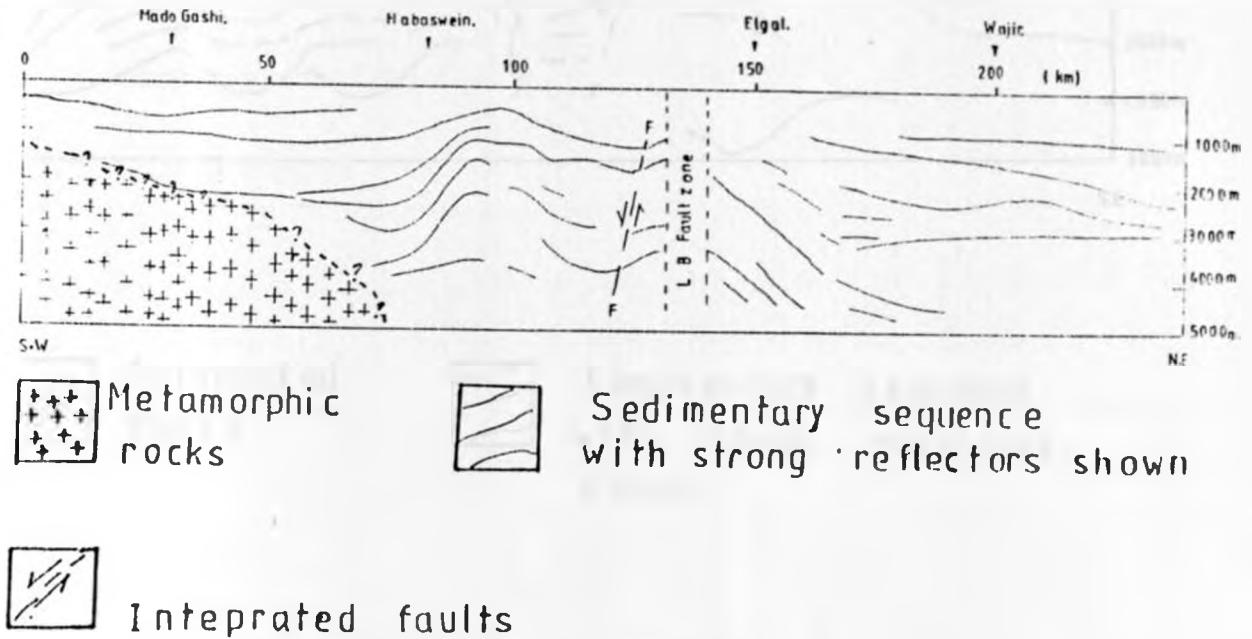
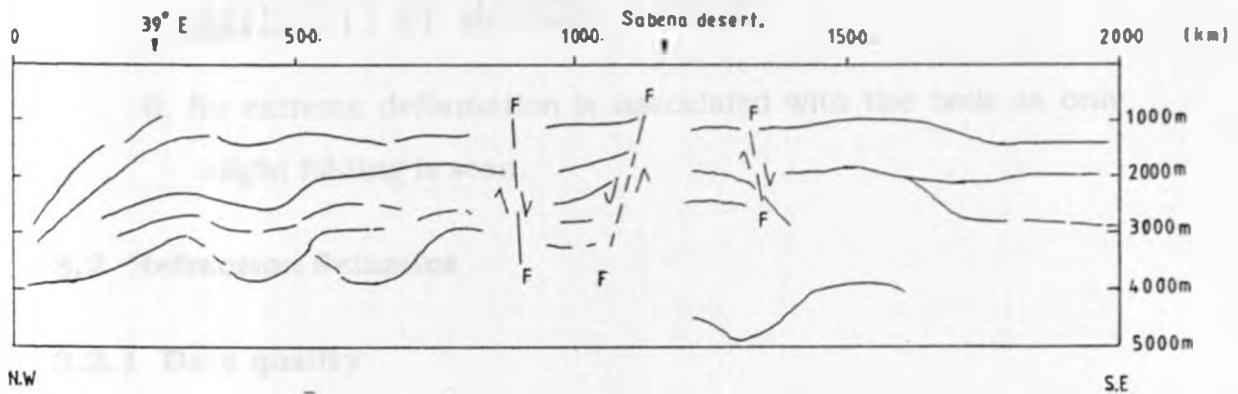


Fig.3.2b: Reflection seismic line REFL2 (interpretation).

a steep easterly dip is apparent. These steep dips are restricted to the older rocks. Young rocks which show good reflections farther east are only gently dipping and are continuous over long distances. The data indicate that Lagh Bogal Fault constitutes a zone up to 10 km wide. The zone is characterized by lack of reflections. This profile also indicates the presence of older beds to the east beyond the fault. Line REFL3 (Fig. 3.2c) and REFL1 are parallel but lie 65 km apart. The former runs from east of Matasade at about $38.75^{\circ}\text{E } 1.5^{\circ}\text{N}$ to 40.1°E and 0.7°N . The profile shows young beds to be horizontal as expected along the strike direction. However the older beds are folded or faulted showing a very irregular and wavy pattern. The beds hardly show any distinct dip.



Interpreted
faults.



Sedimentary sequence
with strong reflectors
shown.

Fig. 3.2c: Reflection seismic line REFLL3
(interpretation).

A number of observations can be made from the examination of the seismic reflection lines:

1. The shallow section of the graben is affected by normal faulting.
2. In the south the apparent dip of the beds is ENE.
3. The boundaries between the sedimentary units are indistinct.
4. There is evidence for intrusives of small size in the extreme south.
5. No basement reflections are observed within the Graben.

UNIVERSITY OF NAIROBI LIBRARY

6. No extreme deformation is associated with the beds as only slight folding is seen.

3.2 Refraction Seismics

3.2.1 Data quality

The locations of the five KRISP90 refraction profiles are as shown in Fig. 3.3. Profile E situated on the western shoulder of Anza Graben is about 400 km long. However only 300 km of the profile was used in the study.

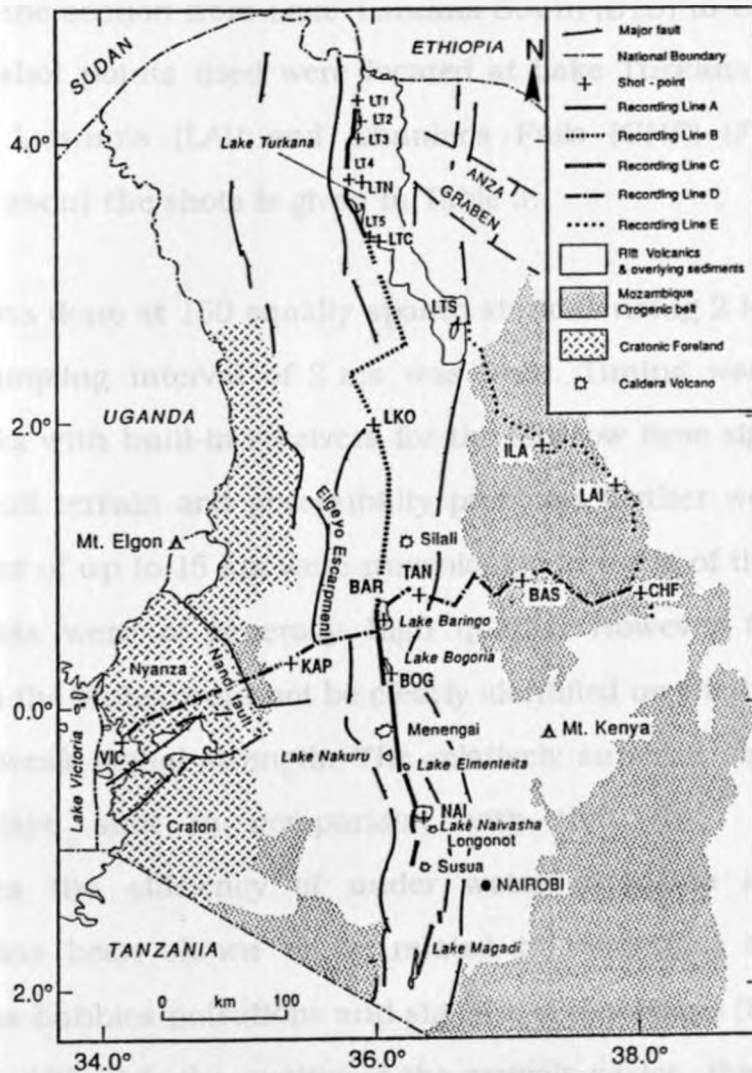


Fig. 3.3: KRISP90 Location map (from KRISP Working Party, 1991).

SHOT	ORIGIN		POSITION		HEIGHT	CHARGE	SHOT TYPE
	DATE	TIME	LAT.	LONG.			
LTS	15.02.90	12.00 00.00	2°41.35N	36°36.95E	340 m	375 Kg	water(80 m)
ILA	13.02.90	17.06 00.60	1°52.11N	37°15.28E	730 m	900 Kg	hole
LAI	13.02.90	17.08 59.95	1°33.40N	37°49.59E	570 m	900 Kg	hole
CHF	13.02.90	17.12 00.00	0°48.39N	38°00.75E	675 m	2000 Kg	hole

Table 3: Data about the shot points LTS, ILA, LAI and CHF (for profile E, Fig. 3.4).

This covers the section from Lake Turkana South (LTS) to Chanler's Falls (CHF). The shot points used were located at Lake Turkana South (LTS), Ilaut (ILA), Laisamis (LAI) and Chanler's Falls (CHF) (Fig. 3.4). The information about the shots is given in Table 3.

Recording was done at 160 equally spaced stations using 2 Hz geophones. A digital sampling interval of 2 ms was used. Timing was done using master clocks with built-in receivers for the Moscow time signal. Because of the difficult terrain and accessibility problems farther west, recording station off-set of up to 15 km were unavoidable in parts of the profile. The resulting data were of generally high quality. However the refraction phases from the Moho could not be clearly identified on the borehole shots due to the weak signal strength. The relatively superior signal obtained from the lake shot in comparison with that from the borehole demonstrates the efficiency of under water explosion sources. This behaviour has been shown to be related to secondary source effects including gas bubbles pulsations and signal reverberations (Burkhard and Veis, 1975). Although the quality of the arrivals varies, the data were of sufficiently good quality to enable correlations and modelling to be done.

The data used in this study were obtained in the form of playback analog reduced time-distance sections with a reduction velocity of 6 km/s. The scales of the plots were 1 cm for 0.5 s and 1 cm for 10 km.

3.2.2 Basic travel time curves and correlations

The term correlation as used in seismic refraction studies implies identifying a phase of a seismic record as representing the phase of another record (Sheriff, 1980). A distinction is made between phase and group correlation. Ideal phase correlation is possible only when the spacing of detectors is smaller than one wavelength. Because this condition is rarely achieved and also because of the influence of inhomogeneities in the subsurface, it becomes necessary to apply a group correlation which sorts the arrival times of a wave group in the record section. The details about the interrelation between the two types of correlations have been outlined by Giese (1976).

Identification of phases on the travel time curves and correlations constituted the first step in the analysis of the refraction data. Preliminary correlation work on all the KRISP90 profiles was done at the KRISP Working Group Workshop held at Malsch near Karlsruhe (Germany) in 1990. The correlation exercise described in this section is a follow-up of this work and was carried out to help identify the initial parameters for the 2D modelling described in this chapter. The correlated record sections (together with ray diagrams and synthetic seismograms corresponding to the end model; see section 3.4) are shown in Figs. 3.4, 3.5, 3.6, and 3.7.

On the record for the shot LTS (Fig. 3.4) the correlation was fairly straight forward as the phases are very clearly represented. The refraction phase

Pg representing basement refraction is traceable up to about 80 km. It is however delayed by about 0.9 s due to the sediments under the lake. This delay agrees well with the two way travel time of slightly less than 2 s obtained by a seismic reflection study conducted in this section (Dunkelman et al., 1989). It is then overtaken by the refraction from the lower crust P*. The P* phase has very strong arrivals up to 222 km. The Moho refraction Pn is weak between 150 and 240 km, but becomes clearly detectable between 245 and 280 km. The Moho reflection PmP is clearly detectable between 90 km and 160 km.

The record for the shot ILA (Fig 3.5) is different from LTS in several ways. The Pg arrival is hardly offset implying that the basement actually outcrops and may only be slightly weathered at the surface. The Pg is correlatable up to about 60 km to the NW and 80 km to the SW. The P* phase is observed here only to the SE. It is however very weak and the arrivals are clear only between 125 km and 150 km. PmP arrivals are detected only to the SE between 90 km and 170 km but less so on the NW. No Pn phase could be detected on this section.

The record for the shot LAI (Fig. 3.6) shows very similar behaviour to ILA. The Pg is detectable up to 70 km in the northern direction but only up to 50 km to the south. Beyond this distance the lower crustal refraction phase P* is detected but only as a weak arrival. They are clearly detected only in the zones 60-90 km to the SE and 70-110 km to NW. The PmP phase could only be correlated between 70 km and 110 km but only to the NW. Refractions from the Moho are not represented on this record.

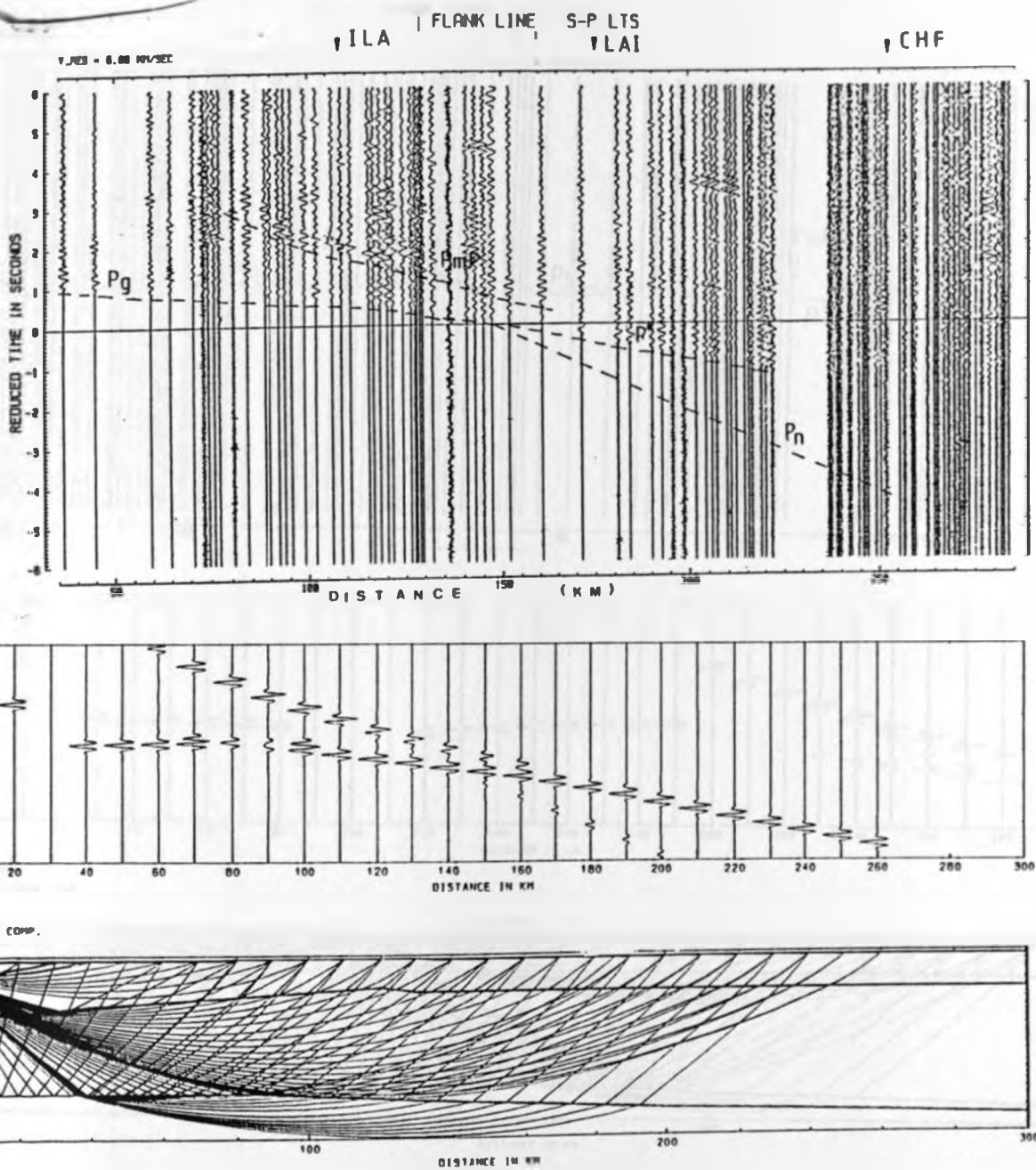


Fig. 3.4: Correlated record section, synthetic seismograms and ray diagrams for S-P LTS.

FLANK LINE S-P ILA

SCALE - 0.00 MPH/SEC

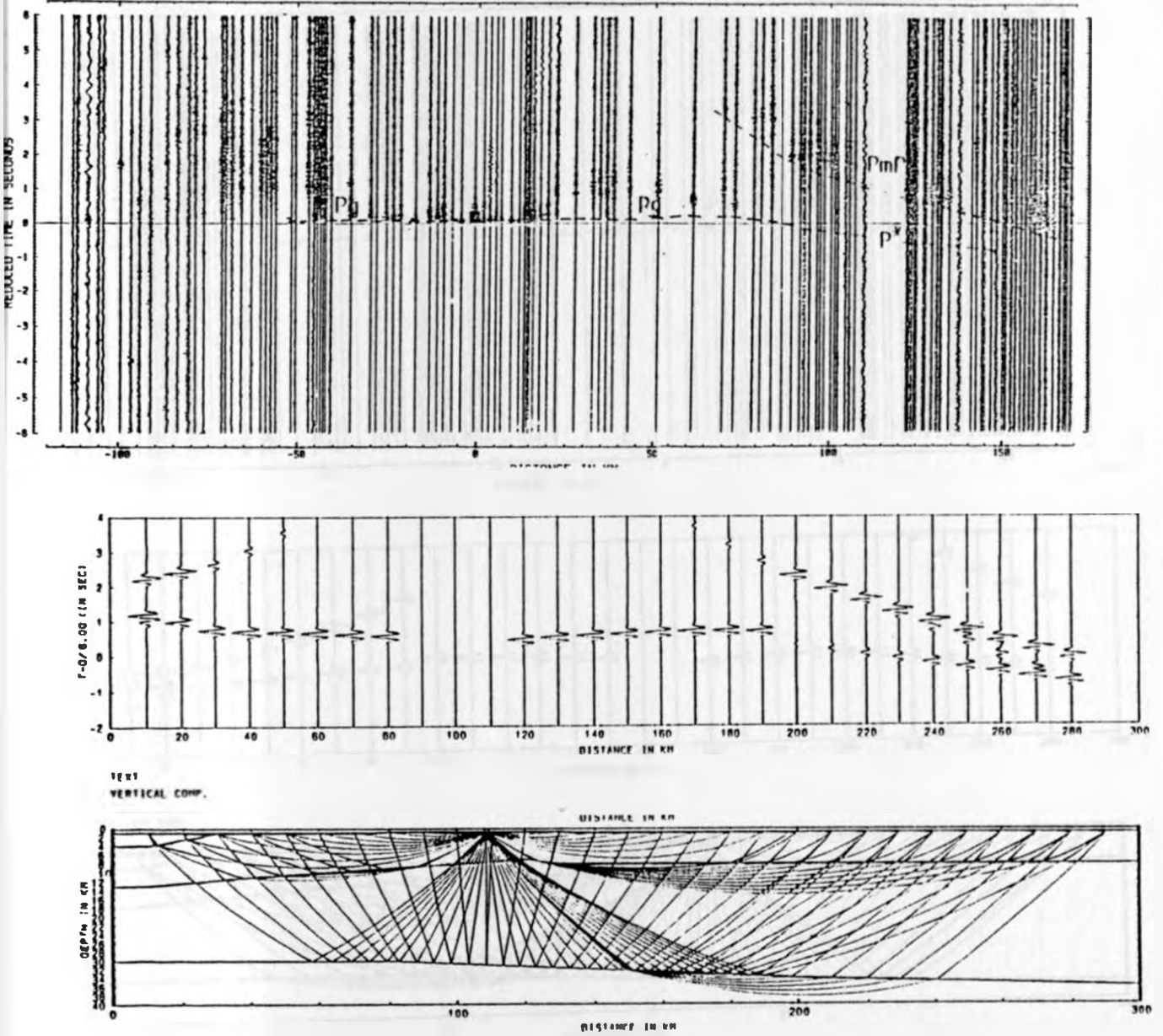


Fig. 3.5: Correlated record sections, synthetic seismograms and ray diagrams for S-P ILA.

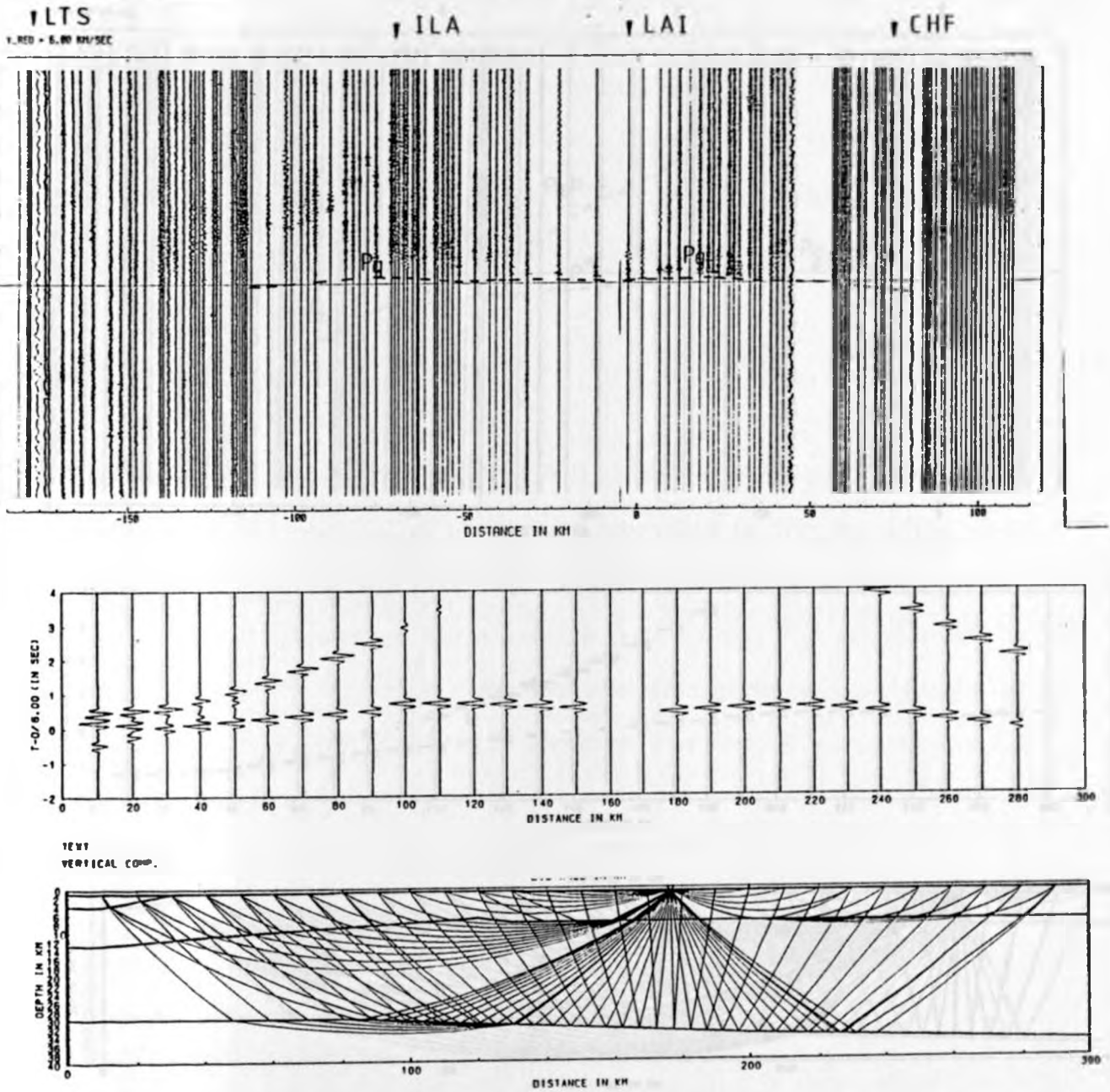


Fig. 3.6: Correlated record section, synthetic seismograms and ray diagram for S-P LAI.

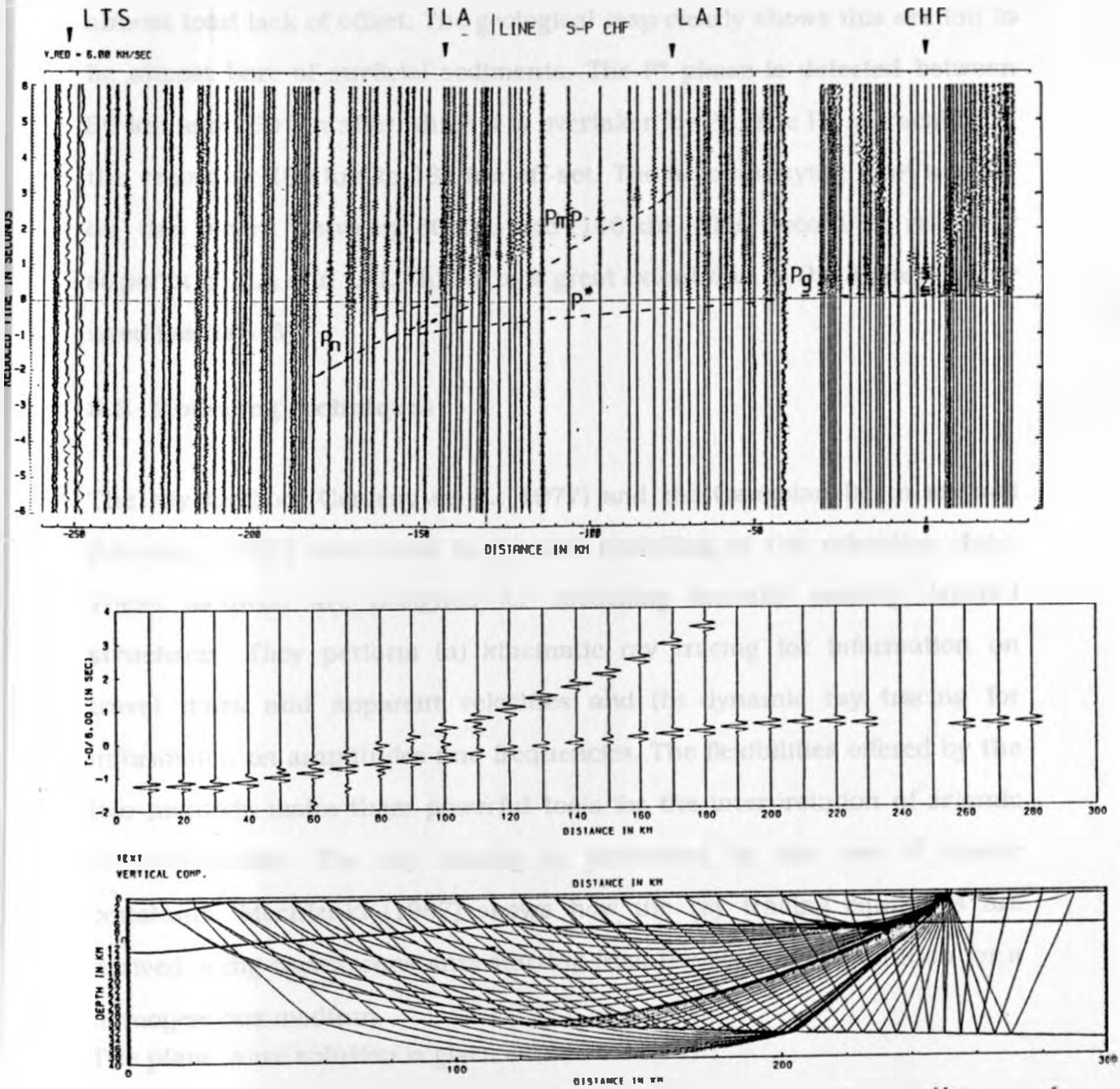


Fig. 3.7: Correlated record section, synthetic seismograms and ray diagrams for S-P CHF.

On the record for the shot CHF (Fig. 3.7), P_g is detectable up to 60 km. That this stretch is directly on an unweathered basement is clear from the almost total lack of offset. The geological map clearly shows this section to be almost bare of surficial sediments. The P^* phase is detected between 50 km and 160 km after which it is overtaken by P_n . The P_n is tracable on the record at 160 km to 185 km off-set. The accompanying P_mP is clear on the record between 60 km and 180 km. This record is relatively superior to ILA and LAI. This is to a great extent due to the higher charge used (see tab. 3).

3.3 Modelling techniques

The ray method (Cerveny et al., 1977) and the Gaussian beam method (Cerveny, 1985) were used in the 2D modelling of the refraction data. These methods are designed for modelling laterally varying, layered structures. They perform (a) kinematic ray tracing for information on travel times and apparent velocities and (b) dynamic ray tracing for information on amplitudes and frequencies. The flexibilities offered by the two methods make them powerful tools for the interpretation of seismic refraction data. The ray tracing is performed by the use of elastic constants. Mochizuki (1987) shows how the ray tracing equations are derived using elastic constants starting from the plane-wave solution for a homogeneous medium.

The plane-wave solution is given as:

$$u_j = A_j \exp(i(k_j x_j - \omega t)) \quad (3.1)$$

u_j : displacement

A_j : amplitude

k_j : wavenumber

w : frequency

x_j spatial coordinates

t : time

The expression is substituted into the equation of motion obtaining:

$$C_{ijkl}k_jk_lA_k = \rho w^2 A_i \quad (3.2)$$

C_{ijkl} : elastic tensor

ρ : density

Equation (3.2) represents an eigenvalue problem and yields three solutions. If only one solution is considered the derivation proceeds as follows:

the polarization vector is normalized by

$$A_i A_i = 1 \quad (3.3)$$

Expressions (3.2) and (3.3) yield:

$$w^2 = (C_{ijkl}/\rho) A_i A_k k_j k_l \quad (3.4)$$

The phase velocity $c = w/k$ ($k^2 = k_j k_j$) is expressed as:

$$c^2 = (C_{ijkl}/\rho) A_i A_k n_j n_l \quad (3.5)$$

$n_j = k_j/k$ is a unit vector parallel to the wavenumber vector.

The eigenvalue equation is solved at each point along the ray path. The ray tracing equations are then obtained as:

$$dX_m/dt = 1/pw(C_{ijklm}A_iA_kk_j) \quad (3.6)$$

$$dK_m/dt = 1/2w(d/dx_m(C_{ijkl}/p)A_iA_kk_jk_l) \quad (3.7)$$

The limitations of the ray method have been discussed by Cerveny (1985).

The three main limitations are identified as follows:

1. The method is applicable only to smooth media in which the characteristic dimensions of inhomogeneities are considerably larger than the prevailing wavelength of the propagating wave.
2. The method fails in the vicinity of some surfaces, lines or points at which the ray field is not regular.
3. The wave amplitudes evaluated by the method are very sensitive to the approximation of the medium and minor details of the model.

The Gaussian beam summation method (Cerveny, 1985) is a generalization of the ray method. The method makes use of the fact that high frequency wave fields propagate mostly along rays. The wavefield is decomposed into contributions corresponding to individual rays. The numerical procedure involves computation of a sufficiently dense system of rays. The rays then correspond to Gaussian beams. Examples demonstrating the applicability of the Gaussian beam approach are given by Cerveny (1985; 1989). It is demonstrated that the method overcomes

singularities associated with the ray method and that it is less sensitive to the approximation of the medium and to minor details of the model.

The method can however not be applied in regions of high velocity gradients (Cerveny, 1989). It also suffers from the disadvantage that several independent elastic constants must be known. The optimum choice of these initial parameters is not fully known.

3.4 Modelling and results

The correlation carried out in section 3.2 led to the identification of the basic parameters which were later used to work out one dimensional velocity depth functions for all the records. The latter provided the starting parameters for the 2D modelling. As this case involves dipping layers, smoothing of the velocities was necessary before performing the ray tracing. The four shot points LTS, ILA, LAI, and CHF were used in the ray tracing. The final model was one for which the computed arrival times agree well with the correlated refraction and reflection arrival times for all the shots. Gradients were also adjusted until a good correspondence between the computed and the observed amplitudes was achieved. The ray diagrams and synthetic seismograms for the end model are shown in Figs. 3.4, 3.5, 3.6 and 3.7.

The model (Fig. 3.8) consists of four layers. The first layer represents the sediments of Lake Turkana. It terminates within 40 km of shot point LTS. The unit is modelled using velocities in the range 3.6 to 4.2 km/s and a maximum thickness of 3 km. The sediments thin out southwards so that

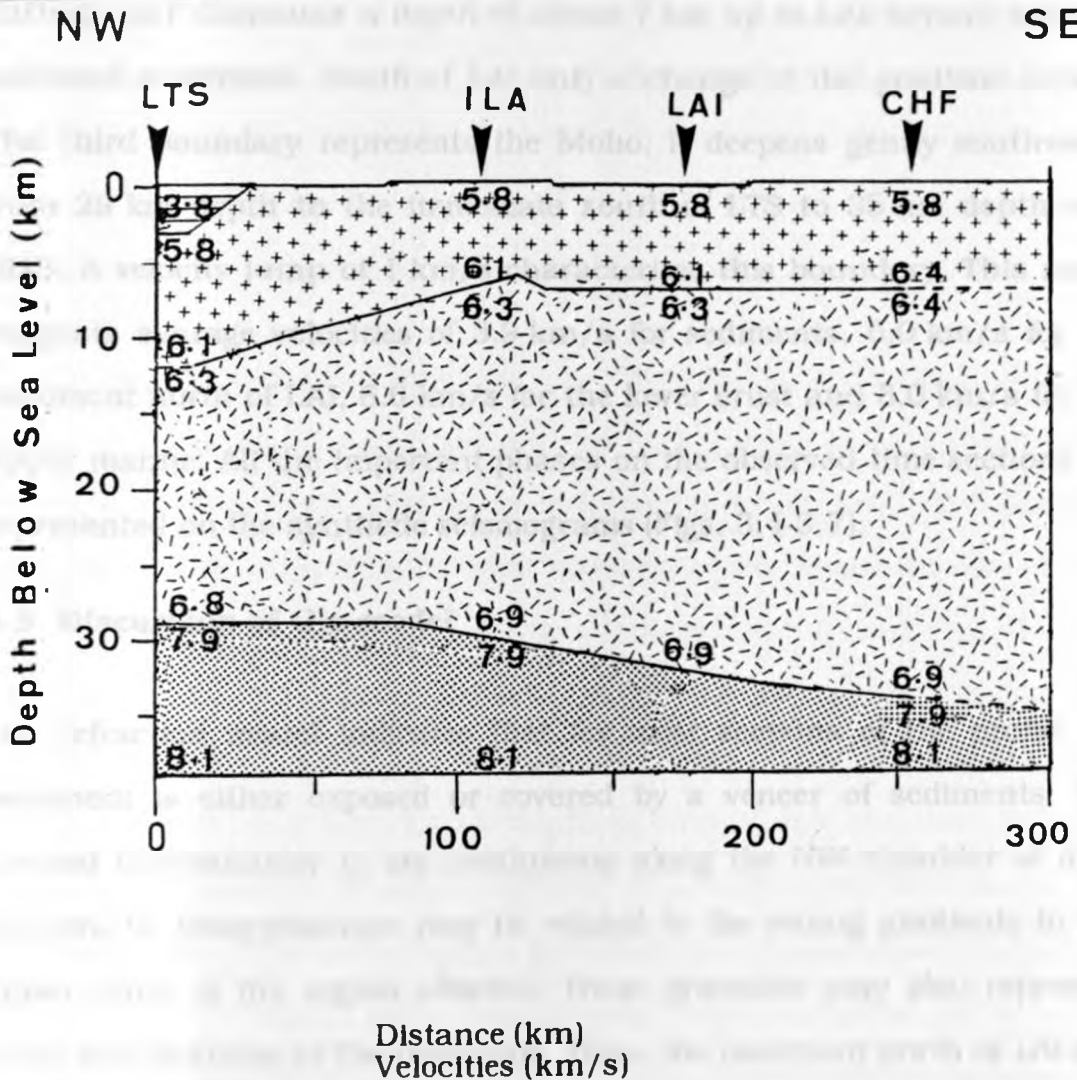


Fig. 3.8: P- wave velocity depth model for KRISP90 Profile E.

the basement layer which occurs at about 3 km below the lake at LTS becomes exposed some 35 km to the south of this shot point. The basement constitutes the upper crust and was modelled using velocities in the range 5.8-6.1 km/s north of LAI but 5.8-6.4 km/s south of LAI.

Stronger basement gradients and relatively higher velocities are indicated for the area south of LAI. The boundary between the lower and the upper crust, commonly referred to as the Conrad Discontinuity, is well defined north of LAI but is not defined to the south. This boundary shallows from about 12 km close to LTS to about 7 km around ILA. Farther south it flattens and maintains a depth of about 7 km up to LAI beyond which it becomes undefined. South of LAI only a change of the gradient occurs. The third boundary represents the Moho. It deepens gently southwards from 29 km depth to the immediate south of LTS to 35 km depth near CHF. A velocity jump of 1 km/s characterizes this boundary. This model suggests average velocities of 3.9 km/s for sediments, 6.0 km/s for the basement north of LAI, 6.6 km/s for the lower crust and 8.0 km/s for the upper mantle. All the important phases on the observed time sections are represented on the synthetic seismograms (Figs. 3.4-3.7).

3.5 Discussion of the model

The refraction model indicates that for most sections of the profile the basement is either exposed or covered by a veneer of sediments. The Conrad Discontinuity is not continuous along the NW shoulder of Anza Graben. Its disappearance may be related to the strong gradients in the upper crust of the region affected. These gradients may also represent some modifications of the basement. Thus, the basement north of LAI can be considered to be a normal granitic upper crust while that to the south as being slightly modified. This anomalous behaviour may be an indicator of the existence of intrusives in this zone. The area between Lalsamis and Chanlers' Falls (Fig. 3.4) is characterized by a scattered occurrence of intrusives. Their ages and structural relationships at depth are however uncertain. There is surface evidence for volcanism in the area during

Tertiary and Quaternary (Key et al., 1987). These evidences are in the form of plateau lavas, craters, cones, and fissures most of which are concentrated in the Laisamis area. The presence of hot springs to the west of Merti (Tole, 1990) close to areas of intrusives and high seismicity (Pointing et al., 1985) suggests that the zone is active and weak. The epicentres in this active zone which is centred on Laisamis are considered to be associated with young volcanics in Marsabit, Laisamis and Nyambeni areas (Hackman et al., 1990). The interpretation of gravity and magnetic data (chapters 4, 5 and 6) also favours the existence of intrusives at shallow depths within the basement.

The present model also indicates that there is no appreciable thinning associated with the western shoulder of Anza Graben. Using the existing data alone, it is not possible to estimate how far west the thinning associated with Anza Graben may have extended. However, the results obtained from the modelling of the shoulder tend to suggest that the profile lies inside the area expected to have been affected by thinning. The gradual shallowing of the Moho in the direction of Lake Turkana is also of special interest. The facts that a depth of only 20 km has been reported under Lake Turkana (KRISP Working Party, 1991) along the Kenya Rift axis and a depth of 29 km only a short distance off the axis to the east indicate that the Moho rises rather steeply NW-wards under the lake. The shallowing of the Moho from 29 km to 21 km occur within a distance of only 100 km.

It is of interest to compare the present results of modelling with those obtained by KRISP Working Party (1991) covering various profiles. A recent paper (KRISP Working Party, 1991) summarises the results. A parallel modelling of the profile to the NW of Anza yields a slightly different

picture from the present model. The uppermost sedimentary layer has a velocity of 3.8 km/s and is about 3 km thick under Lake Turkana. The model suggests the existence of a lens of velocity of 6.4 km/s within the upper crust at a depth of 3.0-4.0 km to the south-eastern end of the profile. It is attributed to intrusive activities in the region. The model favours a continuous but undulating Conrad discontinuity at an average depth of 10 km. The Moho is characterized by a tentative transitional layer having a thickness of 3-5 km. As in the present model, the latter indicates an increase in crustal velocity to the SE of Laisamis. It also favours a gradually shallowing Moho towards Lake Turkana.

Both models assume that the rays travelled in a vertical plane encompassing all the shot points and recording stations. In reality some of the recording stations were offset and the shot points were not all along one straight line. Furthermore, the inhomogeneities in the subsurface may have been such that not all the rays travelled in vertical planes. The existence of 3D effects in the data can therefore not be ruled out. The effect of offset is likely to affect near shot stations more than distant ones. The velocities used in the model for shallow sections may thus be lower than they actually are. The possibility of rays undergoing lateral displacements at depth will have the effect of speeding them up so that in the deeper sections velocities higher than they actually are may have been used along the assumed path. Other 3D features of local extent will have the effect of speeding up or delaying arrivals on a limited number of receivers. Such features also cause local amplitude variations. Localized variations in arrival times and amplitudes possibly emanating from 3D effects were noticeable in the present data.

When tied up with results of other KRISP90 profiles, the present results lead to several observations about the structure of the area in comparison and in relation to the now relatively well known Kenya Rift Valley structure.

Firstly, the sub-Moho velocities east of the Kenya Rift Valley are normal. This is also indicated in the results of an E-W KRISP90 profile which terminates at CHF (Fig. 3.3) (KRISP Working Party, 1991). No appreciable thinning is indicated to the east of the Kenya Rift Valley. This is in direct contrast with the main Kenya Rift Valley axis where abnormal upper mantle velocities of 7.5-7.7 km/s are recorded and a thinning of the crust to about 20 km. occur (KRISP Working Party, 1991). East of the Kenya Rift Valley, profiles D and E (Fig. 3.3) indicate Moho depths of 33-35 km and 29-35 km respectively.

Secondly, although the crust tends to be anomalous on sections of the NW Anza profile, the deviations from the normal velocities are small and are not comparable with those in the Kenya Rift Valley where crustal velocities of 6.8 km/s have been observed.

Thirdly, the abrupt rise of the Moho both from the south and southeast in the Lake Turkana area suggests that the arching of the Moho constitutes an oval or dome-like structure. This correlates well with the regional Bouguer gravity field computed using 5th degree polynomial (Akamaluk, 1989) which reveals an elliptical anomaly trending NNE-SSW centred on Lake Turkana. The gravity anomaly has been attributed to a low density structural lineament in the upper mantle. The refraction and gravity data are thus in good agreement (see chapter 5).

Fourthly, should the NW Anza profile lie within the expected zone of thinning as indications suggest, it will imply that no appreciable thinning is to be expected under Anza Graben itself. This does not however necessarily imply that the original thinning was not appreciable. Bosworth (1989) proposes the lack of appreciable thinned crust under Anza Graben but attributes it to the cooling of the asthenosphere from the time of rifting. This is in line with views expressed in works by Girdler et al. (1969) and Oxburgh (1978) that thinning of the lithosphere is primarily a thermal phenomenon with lithospheric material converted to hotter, less dense asthenosphere material. This implies that with a long time allowed for cooling, the process will tend to reverse.

Fifthly, it is clear from the modelling that crustal variations occur along the NW shoulder of Anza Graben. This is in agreement with the geological mapping which indicates that volcanism and intrusive activities in the area are related to lineaments running NE-SW and hence perpendicular to the shoulder (Hackman et al., 1990).

3.6 Conclusions

The analysis and interpretation of the seismic data has revealed a few aspects of the structure of Anza Graben which are useful for supplementing other data in the geological synthesis. Despite the limitations of signal strength and lack of uniform ground coverage the data have proved to be useful especially for delineating shallow structures both in the Graben and at the shoulders.

The reflection data outline the geometry of the shallow sections well and reveal the existence of faults within and along sections of the Graben

boundaries. Gentle folding has also been detected on some of the records. This folding within the Graben is estimated to be of early Tertiary (Hackman et al., 1990).

Refraction data on the other hand have clearly delineated the shallow and the deep structure over the western shoulder of the Graben. Most important they reveal higher velocities in sections of the crust indicating that at the shoulder properties are not uniform along the strike. Further, the results suggest no appreciable thinning of the crust in the region. The average thickness of the crust in the area is indicated to be about 35 km. Normal sub-Moho velocities of 8.0 km/s are also indicated. The good correlation between observed and computed amplitudes indicates that the gradients used are satisfactory.

However, due to the restriction of the data several informations which are equally important for the understanding of the structure in the region remain unanswered. A refraction profile across the Graben, if shot, should yield accurate data on the basement depth within the Graben. Extension of profile E (Fig. 3.4) into the area between Garissa and Lamu will help to delineate the crustal structure along the entire length of the western shoulder of the Graben.

CHAPTER FOUR

REDUCTION, ANALYSIS AND QUALITATIVE INTERPRETATIONS OF GRAVITY DATA

Gravity data plays the central role in this study. The data were collected by different groups and at different times. These disparities are attributed to the vastness of the area, the history of the geophysical activities in the region and the poor road infrastructure. It therefore follows that the quality and distribution of the data are not uniform. In general, the quality varied with the equipment used and the control maps available at the time, while the distribution and density of the data depended on the objectives of the various groups involved. Before setting out to use the data, an evaluation of their suitability for the study had to be made. It was during this stage that the necessity of doing more work in the area to fill in the gaps and also to check some of the old data became apparent. An evaluation of the existing data sets was considered critical as the accuracy and reliability of the subsequent analysis and interpretation depend strongly on the quality of the data used.

The gravity data used in this study were collected by Leicester University (L1, L2, L4 - 793 stations), British Petroleum (BP- 733 stations), Chevron Oil Company (CH- 685 stations), Burma Oil (BO-151 stations) and Geoprosco/British Petroleum (GBP- 141 stations)(see Tab. 4.1a). These data are contained in a catalogue (Swain and Khan, 1977) which also

Group Cell	L1	L2	L4	CH	BP	BO	GBP	NEW	TOTAL
A	-	86	-	-	-	-	-	-	86
B	-	8	20	266	-	-	-	-	294
C	-	14	105	19	-	-	-	-	138
D	-	12	23	-	6	140	-	-	181
E	-	73	-	-	-	-	-	-	73
F	-	6	-	362	-	-	-	-	368
G	-	32	16	16	-	-	-	169	233
H	-	4	6	-	301	11	-	8	330
I	39	64	5	-	-	-	-	-	108
J	-	38	1	22	-	-	-	-	61
K	-	21	2	-	44	-	-	57	124
L	-	-	-	-	217	-	-	-	217
M	90	27	2	-	-	-	-	-	119
N	31	43	-	-	-	-	-	-	74
O	16	9	-	-	57	-	45	-	127
P	-	-	-	-	108	-	96	-	204
TOTAL	176	437	180	685	733	151	141	234	2737

	37°	38°	39°	40°	41°	
	A	B	C	D		3°
	E	F	G	H		2°
	I	J	K	L		1°
	M	N	O	P		0°
						-1°

Table 4.1 a) Sources of the gravity data
 b) Distribution by latitude/
 longitude cells.

includes measurements from other parts of Kenya. In addition, 234 gravity stations (NEW) were established in the area by the author in 1987. The distribution of gravity data in the study area arranged in one degree squares is shown in Table. 4.1b. The majority of the data covering the Graben were collected by Chevron Oil Company. In the following chapters, the unit mGal is used instead of SI units (m/s^2). 1 mGal corresponds to $10^{-5} m/s^2$.

4.1 Data sources and quality

4.1.1 Leicester University Data

The Leicester data were collected over the periods 1965-69, 1972-73 and 1975. The accuracy of the observed data (after tidal and drift corrections) for the first survey is estimated at 0.4 mGal while the later ones at 0.2 mGal. The stations for first survey were established on 1:100,000 maps. The limitation of these maps was that they included very little detail and hence created difficulties in position determination. In order to reduce the inaccuracies, airphoto print laydowns were made and car odometers used to control the distances. On the basis of Root Mean Square (RMS) errors found on repositioning of 60 stations, on new maps the maximum position inaccuracy is 500 m. Heights for the first survey were measured using the modified leap frog method (Searle, 1969). Later work was done using the normal leap frog. After establishment of the new control points, the 1975 team was able to directly measure the error in some of the 1972-73 data. An RMS error of 2.8 m was indicated using 23 stations located in NE Kenya. Nearly all Leicester stations are confined to roads and motorable tracks.

4.1.2 British Petroleum Data

The British Petroleum data were collected by Geoprosco and Geophysical Services International (GSI). Three surveys were carried out in the years 1955, 1956 and 1960. The 1955 survey done by Geoprosco consisted of 1600 km of widely spaced traverses to the east of 35.5°E and south of the equator. The second survey consisted of 1000 km of traverses in the north of the area of the first survey. The Worden gravity meter No. 212 was used with observation accuracy of 0.1 mGal being estimated. Elevations were determined using theodolites and related to the survey of Kenya datum through bench marks along the southern edge of the area. A height accuracy of 0.3 m was estimated. Positioning was done using aerial mosaics, magnetic compasses and 1:500,000 maps. An accuracy of 30 m was estimated between stations. The absolute accuracy was later found to be in the region of 500 m (Swain and Khan, 1977). The third survey conducted by GSI continued earlier work to 2°N , most stations being located between 40°E and the Kenya-Somalia border. The station spacing was 0.8 km. The Worden meter No. 491 with an estimated accuracy of 0.07 mGal was used. The survey employed tachometry with horizontal control provided by Astrofix and Tellurometer stations. The average vertical misclosure was 1.1 m (max 5.4 m). The stations are estimated to be within 200 m of their true positions. Using the IGSN71 value of the Mombasa base station, a value of 4.44 mGal was subtracted to make them compatible with Overseas Gravity Survey's (OGS) primary gravity net. Good agreement with the Leicester data (within 0.3 mGal) have been noted where traverses coincide.

4.1.3 Chevron data

The Chevron data were collected by Photogravity Co. Inc. in 1974 as an extension of an earlier survey. The work was done by helicopter and covered $38^{\circ}10'E$ to $39^{\circ}E$ and $1^{\circ}N$ to $2^{\circ}30'N$. The lines were run north-south spaced 8 km apart and measurements were made at a spacing of 3 km. Two Worden gravity meters were used. The stations were tied to a 170-station-network which was in turn connected to the Mombasa airport base. Station positions were measured using an electrical system employing transponders. They are considered to be accurate to 10 m. Paulin altimeters in the single base configuration were used to measure the elevations. Later checks indicated an error of 18 m in elevation and usually positive. Reoccupation of 6 Chevron base stations during the Leicester surveys indicated that they were 4.7 ± 1.0 mGal higher than those of Leicester and Burmah surveys. A correction of -4.7 mGal had therefore to be made to the data. Comparison of Chevron heights data with the Leicester ones along the east edge shows differences of 16 ± 6.3 m. Between 2.0° and $2.5^{\circ}N$ the difference is 11.0 ± 1.00 m. A comparison of the Bouguer anomalies for the two overlapping Leicester and Chevron profiles near Wajir road indicated a correction of -25 ± 10 m to the Chevron data.

4.1.4 Burmah data

Burmah surveys were carried out in 1975 by Hunting Surveys Ltd. Stations at intervals of 0.5 km were established along tracks. Two La Coste Romberg gravity meters were used. The survey was tied to the Nairobi base using a light aircraft. The Bouguer anomalies were computed using a density of 2300 kg/m^3 . A correction of 3.48 mGal had to be

subtracted from the observed gravity values which were deduced from the Bouguer anomalies in order to make them compatible with OGS datum. Elevations were measured by precision levelling around closed loops. The maximum closure error is estimated at 0.3 m. Track positions were established first on aerial photos then transferred to 1:100,000 maps. Distances along the tracks were measured using the odometer.

4.1.5 Data from survey during the present study

The survey by the author was carried out in the months of October and November 1987. The main objectives were to attempt to reduce the gaps in the data and to check the accuracy of the old data. A LaCoste Romberg gravity meter (No. G16) was used. Stations were established along roads, motorable tracks and cutlines. An average spacing of 2.5 km was maintained. Two pairs of barometers were employed under the Leap Frog method. Position control was attained by use of 1:50,000 maps, car odometers and by use of intersection of cutlines. A total of 234 stations were established mainly between latitudes 0° to 2°N and longitudes 39°E to 41°E. The accuracy of the gravity measurements was 0.02 mGal. Where height network joined, a correction for the closing error was done manually as the circuits were simple. The closing error was about 5 m for a circuit of about 300 km. The error was distributed within the traverses. The standard error (s.e.) for unadjusted observations was estimated using the formula by Clark (1944). The s.e. for unadjusted observations of unit weight is given by:

$$s.e = \sqrt{\sum(w_i g_i^2)/p} \quad (4.1)$$

W_i : weighting factor

Q_i : corrections to height differences

n : number of traverses

p : number of closed loops

The s.e. at any point in the network can be estimated by multiplying this by m where m is the number of measured height differences from the nearest control point. Multiplying the s.e. by the average number of height differences per traverse gives an average s.e. per station. This estimation is done on the basis that random errors are the main quantities affecting the quality of the survey. A value of 2 m is estimated from the present survey. This contributes to an error of 0.6 mGal to the Bouguer anomaly. Some of the traverses were however not closed. In such cases the estimation of the error was difficult to ascertain. However, such traverses were short and any errors occurring remained within the traverses. The presence of several intersections of well controlled oil exploration cutlines and better basemaps (1:50,000) helped to improve the position control. It is estimated to be accurate to 50 m. The overall accuracy of the Bouguer anomaly values taking into account uncertainties in elevation is estimated at 0.5 mGal. In the present survey a number of old stations particularly those located at road intersections were reoccupied. The agreement with the observed data in these cases are within 1 mGal.

4.2 Computation of the Bouguer anomalies

All previously existing data which had already been reduced are referred to IGSN71. In order to ensure uniformity, the data from the present survey have been reduced to the same format and in the same way. The theoretical sea level gravity of the latitude θ were calculated using the formula:

$$r = 9780318.5(1 + 0.005278895 \sin^2\theta + 0.000023462 \sin^4\theta) \quad (4.2)$$

This formula is an approximation of the 1967 gravity formula (Geodetic Reference System, 1967) given by Torge (1989) as:

$$r = 9780318(1 + 0.00532024 \sin^2\theta + 0.000,0059 \sin^2 2\theta) \quad (4.3)$$

The approximation formula (4.2) is accurate to 0.004 mGal. Free air anomalies (FAA) were then calculated by continuing upward the sea level theoretical gravity to the station height (h), using the free air correction factor and subtracting this from the observed gravity:

$$FAA = g_o - (r - 0.3086h) \quad (\text{in mGal}) \quad (4.4)$$

Simple Bouguer anomalies (SBA) which are used in this study were calculated by subtracting from the FAA the effect of the infinite horizontal slab of thickness equal to the station height (h) and density 2.67 g/cm^3

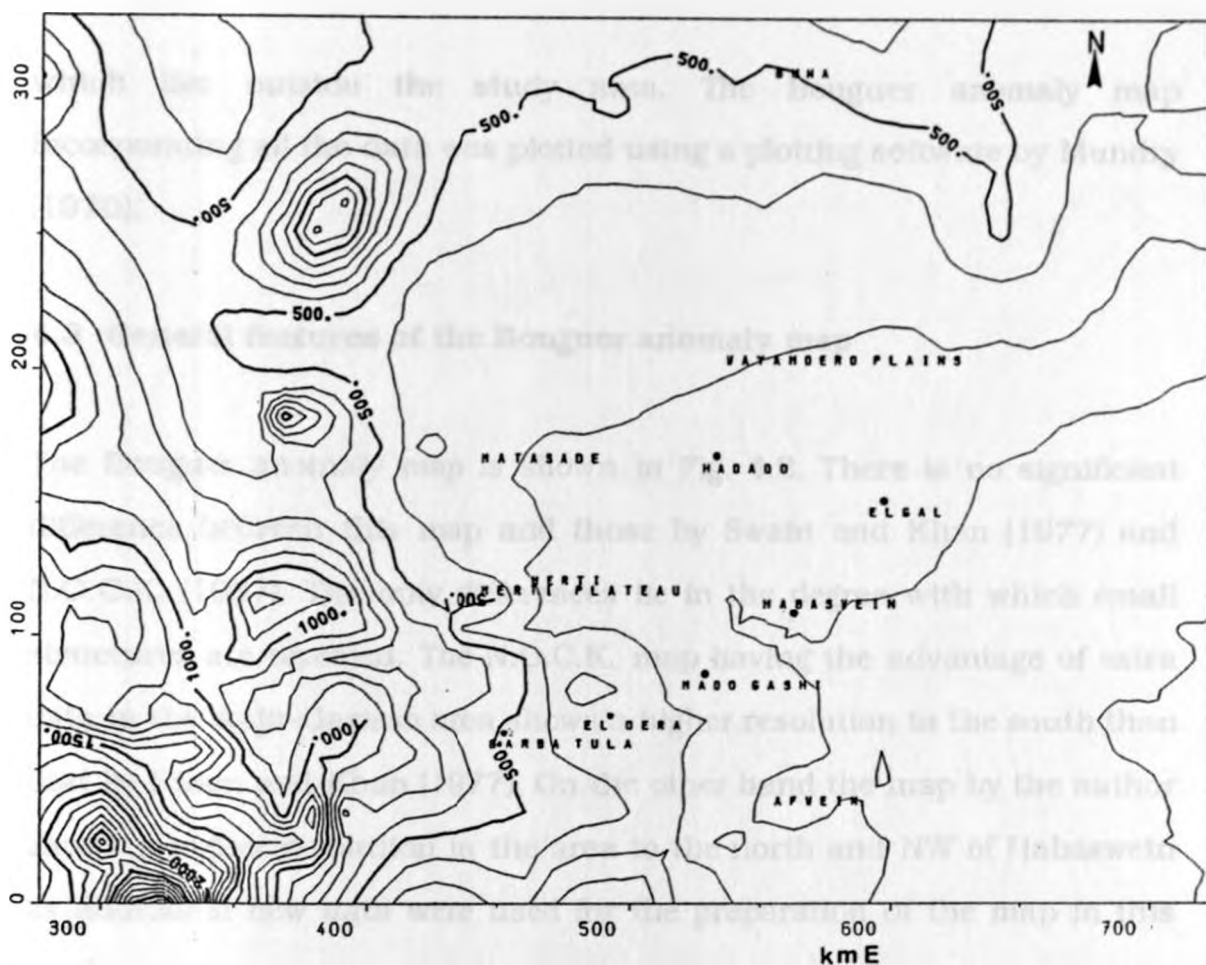


Fig. 4.1: Elevation map of the study area and the surrounding areas, contour interv: 100 m.

(in this case expressed in cgs units). The expression is:

$$\text{S.B.A} = \text{FAA} - 2\pi\text{G}\rho h = \text{FAA} - 0.1119h \text{ (in mGal)} \quad (4.5)$$

Complete Bouguer anomalies (CBA) were also computed but were not much different from the SBA as height changes involved are not large. In the area surveyed by the author, the average height of the stations is 242.0 m. The area is generally flat as can be seen from the elevation map (Fig. 4.1). The terrain effect is thus small and can be ignored. The strong gradients at the SW corner of map represents the slope of Mt. Kenya

which lies outside the study area. The Bouguer anomaly map incorporating all the data was plotted using a plotting software by Mundry (1970).

4.3 General features of the Bouguer anomaly map

The Bouguer anomaly map is shown in Fig. 4.2. There is no significant difference between this map and those by Swain and Khan (1977) and N.O.C.K. (1987). The only differences lie in the degree with which small structures are revealed. The N.O.C.K. map having the advantage of extra data in the Wajir-Garissa area shows a higher resolution in the south than that by Swain and Khan (1977). On the other hand the map by the author shows a higher resolution in the area to the north and NW of Habaswein as additional new data were used for the preparation of the map in this section.

The map clearly delineates the Anza structure. A change of the anomaly trend occurs halfway along the structure changing from $N50^{\circ}W$ in the south to $N30^{\circ}W$ in the north. The eastern shoulder is characterized by a very steep gradient reaching 0.005 mGal/m , indicating the presence of a very large displacement of the rocks along this zone. Estimates of fault throw were carried out by extrapolating the flat regional anomaly surface to the fault and ignoring the positive anomaly at the shoulder. A value of more than 7 km is obtained assuming density contrasts of -400 kg/m^3 . The western margin is not well defined due to the presence of interfering structures joining on to the main structure from the southwest. The average gradient is gentle being about 0.0005 mGal/m . To the south,

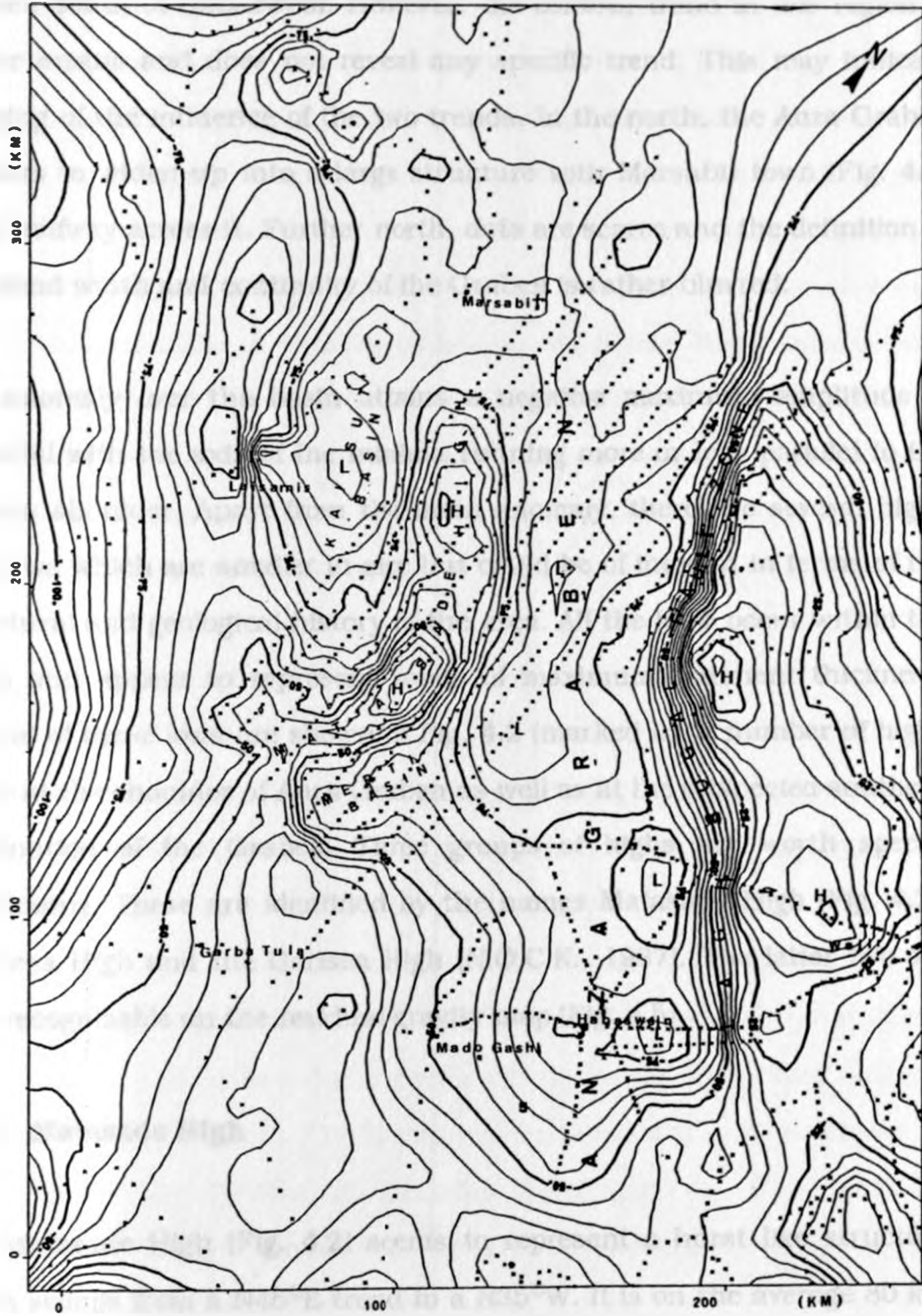


Fig. 4.2: The Bouguer anomaly map of the Anza Graben (on a local grid; contour interv. 5 mGal).

there is a steepening of the gradient suggesting that a high bounds the Graben south of Habaswein. However, the contour trend in this region is rather erratic and does not reveal any specific trend. This may indicate merging of the influence of the two trends. In the north, the Anza Graben appears to widen up into a large structure with Marsabit town (Fig. 4.2) lying halfway across it. Further north, data are scarce and the definition of the trend width and continuity of the Graben is rather blurred.

The anomaly over the basin attains a negative maximum amplitude of 80 mGal with the axis of the minima running more or less parallel to the Graben shoulder. Apart from the main anomaly, there are several highs and lows which are smaller in size but could be of interest in terms of the structural and geological history of the area. All the lows occur within the basin and appear to represent zones of maximum sediment thickness. Several of these lows are shown in Fig. 4.2 (marked L). A number of highs occur at the shoulder of Anza Graben as well as at the suspected southern termination of the Graben. Three groups of highs are worth special mentioning. These are identified by the names Matasade High (Fig. 4.2), Mochesa High and the Garissa High (N.O.C.K., 1987). The latter two are best recognizable on the residual gravity map (Fig. 4.5).

4.3.1 Matasade High

The Matasade High (Fig. 4.2) seems to represent a horst like structure which swings from a $N45^{\circ}E$ trend to a $N35^{\circ}W$. It is on the average 80 km long and about 30 km wide. It is flanked on both sides by basins one of which is here referred to as the Merti Basin and the other has been referred to as the Kaisut Basin (N.O.C.K., 1987). Merti Basin has a NE-SW

trend. This basin seems to terminate on the basement rocks to the north of Garba Tula (Fig. 4.2). However, the gravity data are too sparse to help to define the termination. The Kaisut Basin on the other hand, has a NW-SE trend parallel to the Anza trend, but shielded off Anza by the Matasade High. The geological map indicates the presence of rocks of the Jurassic age over this high occurring as inliers. Several pockets of intrusive rocks occur along this structure especially at its southern end. The outcrop of the intrusives show a good correlation in trend with the Matasade High. Although the existence of the horst like structure can be attributed to block faulting or uplift, its curved outline is unusual. The Matasade structure appears to deepen towards the Anza Graben as can be inferred from the broadening of the anomaly signature and decrease in gradient.

4.3.2 Mochesa High

The Mochesa High is located to the east of the southern section of Anza Graben some 100 km south of Wajir and to the north of Hagadera. (Fig. 4.5). It is more than 100 km long (extending into Somalia) and about 50 km wide. Along the same axis in the region between Garissa and Habaswein, a number of gravity highs occur. The Bouguer anomaly over Anza closes just before the appearance of these highs. They are best defined on the N.O.C.K. (1987) map where they form a crescent-like arc around the Anza Graben. In fact, the highs define a rather weak but noticeable ENE-WSW trend. This weak trend is probably marks the SW continuation of the Mochesa High.

4.3.3 Garissa High

The Garissa High (Fig. 4.5) trends NW-SE. Its pronounced section is about 80 km long and 40 km wide. The structure appears to deepen SE-wards. It conforms to the Anzan trend and is separated from the Anza Graben by structures associated with Mochesa High. It is displaced SW-wards by about 100 km from the axis of the Anza Graben.

4.4 Techniques used in the data analysis

A given potential field data can be treated by the so called automatic methods so as to present the same field in different forms or at different height levels. Transformations of this type are usually aimed at presenting the data in a form suitable for further interpretation. Depending on the structural set up of the area in question, such transformations may make structures of interest more readily discernible and can help to resolve structures having overlapping anomalies. The relevance of the automatic methods can be appreciated from works done on potential field anomalies worldwide (Hinze, 1985). In order to carry out the transformations, it is most convenient to operate in the frequency domain. The Fourier Transformation Technique (Cooley et al., 1967) makes these computations easily attainable. The filtering operations are done in the frequency domain by multiplication of the transfer function $\Psi(k_x, k_y)$ with the Fourier transform $F(k_x, k_y)$ of a given data $f(x, y)$ (Black and Scollar, 1969; Degro, 1986). The final results are transformed back into the space domain by inverse Fourier transform:

$$\theta(x, y) = \mathcal{F}^{-1}(\Psi(k_x, k_y) \cdot F(k_x, k_y))(x, y) \quad (4.6)$$

In order to perform this transformation, the data have first to be interpolated on to a square grid. In doing this, care must be taken in the selection of the sampling interval and in the choice of the total number of data points per side of the square grid. The choice of the sampling interval depends on the wavelength of interest. The shortest wavelength present is twice the data interval while the longest is the data length. Wavelengths shorter than twice the sampling interval unfortunately still interfere and are in fact added to longer wavelengths, a process referred to as aliasing (Kanasewich, 1975). In order to minimize these effects, it is necessary to remove wavelengths below those corresponding to Nyquist frequency by use of an alias filter before sampling or to select a sampling interval which includes all important short wavelengths present in the data (Swain, 1979). A general rule to choose a sampling interval is to use half the measured data spacing (Swain, 1979). The total number of data points per side is limited by the storage capacity of the computer used. A further restriction on the data points per side is imposed by the requirement of the F.F.T routines that the data must be on a grid of the form $2^N \times 2^M$ where N and M are integers (Kertz, 1970; Marple, 1987).

In performing an F.F.T. computation of a time series, it is assumed that the data repeat themselves periodically. Since the real data in the case of potential field computations are finite, discontinuities at the end of the data sets affect the results. The effects are seen in the form of large amplitude, short-wavelength components and their aliases. These edge effects can be minimized either by surrounding the data with zeros by use of a suitable taper or by expanding the data at the margins (Black and Scollar, 1969). In this study an expansion of 20% was made at the margins and more data added in the margins before performing the

transformation. Once the data have been appropriately presented, the next task is to select suitable filters that would bring out the desirable features in the data.

The techniques used in the analysis of the gravity data are polynomial fitting, wavelength filtering and vertical gradient determination. These techniques are discussed at length in text books of geophysics (e.g. Telford et al., 1990; Robinson and Coruh, 1988) and by Degro (1986).

4.4.1 Polynomial fitting

In polynomial fitting (Telford et al., 1990), as applied to 2D data, a given gravity field is approximated by a 2D polynomial. A least square operation is then carried out to find out the best fitting surface. The closeness of the fit depends on the order of the polynomial used. Lower order polynomials approximate the regional field. With increasing order, the polynomial begins to mimic the observed field surface. As fitting is generally for the purpose of the regional surface determination, polynomials of order greater than two are rarely used (Telford et al., 1990). The weakness of this technique of regional separation is that the fitting aims at obtaining the average surface. Thus, it is bound to yield positive and negative residuals which may not be justifiable in reality. In this study only polynomials of up to the second order were used.

4.4.2 Wavelength filtering

It is usually of great value to separate an observed gravity or magnetic field into regional and residual parts. This enables anomalies associated

with various depths below the surface to be identified in a qualitative way. It also helps to distinguish between large and small structures in a given study area. Wavelength filtering involves associating certain components of the anomaly with certain wavelengths by harmonic analysis. It is assumed that the observed field is made up of:

1. long wavelength components the sources of which are deep-seated and of regional character and;
2. short wavelength components the sources of which are shallow and of local character.

These assumptions have their weaknesses, mainly due to the principle of equivalence and the integrated effect. Some of the long wavelength terms in the harmonics are related to local anomalies. Further, in the case of magnetic anomalies the assumptions hardly hold due to erratic and large amplitude characteristics. It is therefore important to note that perfect separation is not possible (Robinson and Coruh, 1988). The positive contribution of the technique, however, generally outweighs the limitations.

In the separation of regional and residual fields a certain cut-off wavelength λ_c is identified. Anomalies for which $\lambda \leq \lambda_c$ are suppressed or isolated are referred to as residuals. The choice of a cut-off wavelength must be related to the depth of the disturbing body. The approximate relationship between the maximum depth z_s of a causative body and the half width $b^{1/2}$ of the anomaly is given by Jung (1961) as:

$$z_s = 0.5 b^{1/2} \text{ (2 dimensional)} \quad (4.7)$$

$$z_s = 0.652 b_{1/2}^{1/2} \text{ (3 dimensional)} \quad (4.8)$$

An approximate formula for the selection of the boundary wavelength is given as:

$$\lambda_c = 3z_s \text{ (3 dimensional)} \quad (4.9)$$

This can also be obtained from the anomaly map as:

$$\lambda_c = 2b_{1/2} \text{ or } \lambda_c = 2b \quad (4.10)$$

The filtering characteristics of an ideal low or high pass filter depend on the cut-off wavelength λ_c . In practice, it is noted that the sharp cut-off associated with ideal filter results in a lot of high frequency noise on the inverse transformation. It is therefore practical to fit a function to the filter which ensures a smooth cut-off. In the program package used (INTERP, see appendix) this was accomplished by use of a Gaussian function of the form:

$$G(k) = e^{-k^2/a} \quad (4.11)$$

where a is given as:

$$b_{1/2} = 2(2 \ln a)^{1/2} \quad (4.12)$$

The transfer function used is of the form:

$$\Psi_1(k) = \begin{cases} 1 & |k| \leq |k_c| \\ e^{-\frac{(k-k_c)^2}{a}} & \text{for } |k| \geq |k_c| \end{cases} \quad (4.13)$$

for low pass filtering and

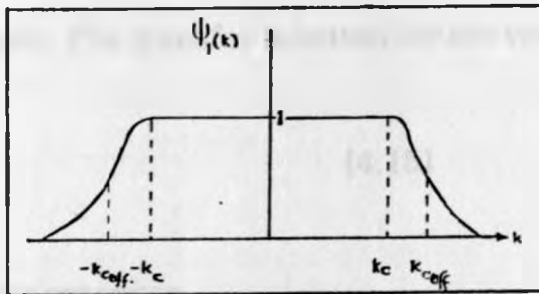
$$\Psi_2(k) = \begin{cases} e^{-\frac{(k-k_c)^2}{a}} & \text{for } |k| \leq |k_c| \\ 1 & \text{for } |k| \geq |k_c| \end{cases} \quad (4.14)$$

for high pass filtering

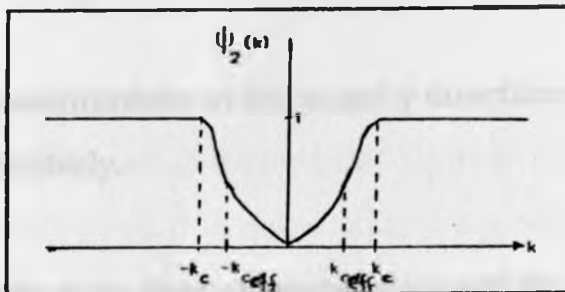
k : wavenumber

k_c : cut-off wavenumber.

In 2D these filters have the appearance shown in Fig. 4.3a and Fig. 4.3b respectively.



a



b

Fig. 4.3a and b: Filter characteristics of frequency domain low pass and high pass filters (after, Degro, 1986)

4.4.3 Vertical gradient of gravity

The vertical gradient of gravity is simply the change of gravity with the height (Degro, 1986). Although a constant gradient is usually assumed in the free air correction, the gradient varies from place to place depending on the densities of the subsurface masses at the point. Variations of up to 10% of the normal value have been reported (Tsuboi, 1983). The vertical gradient can be calculated from measurements taken at two different levels or mathematically by the use of an appropriate operator. The vertical gradient is useful in structural interpretation because the filter enhances near surface features. Of greater significance to this study however is that such data are on a degree of derivative most realistically comparable with the vertical component of the magnetic field or the field reduced to the pole. The transfer function for the vertical gradient is:

$$\Psi(k_r) = k_r \quad (4.15)$$

$\Psi(k_r)$: filter response

k_r : wavenumber

$$k_r^2 = k_x^2 + k_y^2 \quad (4.16)$$

k_x & k_y : wavenumbers in the x and y directions respectively.

This filter has high pass filter characteristics and for this reason has to be tapered to minimize power leakages from the higher to the lower frequency portions of the spectrum. It is also possible to compute the gradient at

continued levels in the cases where some of the surface features may have been deemed to have undesirable effects. The expression then becomes:

$$\Psi_{z_0}(k_r) = e^{k_r z_0} k_r \quad (4.17)$$

The filter characteristics of this filter are shown in Fig. 4.4.

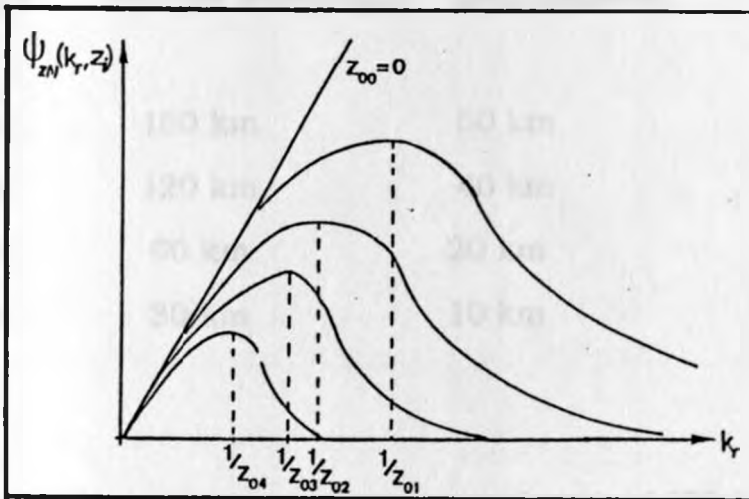


Fig. 4.4: Filter characteristics of a vertical gradient filter (from Degro, 1986).

4.5 Filtered gravity maps

The residual map obtained after fitting the trend surface of the second degree is shown in Fig. 4.5. A total of 2737 gravity stations were used over an area of 222,000 km². The map depicts negative residuals over the basin but positive ones on the shoulders. The ENE-WSW trend which is only weakly defined on the original maps is clearly defined here.

Wavelength filtered maps are presented in Fig. 4.6 a-d. One of the main objectives of the wavelength filtering was to attempt to relate the anomalies to their depths of origin and to identify persistent trends at various wavelengths of cut-off. The estimations of the depths of origin were made by using the 3D approximation equations given in section 4.4.2. The wavelengths selected in this study are as follows:

wavelength	effective wavelength	depth(approx)
190 km	180 km	60 km
130 km	120 km	40 km
65 km	60 km	20 km
32 km	30 km	10 km

The regional anomaly with an effective wavelength of 180 km (Fig. 4.6a) is characterized by broad circular to elliptical anomalies the origin of which can be attributed to depths of about 60 km. A trend very close to NNW-SSE is defined which could be related to the Kenya dome. Except for the trend, the features of the Graben including the Graben margins are hardly recognizable.

Fig. 4.6b is a case with an effective wavelength of 120 km. In this case the Anza trend becomes better defined. The crescent-like positive peaks marking the shoulders and southern termination of Anza Graben become clearly defined. At this wavelength, anomalies associated with small features are almost absent.

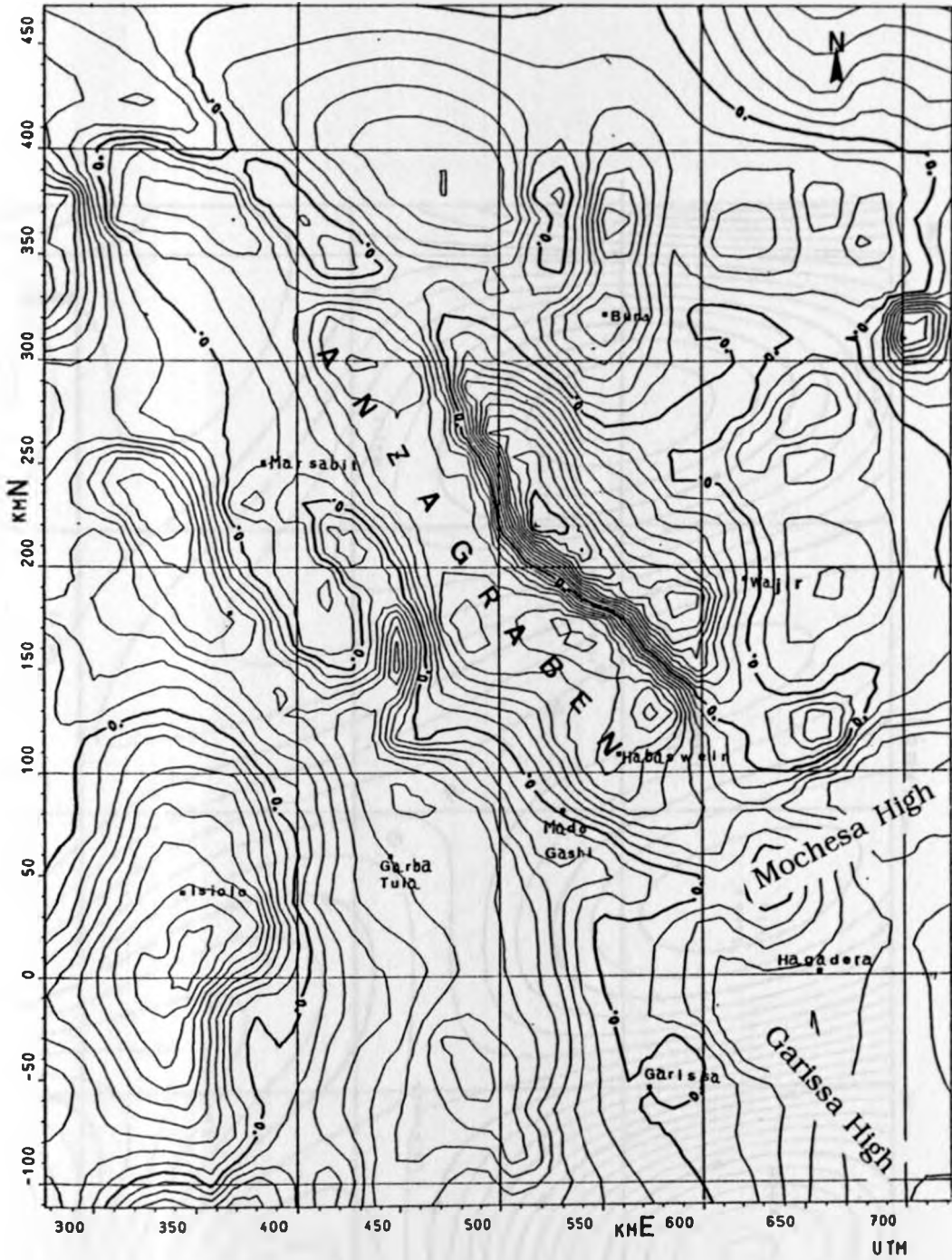


Fig. 4.5: The residual gravity field using a polynomial of the second degree.

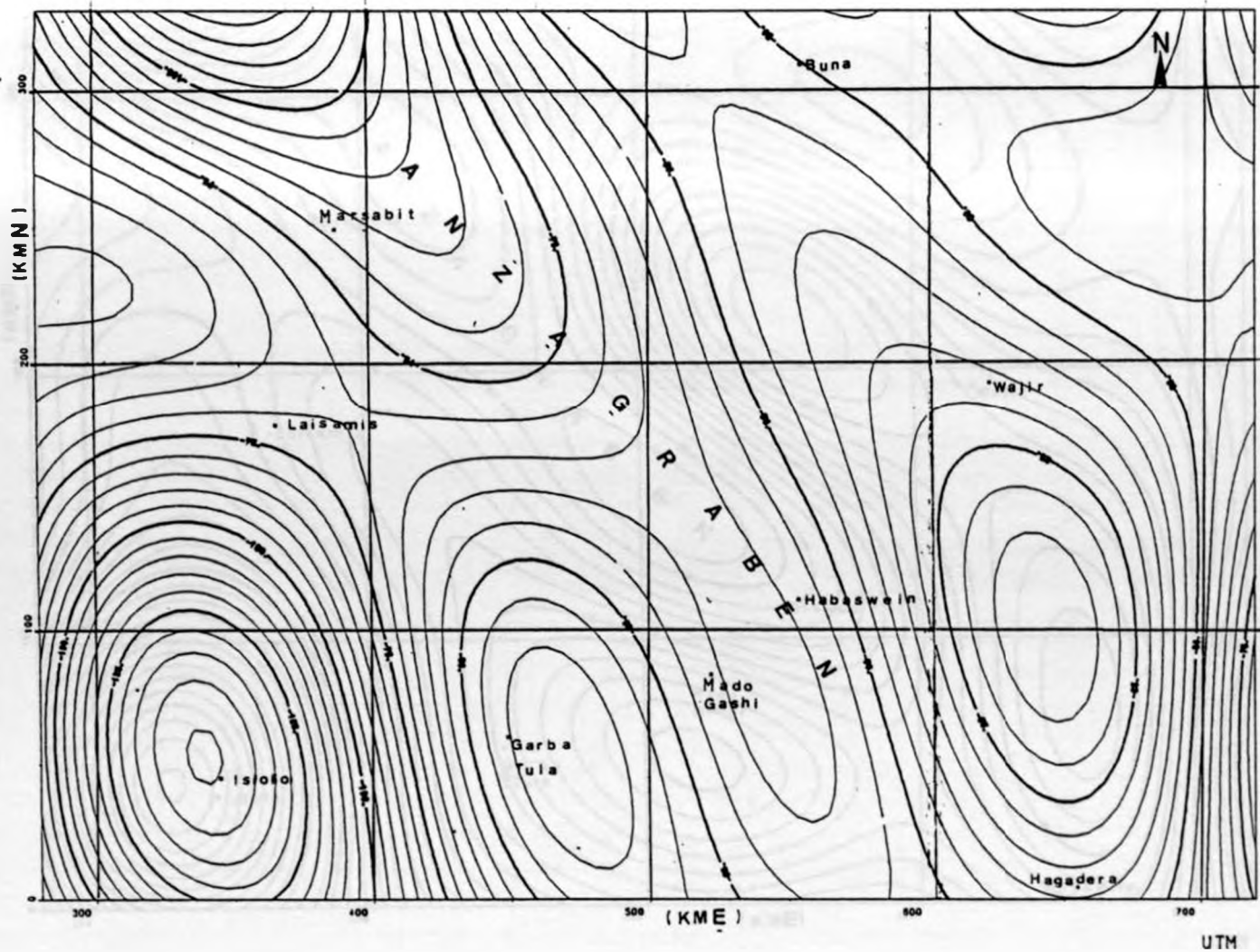


Fig. 4.6a: Regional gravity field with wavelength of 190 km ; effective cut-off wavelength of 180 km.

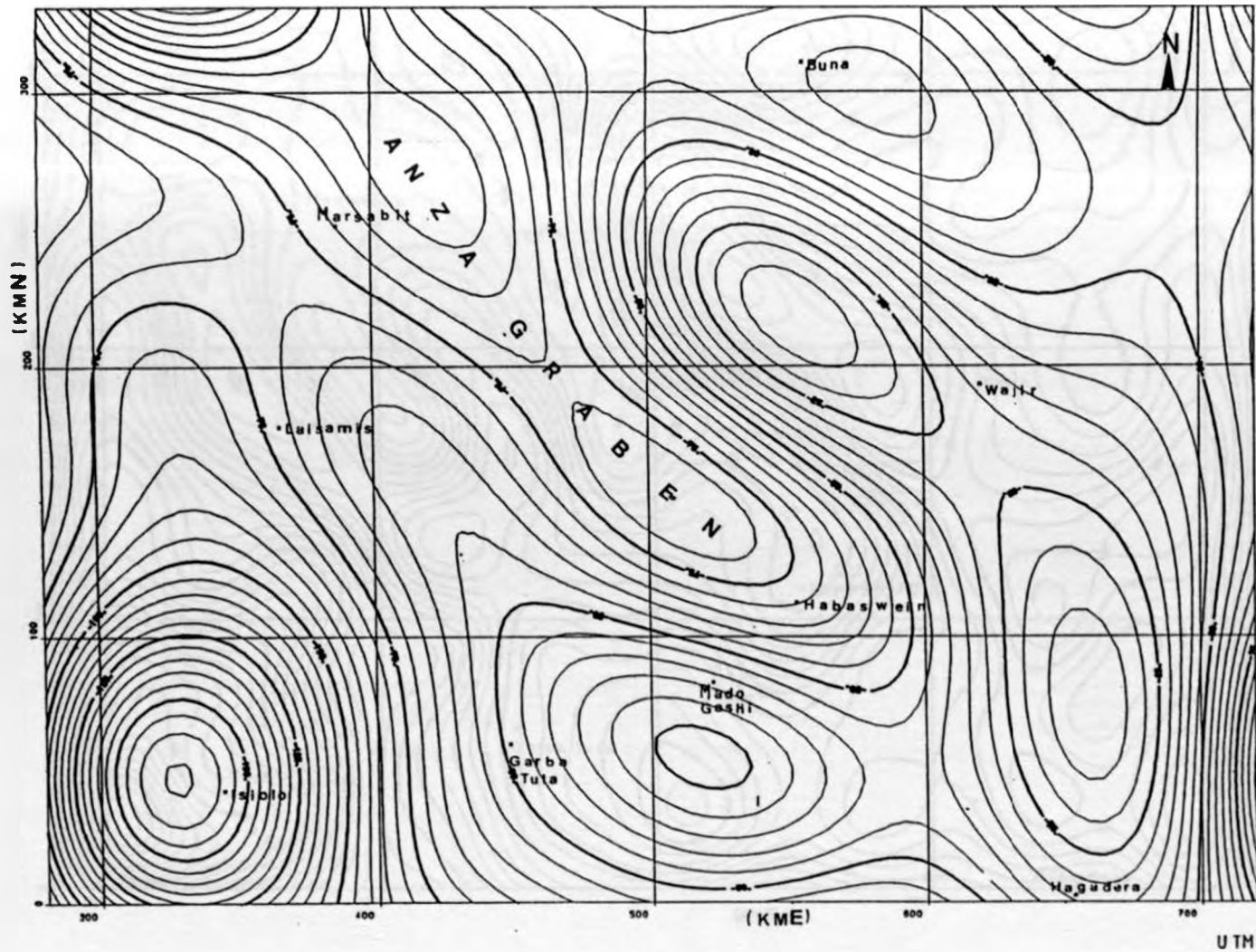


Fig. 4.6b: Regional gravity field with wavelength of 130 km.; effective cut-off wavelength of 120 km.

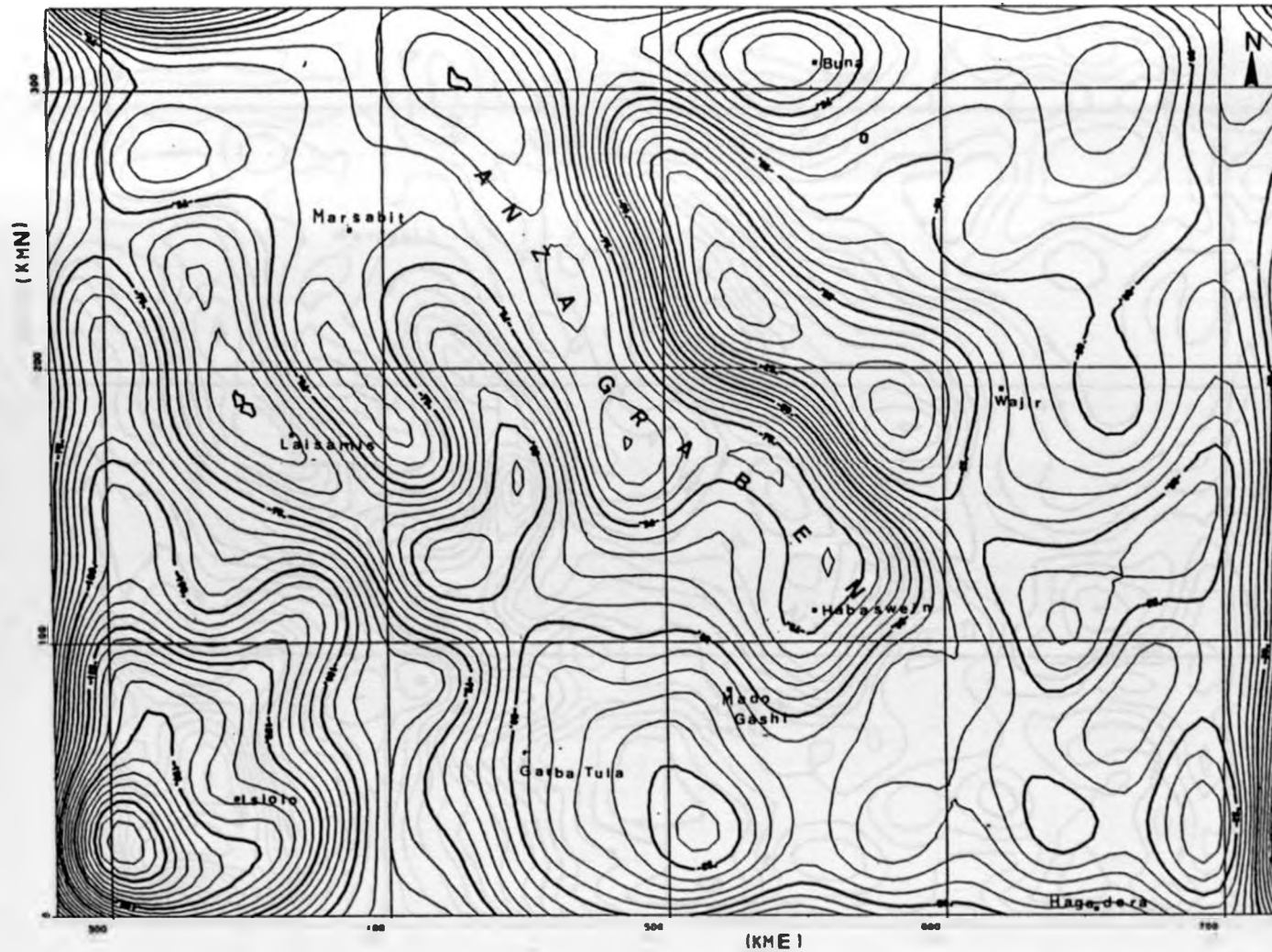


Fig. 4.6c: Regional gravity field with wavelength of 65 km; effective cut-off wavelength of 60 km.

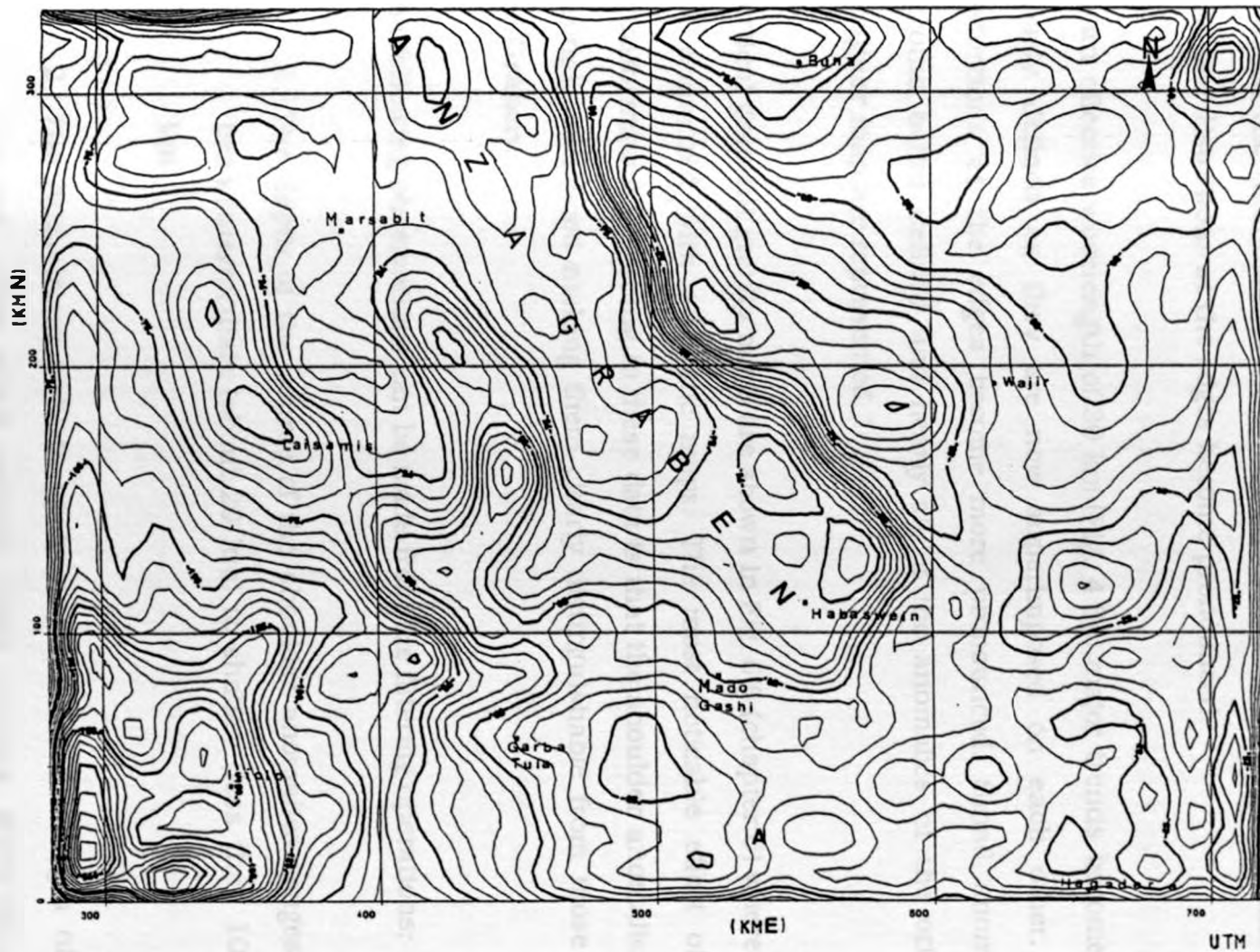


Fig. 4.6d: Regional gravity field with wavelength of 32 km; effective cut-off wavelength of 30 km.

At an effective wavelength of 60 km (Fig. 4.6c), most features of the original Bouguer map (Fig. 4.2) appear. The shoulder anomalies are better defined but the trends less clear. At the southern termination of Anza Graben, the NEE-SWW trend is best defined. It is noticeable on this map that the distortions at the edges become pronounced.

At an effective wavelength of 30 km (Fig. 4.6d) major trends become less clearly defined as they are now superimposed on each other. The distortions at the edges become more pronounced. Small anomalies become better defined and nearly all of the anomalies of the original Bouguer map are represented.

Vertical gradient gravity maps are shown in Fig. 6.6 (chapter 6) where they are compared with magnetic maps. The most noticeable effect of the transformation according to these data is that the shoulder anomalies are strongly enhanced making them clearly distinguishable from those over the Graben.

The following observations can be made from the filtering operations:

1. The depth of the source of the shoulder anomalies ranges from intermediate (about 20 km) to shallow (less than 10 km).
2. The Anza trend persists up to an effective wavelength of 180 km, after which another trend running WNW-ESE probably related to the Kenya dome dominates.

CHAPTER 3

3. The ENE-WSW trend occurring to the southern termination of Anza Graben disappears after an effective wavelength of 60 km suggesting that the trend has shallow to intermediate depths.

4. Well defined structural trends persist even with long cut-off wavelengths probably indicating possibilities of sub-Moho trends.

CHAPTER FIVE

MODELLING OF THE GRAVITY DATA

5.1 Choice between 2D and 3D modelling

The basis for defining a potential field source as two dimensional (2D) is that its strike length must be at least three times its width (Jung, 1961). The properties of the causative body are in this case assumed to be constant along the strike. All sections taken across the structure are expected to share the same parameters such as density, geometry etc. Situations where properties in the strike direction vary call for 3D models. In 3D, the model representation is complicated and requires somewhat laborious definition of body parameters. The computations require considerably more computer time than for 2D cases. It is also not easy to 'see' what the model is doing unless several presentation formats for the results are available, such as in the form of contour maps and cross sections in various directions. These problems have been to a great extent overcome during the recent years so that efficient data representation for 3D modelling of basins is easily attainable. The choice between 2D and 3D is therefore not so much dictated by the limitations of the parameterization problems or computer time as by the type of structure under investigation. Algorithms for 3D model representation are now available. Examples of these are those by Götze and Lahmeyer (1988) and Richardson and MacInnes (1989). The main advantages offered by 3D modelling are:

1. The influence of bodies from adjacent areas on a given profile can be detected and accounted for.

2. The technique limits the number of possibilities of free modelling.

3. The addition of a third dimension provides a more realistic representation of the subsurface structure.

Through representation by 3D of basins previously modelled by 2D, new and interesting results have been reported in a number of areas (e.g. Götze, 1984; Wagener and Götze, 1989). 3D gravity modelling has however been applied in a very limited way to the rifts in Kenya. Most of the models attempted so far have been 2D. It is however evident from both the geological and geophysical data that the Kenyan rifts show appreciable variations along their strikes (Baker et al., 1972; KRISP Working Party, 1991). In the case of Anza Graben the variations along the strike are indicated by the following:

1. The Graben is not straight but shows a curving half way along its strike.

2. The borehole data indicate variations in depths to specific horizon both perpendicular to and along the strike.

3. The properties of the rocks constituting the flanks of the Graben are not uniform along the strike.
4. There are small basins such as Kaisut and Merti which join the Graben at distinct positions.

On the basis of the above points, the modelling of the gravity data was performed using 3D.

5.2 Techniques used in the modelling

5.2.1 The method of the plane distribution of mass

The basement depth in the case of a sedimentary basin can be estimated by assuming a plane distribution of mass. Tsuboi (1983) showed that if two layers of densities β_1 and β_2 are separated by an interface of undulation of amplitude $h(x)$, the mass distribution may be approximated by a plane distribution of mass $(\beta_1 - \beta_2) h(x)$ condensed on the average depth of the interface as shown in Fig. 5.1. It is in this way possible to obtain the observed gravity effect.

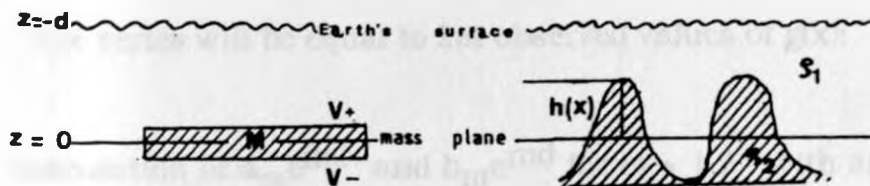


Fig. 5.1: The representation of the mass plane at depth d and the undulation of the interface (after Tsuboi, 1983).

The underground mass distribution is obtained by the evaluation of the series:

$$M(x) = 1/2\pi G \sum (a_m e^{md} \cos mx + b_m e^{md} \sin mx) \quad (5.1)$$

at $2m$ equidistant points

$M(x)$: total mass

G : universal gravitational constant

a_m, b_m : Fourier coefficients

m : a positive integer

d : depth of the interface

The important steps are as follows:

1. analysis of a given field $g(x)$ into a Fourier series by determination of $2m$ coefficients a_m and b_m such that the series will be equal to $2m$ observed values of $g(x)$;
2. calculation of $a_m e^{md}$ and $b_m e^{md}$ for $m = 1, 2, \dots$ with an assumed depth d ;
3. synthesis of the series:

$$M(x) = 1/2\pi G \sum (a_m e^{md} \cos mx + b_m e^{md} \sin mx) \quad (5.2)$$

to find $M(x)$.

The next step is to find the depth of the mass. This can be based on geological information or estimated mathematically. In the latter case we take a surface distribution of gravity to be given by:

$$g(x) = B_m \cos mx \quad (5.3)$$

The plane mass at depth d that will produce this gravity distribution is:

$$M(x) = (B_m e^{md} \cos mx) / 2\pi G \quad (5.4)$$

Now if this mass is due to an undulation, the amplitude of the undulation of the interface will be given by:

$$h(x) = (B_m e^{md} \cos mx c_m) / 2\pi G (\beta_2 - \beta_1) \quad (5.5)$$

It is obvious that $h \leq d$

or

$$\ln B_m / (2\pi G (\beta_2 - \beta_1) + md) \leq \ln d \quad (5.6)$$

Thus, d is limited depending on $\beta_2 - \beta_1$ and B_m . Once the limiting value of d is determined, the undulations can be drawn. These calculations

assume a simple case of two layers with homogeneous density distribution. The extension of the equations to 2D data where the plane becomes a surface is also straight forward.

5.2.2 The 3D interactive modelling technique

3D interactive modelling was done using a program package based on an algorithm developed by Götze (1984, appendix). The elementary body of the model is taken as a polyhedron with plane surfaces. The attraction of such a homogeneous polyhedron at a station P is based on the potential relation.

$$U(P) = G \iiint 1/R \, dm \quad (5.6)$$

U(P): gravitational potential at P

R: distance between P and dm

G: gravitational constant

$$dm = \beta dv = \beta dx dy dz \quad (5.7)$$

The derivative of the potential with respect to the vertical axis (z component) leads to the gravity effect:

$$g_z(P) = G\beta \iiint d/dz (1/R) \, dV \quad (5.8)$$

By use of the Green equation, the volume Integral above can be expressed as a surface integral, thus:

$$g_z(P) = G \beta \iint \cos(n, z) (1/R) dS \quad (5.9)$$

As shown in Fig. 5.2 the cosine term determines the direction of the surface element dS with relation to the Cartesian coordinate system.

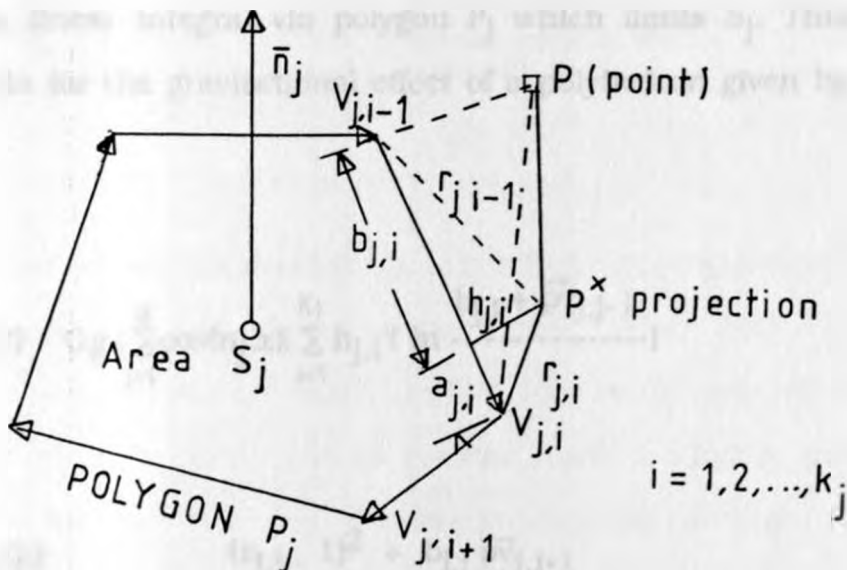


Fig. 5.2: Presentation of an arbitrarily structured polygon (after Götze and Lahmeyer, 1988).

Since $\cos(n_j, z)$ is constant for any polyhedron surface S_j ($j = 1, \dots, m$, the number of surfaces), the attraction effect of its individual surfaces S_j can

be expressed as:

$$g_z(P) = G\beta \sum_{j=1}^m (\cos(n_{j,z}) \iint_{S_j} (1/R) dS_j) \quad (5.10)$$

In practice, a transformation of the coordinate system is required such that the simplest possible expression is maintained in the evaluation of the line integral. Thus, a surface oriented system x',y',z' is used. The x' -axis runs parallel to the surface normals and y is orthogonal to the x' - and z' - axes (see Fig.5.2). The next step is the conversion of the surface integral into a linear integral via polygon P_j which limits S_j . This leads to the formula for the gravitational effect of a polyhedron given by Götze (1984) as:

$$g_z(P) = G\beta \left(\sum_{j=1}^m \cos(n_{j,z}) \left(\sum_{i=1}^{K_j} h_{j,i} \left(\ln \frac{b_{j,i} + \bar{p}v_{j,j-1}}{(r_{j,i} - 1)^2 + b_{j,i} \bar{p}v_{j,i-1}} \right) + \frac{\bar{p}p_j^*}{h_{j,i}} \left(\arctan \frac{(r_{j,i} - 1)^2 + b_{j,i} \bar{p}v_{j,i-1}}{|pp_j^*| |h_{j,i}|} \right) - \frac{\arctan(r_{j,i}^2 + a_{j,i} \bar{p}v_{j,i})}{|pp_j^*| |h_{j,i}|} \right) + 2\pi \bar{p}p_j^* \delta \epsilon \right) \quad (5.11)$$

$$\delta = \begin{cases} 0 \\ 1 \end{cases}, \text{ if } p^* \begin{cases} \notin S_j \\ \in S_j \end{cases}, \quad \epsilon = \text{factor}$$

where the various parameters are as shown in Fig. 5.3. δ assumes a value of zero or one depending on whether P^* lies on the polygon or not.

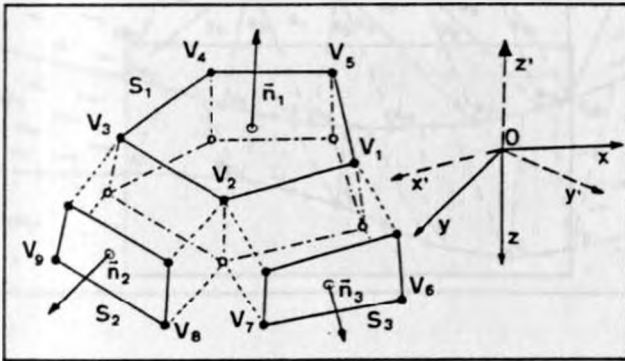


Fig. 5.3: Presentation of polyeder surface with parameters of equation (5.11) (after Götze, 1984).

It is the above expression (5.11) which is programmed (Götze and Lahmeyer, 1988). In setting up the model, certain basic elements of the data structure must be clearly defined. The model selected is divided into vertical sections referred to as planes. These are not to be mistaken for profiles as they are not necessarily passing through actual gravity stations. All the elements of the data structure are to be found in these planes. The planes are the carriers of the geometrical and material parameters. The main elements of the data structures are planes, lines, layer boundaries and triangular planes (Fig. 5.4). The planes are vertical and should be placed parallel but not necessarily equidistant from each other. In the planes, the substructure is marked by a series of interconnected points v_i . The series of vertices comprise a line. A closed

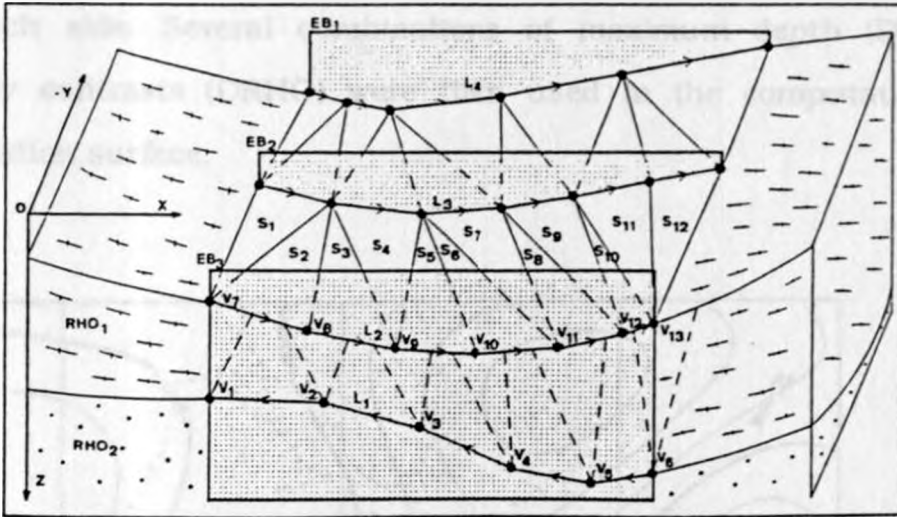


Fig. 5.4: Presentation of a simple two layer substructure (after Götze and Lahmeyer, 1988).

line (polygon section) marks the intersection of a layer boundary with the respective plane. There may be opened or closed lines as well as lines which have only one point. Layer boundaries stabilize the 3D structure by encompassing lines of neighbouring planes which are separated by identical density values. Each layer boundary consists of triangles with v_1 as the vertices. The model is completely defined with an input of a set of point coordinates and material parameters. This 3D modelling approach does not eliminate the ambiguities caused by the equivalence principle.

5.3 Inversion of the gravity data by the method of plane distribution of mass

The main purpose of inverting the gravity data by the method of plane distribution of mass (Tsuboi, 1983) was to determine the most ideal start model for the 3D interactive modelling. The 2D gravity data were first

interpolated on to a 60 * 80 grid of spacing 5.3 km and widened by 8 units on each side. Several combinations of maximum depth (Dmax) and density contrasts (DRHO) were then used in the computation of the undulation surface.

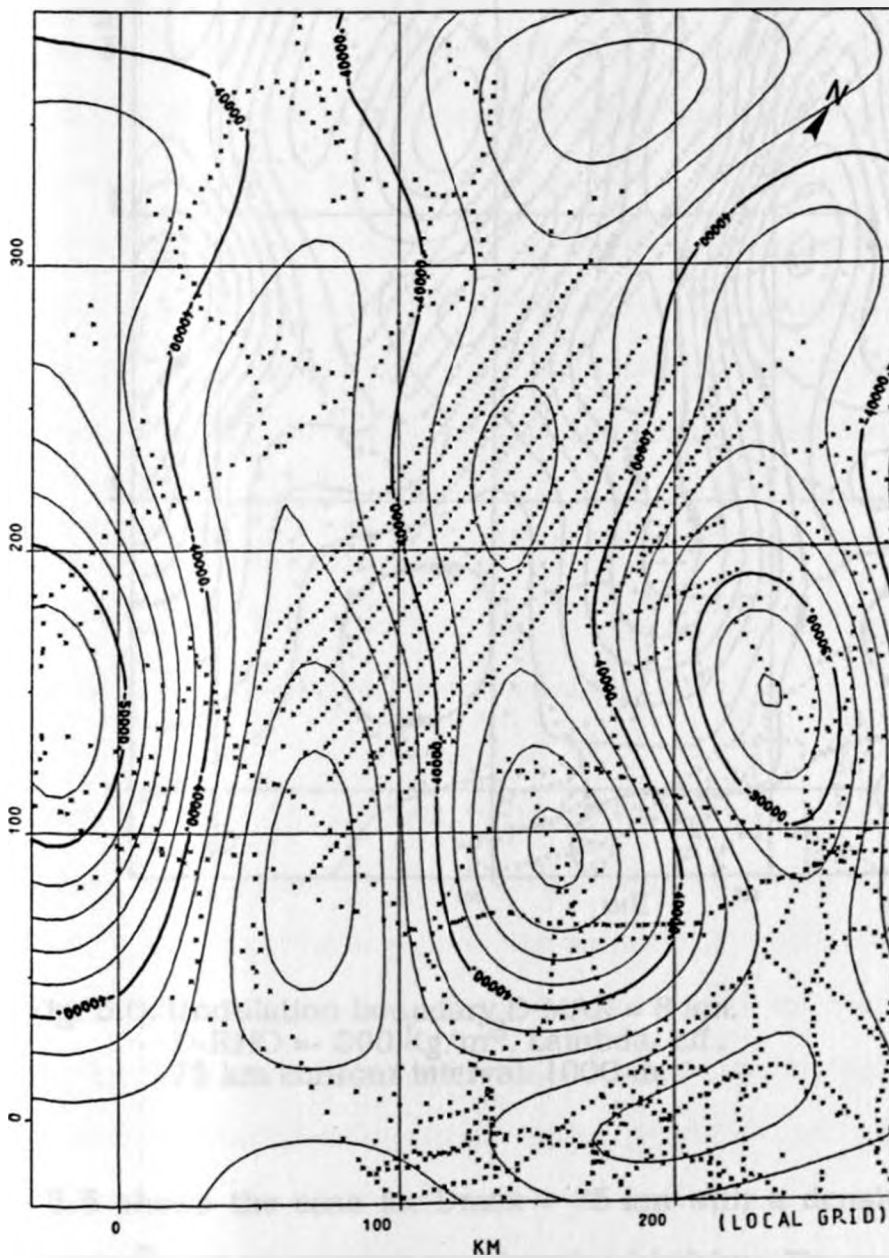


Fig. 5.5: Undulation boundary, D-MAX = 35 km,
D-RHO = -350 kg/m^3 . Lambda-eff., 140 km
contour interval 2000 m.

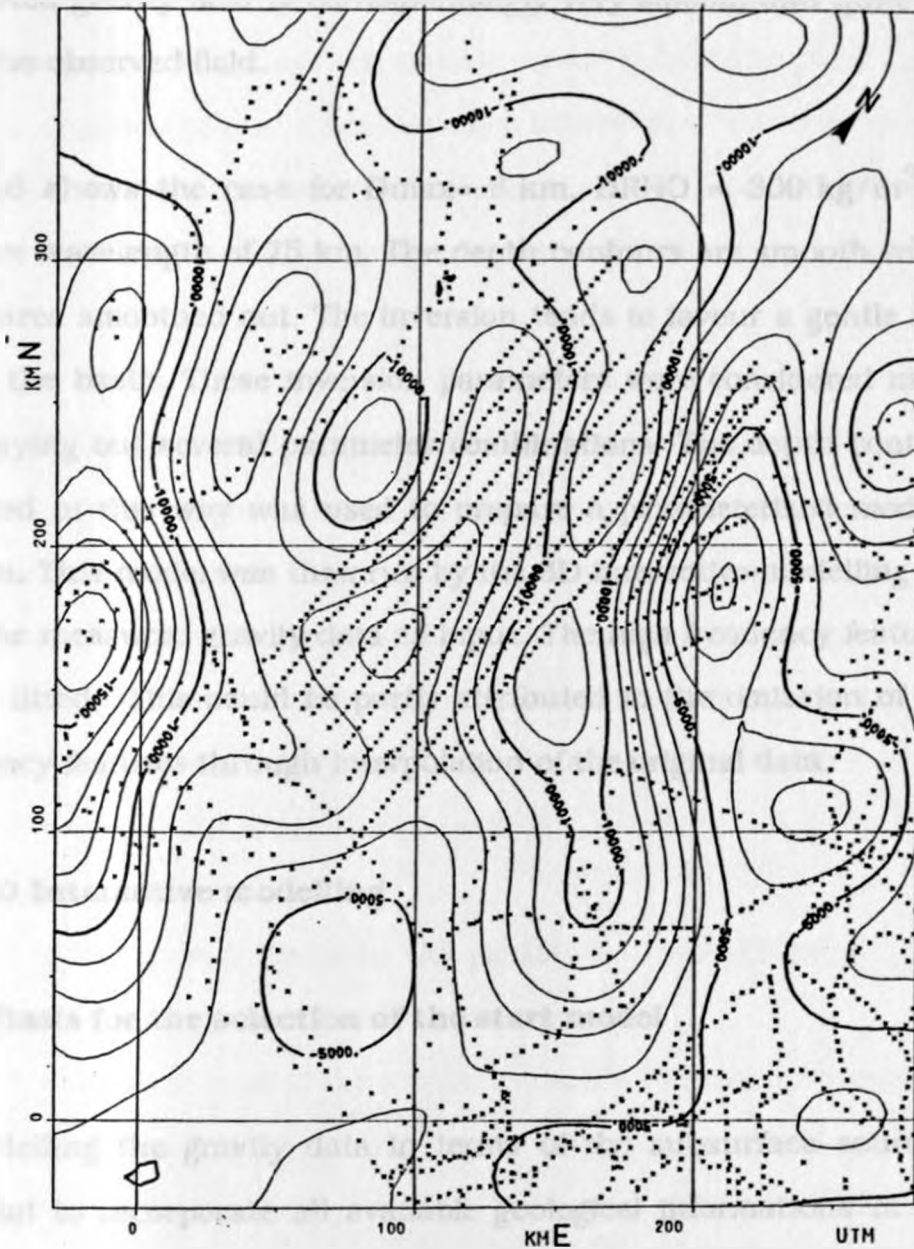


Fig. 5.6: Undulation boundary, $D\text{-MAX} = 8 \text{ km}$,
 $D\text{-RHO} = -300 \text{ kg/m}^3$, Lambda-eff. ,
 75 km contour interval: 1000 m.

Fig. 5.5 shows the case for $D_{\text{max}} = 35 \text{ km}$ with a density contrast of -350 kg/m^3 and an effective wavelength of 140 km. The map is on a local coordinate system. The surface obtained is quite smooth and shows the type of features which could probably be associated with the Moho. The

computed gravity field is correspondingly very smooth and quite different from the observed field.

Fig. 5.6 shows the case for $D_{\max} = 8$ km, $\Delta\rho = -300$ kg/m³ and an effective wavelength of 75 km. The depth contours are smooth with minor structures smoothed out. The inversion tends to favour a gentle northerly dip of the basin. These inversion parameters were considered most ideal after trying out several parameter combinations. The depth contour map obtained in this way was used to prepare a parameterized model of the Graben. This model was then run by the 3D interactive modelling program with the measured gravity data as input. The high frequency features were poorly fitted. This could be partly attributed to the omission of the high frequency features through interpolation of the original data.

5.4 3D Interactive modelling

5.4.1 Basis for the selection of the start model

In modelling the gravity data in terms of the subsurface sources, it is essential to incorporate all available geological informations in order to reduce the degree of ambiguity or the number of possible solutions. In the case of sedimentary basins, valuable informations to incorporate into the model include shapes and orientation of structural features, sediment thicknesses, basement depths, rock densities and borehole data. Constraints imposed by these informations help in the construction of a geologically plausible start model and reduce the ambiguity of the resulting models.

A start model can also be obtained by inversion of data as it was done in the previous section. However, such a model tends to contain more of the general characteristics than specific information on the structure of interest. Although it is an approximation method, a reliable start model can be obtained if a good control on the inversion input parameters is possible.

In this study, both of the approaches mentioned above were considered. Using the first approach, the start model was obtained by parameterizing the estimated basement depths from the structural contour map of Kenya. In the second approach the results of the inversion of gravity data (section 5.3) were used. Since these two start models are totally independent of each other in terms of origin, comparison of the two offered a further chance to assess the attributes of each.

5.4.1.1 Start model based on the structural map of Kenya

Fig. 5.7 shows the part of the structural map of Kenya covering the study area. The map suggests a gently and uniformly dipping unfaulted western shoulder for Anza Graben and a steep eastern shoulder characterized by Lagh Bogal Fault. In the area where the floor of the Graben has not been disturbed by faulting, the deepest parts are indicated to lie along the axis through the centre of the Graben floor. According to the presentation, the Graben consists of several isolated zones of maximum depth peaks. The deepest parts range from 6 km in the north through 8 km in the central zone to 10 km in the SE.

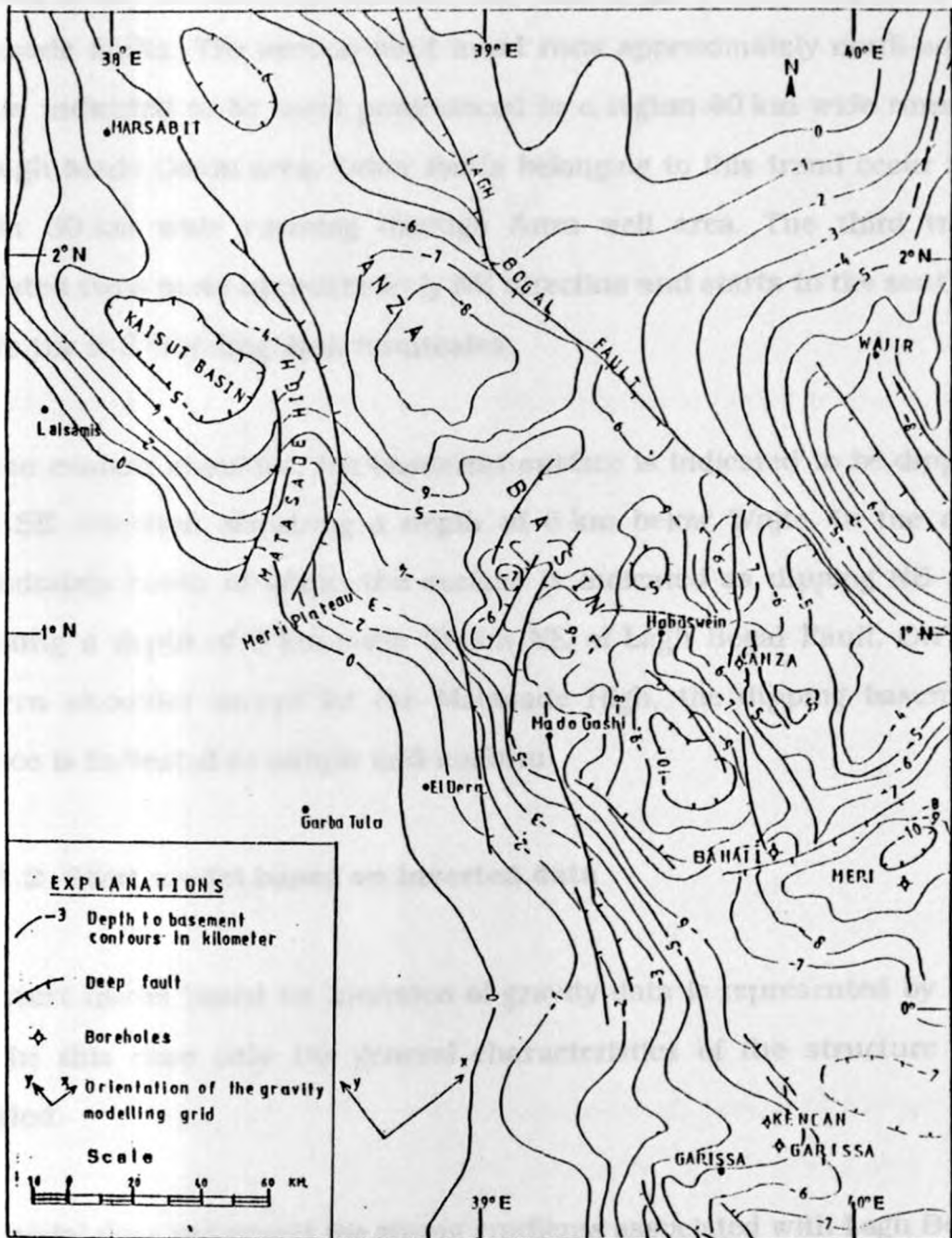


Fig. 5.7: The structural map of the study area, (after N.O.C.K. 1986).

Three trends of major faulting are shown on the map. The first trend runs parallel to the Graben and includes the Lagh Bogal Fault and part of the Matasade faults. The second fault trend runs approximately north-south and is indicated to be most pronounced in a region 40 km wide running through Mado Gashi area. Other faults belonging to this trend occur in a region 30 km wide running through Anza well area. The third trend indicated runs in an approximately NE direction and starts to the south of where the N-S trending fault terminates.

On the eastern shoulder, the basement surface is indicated to be dipping in a SE direction acquiring a depth of 6 km below Wajir. In the area immediately south of Wajir, the surface is indicated as dipping NE and attaining a depth of 9 km some 20 km NE of Lagh Bogal Fault. On the western shoulder except for the Matasade High, the dipping basement surface is indicated as simple and uniform.

5.4.1.2 Start model based on inverted data

The start model based on inversion of gravity data is represented by Fig. 5.5. In this case only the general characteristics of the structure are revealed.

The model does not reveal the strong gradients associated with Lagh Bogal Fault. It presents a symmetrical rather than asymmetrical model for the Graben. In contrast to the structural map, the inverted model suggests a general northerly dip for the Graben. The sides of the Matasade High are represented as very gently dipping so that the suspected steep fault margins are not revealed. In general, the influences of the faulting are not

highlighted. Although this model shares some of the characteristics expressed in the structural map, it is lacking in details. Some of the structures known geologically to exist are not revealed. The model based on the structural map model was therefore preferred for use in the 3D interactive modelling.

5.4.2 Problems of the determination of the model parameters

The critical control parameters for modelling include depth to basement, densities, density contrasts for the various parts of the model and location of the Graben boundaries. Not all of these parameters had been defined by the start model. Further, the defined parameters had not been uniquely determined. The involvement of several data types in this study provided an opportunity for a critical evaluation of the already defined parameters and the estimation of the non-defined ones.

5.4.2.1 Basement depth

The structural contour map giving the depth to basement although based on existing data is very subjective in the region of Anza Graben. In this region no boreholes were able to strike the basement except in the area to the north of Marsabit. Thus, the basement contours given are approximations based on correlations and estimations from variation in thicknesses of the overlying beds. As indicated in chapter 2, these tools for estimating depths have a rather limited value for Anza Graben because of the oscillatory sedimentation history of the region. The depth values used for the start model were thus not strictly constrained. This is especially

true for the deepest sections of the Graben. In the shallow sections, the contours are fairly reliable as evidenced by the reflection data.

5.4.2.2 Rock densities

In view of limited density information of rocks in this area, the values adopted for the start model were derived from the evaluation of the measurements in a few boreholes in the area and of measurements on similar rock units in adjoining areas.

In the case of the sedimentary rocks, the density information available cannot be considered as representative. The density data on rocks within Anza Graben are from boreholes Duma, Ndovu and Sirius (Fig. 2.1). In Duma, the density informations are given only on shale formation and only in the interval from 845 m to 2320 m.(Tab. 5.1). The range is relatively large (2330 kg/m^3 to 2680 kg/m^3) and shows a tendency for the density to increase with depth. Since shale constitutes only a small portion of this interval, the data are not good enough for the purpose of generalization.

Depth range	No. of samples	Mean density
800- 900 m	6	2.33
1400-1500 m	3	2.48
1500-1600 m	6	2.53
1800-1900 m	9	2.70
1900-2000 m	11	2.64
2200-2300 m	10	2.68

Table. 5.1: Shale densities in Duma (* 10^3 kg/m^3).

Depth range	Bulk density	Matrix density
1022-1180 m	2.25	2.65
1225-1435 m	2.20	2.65
1455-1707 m	2.15	2.65
1710-2105 m	2.50	2.68
2110-3100 m	2.43	2.68
3100-4267 m	2.60	2.68

Table 5.2: Shale densities in Ndovu (* 10^3 kg/m^3).

Limited density measurements were also obtained from Ndovu (Tab. 5.2). In this case, the densities also appear to increase with the depth. They range from 2250 kg/m^3 at the top of the interval to 2600 kg/m^3 at the bottom. The values for the bulk density are much lower than in Duma. However they also represent only part of the interval and cannot be considered as representative.

Further measurements were obtained from Sirius (Fig. 2.1). In this case the measurements were not confined to shale formation but rather covered all the units within the interval sampled. Shale occurrence in this well is very limited. The density measurements obtained are correspondingly low (Tab. 5.3). No distinct increase of density with depth can be detected.

There are a number of techniques for computing depth density functions for modelling (Maxant, 1980; Litinsky, 1989). However, the development of such functions usually requires a large amount of density data to be

Depth range	Density
230- 435	2.15
435- 971	2.20
971- 994	2.35
994-1006	2.17
1006-1016	2.15
1016-1034	2.18
1034-1146	2.17
1146-1276	2.22
1276-1289	2.27
1289-1485	2.18

Table 5.3: Density measurements in Sirius
(* 10^3 kg/m³).

available and if possible in several boreholes. Some of the boreholes should have penetrated the entire sedimentary sequence. Since Sirius penetrated the sequence, an attempt was made to obtain the effective density values using data from it. A value of -400 kg/m^3 was obtained for the contrast taking the basement to be 2700 kg/m^3 . The formula used is:

$$\bar{\Delta\rho} = \frac{\Delta\rho_1 h_1 + \Delta\rho_2 h_2 + \dots + \Delta\rho_n h_n}{h_1 + h_2 + \dots + h_n} = \frac{\sum_{i=1}^n \Delta\rho_i h_i}{H} \quad (5.12)$$

n : number of layers h_i : thickness ρ_i : density contrast

However, as the borehole is relatively very shallow, these results could not be assumed to apply to the entire basin. In general the data from the boreholes were of limited use for the following reasons:

1. The measurements were made mainly on one component (i.e. shale) of the rocks drilled through.

2. The measurements are only in the intermediate interval with the shallow and deeper parts not represented.
3. The older rock units of Permo-Triassic and Jurassic which are suspected to occur at depth are not represented by the borehole data;
4. The data represents only three locations in a basin of an area of over 30000 km².

It was therefore necessary to consider density information especially for the older rocks from correlatable units elsewhere within the sedimentary belt of Kenya. Measurements made on the older members of the sedimentary sequence from coastal Kenya (Dindi, 1983; 1986 and Dindi and Swain, 1988) yielded the densities shown below (Table. 5.4). The density values are generally high and are attributed to compaction related to the age and the depth of burial. These values probably constitute the highest values to be expected for the sedimentary rocks in the region.

In view of the scarcity of the existing density data and the large variations in densities indicated, they could not be used directly without special consideration about which values to use. Several factors led to the ruling out models with several densities for the sediments. These factors include:

1. lack of clear cut consistency in the density depth relationship;

2. lack of clear cut indication of linear increase of density with depth;

Source	No. of samples	Mean dry density	Mean wet density
Maji ya Chumvi formation (shale)	39	2.58	2.61
Mariakani formation (sandstone)	8	2.48	2.53
Mazeras formation (sandstone)	20	2.53	2.60

Table 5.4: Densities of Permo-Triassic rocks at coastal Kenya ($\times 10^3 \text{ kg/m}^3$).

3. lack of basis for defining density boundaries or associating density boundaries with lithological boundaries;
4. limited information on the density distribution within the basin due to limited borehole data.

On the basis of all the data examined it was considered most appropriate to assign the sediments densities in the range of 2300 kg/m^3 to 2500 kg/m^3 as the mean values for the start model.

The data used for assigning densities to the metamorphic basement rocks were obtained from Swain (1979). Samples on which the data are based were collected during the Leicester surveys and include areas located on

the western shoulder of Anza Graben. The methods used for the density measurements by Dindi (1982) and Swain (1979) are similar and have a measurement error of 10 kg/m^3 . The average composition of the metamorphic rocks in most of Kenya is the gneiss. The data indicate a value of 2650 kg/m^3 for this composition. Where amphibolites occur, the densities vary between 2800 and 3000 kg/m^3 ; but these are isolated in occurrence. Thus, densities in the range of 2700 to 2800 kg/m^3 were considered appropriate for the metamorphic rocks. In this study a value of 2700 kg/m^3 was selected as the most ideal.

Intrusives caused the major problem in the selection of modelling densities. They show variable compositions (Hackman et al., 1991) and hence are likely to have a wide density variation. In Sirius well, an intrusive rock sample gave a density of 2950 kg/m^3 . Measurements on samples from the immediate west of Anza Graben (Swain, 1979) yield densities of about 2800 kg/m^3 with a few samples giving 3000 kg/m^3 . The rocks in this case have been described as dolerites and gabbros. In this study a value of 3000 kg/m^3 was considered to represent the extreme case so that a maximum value of 2800 kg/m^3 was considered most representative.

5.4.2.3 Margins of the structure

The transition zone from the Anza Graben to its shoulders is not easily defined due to the coverage of young sediments and volcanics extending beyond the margins of the Graben. In the east, because of the abrupt changes of gravity and magnetic gradients, the position of the boundary could be estimated reasonably well. However in the west, the location of

the boundary could not be easily ascertained except where reflection data existed. The western termination of the Graben was therefore approximated to coincide with the contact of the Quaternary and the exposed metamorphic rocks.

5.4.3 Model data preparation

The first step in the model data preparation was the selection of an appropriate grid. In order to cover the entire extent of the structure as defined in chapter one, 20 parallel planes (Fig. 3.1) were used. Their spacing varied from 10 km to 20 km depending on how rapidly the structure appeared to change along the strike. The profile lines were oriented approximately perpendicular to the axis of Anza Graben.

The origin of the coordinate system was located at $38^{\circ}44'E$ and $0^{\circ}21'S$. The coordinates of the basement depths as estimated by the structural contour map were then taken for all the planes. In order to facilitate the comparison of the computed gravity effect and the observed, the latter data were also transformed to the local coordinate system. The Bouguer and not the residual (Bouguer anomaly minus regional anomaly) values were used as the modelling involved both shallow and deep structures.

5.4.4 Tentative models

The strategy adopted in modelling was to incorporate models of the structure piecewise until both shallow and deep structures had been modelled. One advantage of this approach is that one has a better control on the model as it becomes more sophisticated. Initially, only the basin was modelled. The geometry of the start model was adjusted until the

computed anomaly mimicked the observed in the section over the Graben. The fixed density contrasts were then varied between -200 kg/m^3 and -400 kg/m^3 to determine the effect on the computed anomaly amplitude. Contrasts outside this range were ruled out as unrealistic on geological grounds. Models with contrasts -200 , -250 , -300 , -350 and -400 kg/m^3 were generated. A contrast of -400 kg/m^3 produced a much larger amplitude than the observed while that of -200 kg/m^3 a much smaller one. The two cases favour a much shallower and a much deeper basin respectively. A contrast of -300 kg/m^3 yielded a relatively superior correlation between the computed and the observed anomaly. This value was assigned to the modified version of the start model in its further development.

The next step was the incorporation of models to account for the short wavelength part of the shoulder anomalies. In this case there is hardly any reliable geological control on the position or density. Thus, boundaries were rather subjectively defined with control only from the gravity and magnetic data. Density contrasts of up to -200 kg/m^3 were used. Higher contrasts were considered geologically unrealistic and hence were not used. Again the geometry of these models was varied until the computed shoulder anomalies almost mimicked the observed. Models with various contrasts were then generated. Contrasts yielding the closest agreement between the observed and the calculated were then adopted for further development of the model.

The model was then extended to include the deep structure up to the Moho. It was constructed to incorporate thinning to account for the long wavelength components of the shoulder anomalies. In the absence of deep

refraction data directly over the Graben, values for the Moho depth had to be based on studies done elsewhere in the country. Bonjer et al. (1970) recorded a normal crustal thickness of 42 km below Nairobi on the eastern flank of the Kenya Rift Valley. Henry et al. (1990) report a Moho depth of 34 km beneath the central sector of the Kenya Rift Valley indicative of a thinned crust. Keeping the Moho depth closer to this order of value it was placed at 40 km away from the shoulders thinning to 35 km at the shoulders and under the Graben. This agrees in part with the results of the refraction modelling of the KRISP90 data along Profile E which indicates a depth of about 35 km for the Moho at the SE end of Profile E (see Fig. 3.9). Again several models were generated with sub-Moho densities ranging from 3000 to 3400 kg/m³ in order to study the influence on the calculated anomaly.

While the fit at the flanks was not seriously affected, densities of 3300 kg/m³ and 3400 kg/m³ reduced the fit over the basin. A density of 3200 kg/m³ improved the fit at the shoulders and maintains a good fit over the Graben. This value which is normally taken as the standard for normal sub-Moho rocks (Sheriff, 1980) was used in the further improvement of the model. Having fixed the sub-Moho densities as well as those of the bodies at the shoulders, a test was made using contrasts of -200 kg/m³ and -400 kg/m³ for the sediment infill to determine necessary changes to the model in order to achieve a fit. It was observed that with -200 kg/m³ the maximum sediment thickness required is over 10 km.

Although the value of 10 km is in agreement with the basement depth estimates from aeromagnetic data, it suggests contrasts which are not consistent with the order of densities of dominant lithological units

encountered in boreholes. If this should be the actual subsurface situation, it will imply a very rapid drop in contrast beyond the depth reached so far by drilling. Only the shales which are not well developed in the area had densities of 2500 kg/m^3 . Applying a contrast of -400 kg/m^3 , the maximum thickness required is only 5 km. However, existing data show that boreholes drilled in sections not considered to be the deepest parts of the Graben attain depths of up to 4.5 km without any indications of approaching the basement.

5.4.5 The final model

A sediment/basement density contrast of -300 kg/m^3 was used in the final model. Deviations of upto 50 kg/m^3 still yield reasonable models. Higher deviations however make it difficult to reconcile the models with geological data (see section 5.4.4). The ensuring model with density contrast -300 kg/m^3 ties in well with most of the data available to date. As the control on the densities of the intrusives at the shoulders was not rigid, the final refinements of the model also involved inversion of these densities. The final density contrasts for these bodies were obtained by inversion as 20 kg/m^3 and 50 kg/m^3 . Various sections of the final model were generated. Two of these sections are shown in Figs. 5.8 and 5.9. A 3D perspective picture is shown in Fig. 5.10.

The important attributes of the model are:

1. The densities used are 2400 kg/m^3 for the sediments in the Graben, 2700 kg/m^3 for the normal basement, 2720 kg/m^3 and 2750 kg/m^3 for the bodies at the western and eastern shoulders respectively, 2900 kg/m^3 for the lower crust and 3200 kg/m^3 for the upper mantle.

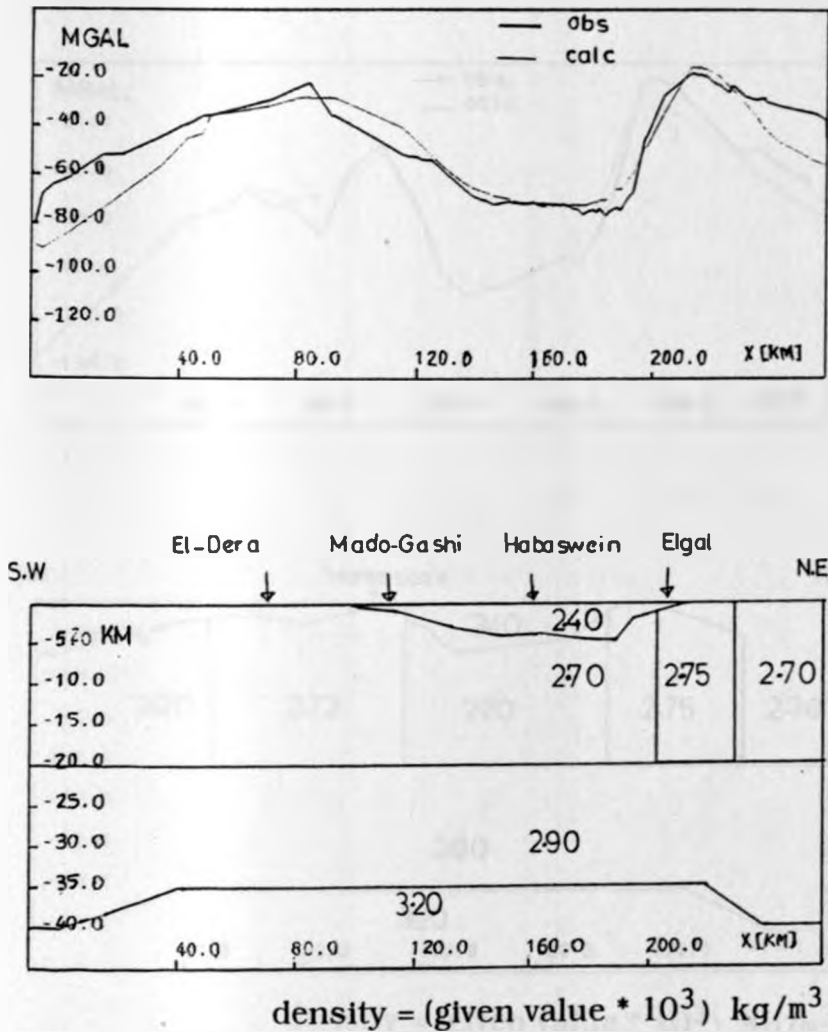
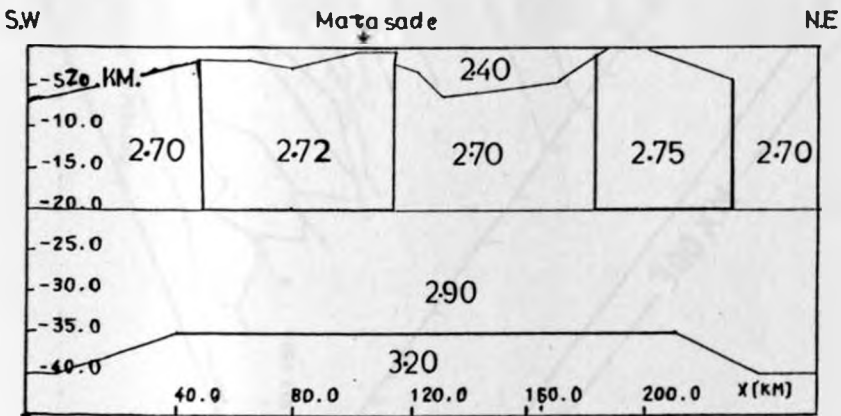
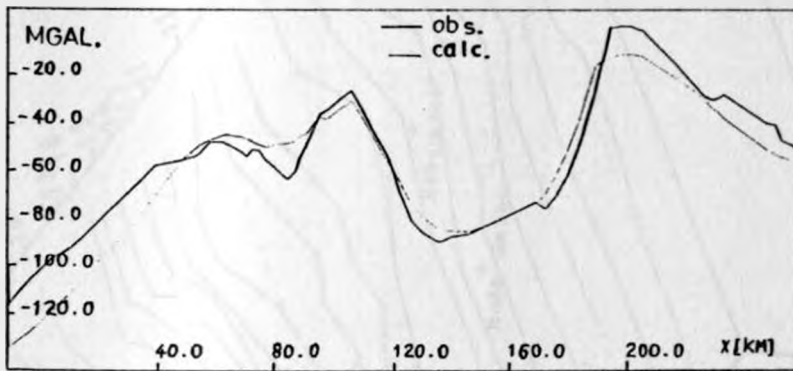


Fig. 5.8: The section through the model along plane 7 (Fig. 3.1) in the southern part of Anza Graben.



density = (given value * 10³) kg/m³

Fig. 5.9: The section through the model along plane 12 (Fig. 3.1) in the northern part of Anza Graben.

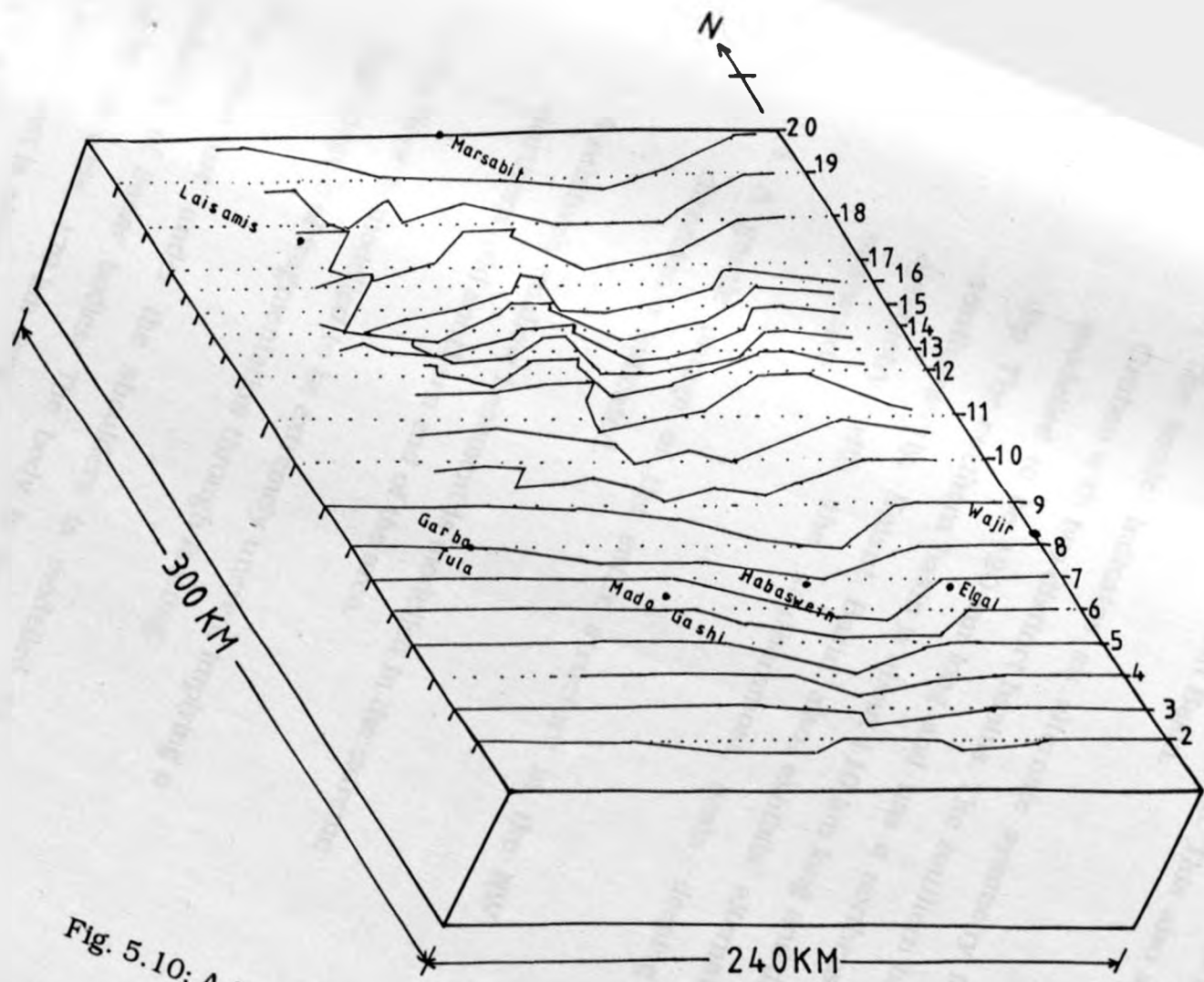


Fig. 5.10: A 3D-perspective picture of the model.

2. The maximum depth of the Graben according to the model is of the order of 8 km. This also applies to the neighbouring Kaisut Basin.
3. The model indicates an alternate symmetry for Anza Graben with two distinct basins. The southern basin is modelled to be 120 km long and has a northeasterly dip. The northern basin is about 110 km long and dips southwesterly. Kaisut Basin also exhibits alternate symmetry with the southernmost basin deeping eastwards.
4. A gentle plunge of the entire structure in the NW direction is indicated.
5. A relatively shallow basement is modelled in the extreme northern and southern end of the area.
6. The floor is modelled to be extremely uneven, implying a high degree of fragmentation through faulting.
7. The structure under the shoulders is modelled as consisting of linear bodies. The body to the west is 30 to 80 km wide, 170 km long and 4 km deep. The body to the east is about 40 km wide, 240 km long and about 1 km deep.

8. The model includes a thinning of the crust by 5 km below Anza Graben.
9. The sub-Moho density remains uniform below the Graben and the shoulders.

Most of the residuals obtained after fitting the model are close to zero. Residuals of up to 5 mGal over the Graben are considered tolerable especially since the model is controlled by only 20 planes. The large residuals along the margins of the grid lie outside the section for which a fit was sought. Due to the level of accuracy of the data and the known non-uniqueness of gravity modelling, no attempt was made to achieve a perfect fit. Deters (1990) has used this final model for inversion studies using the algorithm by Richardson and MacInnes (1989). No substantial changes in the geometry resulted from the inversion.

CHAPTER SIX

MAGNETICS

The aeromagnetic data used were flown by Kenting Exploration Company in 1982 (P.E.P.P., 1983). These data cover about 70% of the study area. The section east of 39.5°E is however not covered. The data exist in the form of contour maps at a scale of 1:250,000. The profiles are at a spacing of 5 km oriented $\text{N}30^{\circ}\text{E}$. Orthogonal control lines are spaced 25 km apart. West of 38°E the ground clearance was 1830 m above sea level while to the east 915 m. The proton precession magnetometer used had a resolution of 0.10 nT. The flight path of the survey aircraft was recovered from a 35 mm tracking film onto aerial photos and transferred to topographic maps. A Doppler system was used in navigation.

At the beginning of this study, the author carried out ground magnetic measurements in the southern section of the Graben. Two proton precession magnetometers were used. Accessibility problems however made it difficult to conduct ground magnetics in the northern section of the Graben.

6.1 The basis of the magnetic method

The basis of the magnetic method is presented in various geophysical text books (e.g. Jung, 1961; Telford et al., 1990; Grant and West, 1965). The brief outline which follows is as given by Telford et al. (1990).

Neglecting the influence of the external field, the measured total magnetic field on the earth's surface can be considered to consist of two components. One is the effect of the earth's normal field and the other that of the near surface geological sources. The disturbances due to the latter can be represented by $\vec{\Delta T}$ (see equation 6.1). These anomalies are much smaller than the normal earth's field represented by \vec{T}_0 . Since the measured field \vec{T} and \vec{T}_0 are different, the anomaly is represented as:

$$\vec{\Delta T} = \vec{T} - \vec{T}_0 \quad (6.1)$$

The anomalous part of the observed field is due to magnetization of magnetic bodies within the crust. The magnetization here consists of two parts, the induced and the remanent magnetization.

The induced magnetization is caused when rocks are subjected to a magnetizing force. The induction field H and the induced magnetization M_i are related by the expression:

$$\vec{M}_i = k \vec{H} \quad (6.2)$$

k : magnetic susceptibility.

A more accurate expression includes the effects of demagnetization (Grant and West, 1965) and that of the mineral components of the body. The exact expression for the effective magnetization is then given (Telford et al., 1990) by:

$$\vec{H}_{\text{eff}} = \vec{H} + \vec{H}_{\text{dem}} = \vec{H} + N \cdot \vec{M}_1 \quad (6.3)$$

N: demagnetization factor.

It follows that:

$$\vec{M}_1 = k / (1 + kN) * \vec{H}_{\text{eff}} = k' \vec{H}_{\text{eff}} \quad (6.4)$$

$$\text{and } k' = \vec{M}_1 / (H_{\text{eff}} \cdot \vec{M}_1 \cdot N) \quad (6.5)$$

k': apparent susceptibility of the body.

k' is a function of the material and its form. For most rocks, the magnetization is very small compared to the earth's field. The demagnetization vector can therefore be ignored. In general, the overall susceptibility is influenced by several factors which include:

1. content of ferromagnetic minerals and their sizes, forms and distribution;
2. strength of the field;
3. temperature.

The remanent magnetization is part of the natural magnetization of rocks which persists when the external field is removed. The carriers of Natural Remanent Magnetization (NRM) are ferrimagnetic minerals such as magnetite. NRM is independent of the direction of the present earth's field

and is usually smaller in magnitude. It can however in some cases be as great as the induced magnetization (Green, 1960; Books, 1962). If the influence of remanence is not taken into account, it may lead to erroneous interpretations. A measure of the remanence is given by the Königsberger ratio (Sheriff, 1990) defined by:

$$Q = M_r / M_i \quad (6.6)$$

M_r : remanent magnetization

For most rocks Q lies between 0 and 10 but can be as high as 100. On the basis of occurrence and stability there are different types of remanent magnetization. The most significant is the thermoremanent magnetization associated with cooling. Others include chemical remanent magnetization, isothermal remanent magnetization, and viscous remanent magnetization (Telford et al., 1990). Generally sedimentary rocks have smaller remanence ($Q < 1$) than extrusive rocks ($Q > 1$).

The anomalous magnetic field may therefore be represented vectorially as:

$$\vec{M} = \vec{M}_i + \vec{M}_r \quad (6.7)$$

Due to the fact that the remanent magnetization is usually much smaller than the induced magnetization, the vector $\Delta \vec{T}$ (equation 6.1) can be approximated to be in the direction of the earth's normal field ($\Delta \vec{T} \ll \vec{T}_0$).

In the modelling of the magnetic data temperature gradient of a given area has to be taken into account. The Curie temperature which is the

temperature above which rocks lose their magnetization is for most rocks less than 600°C and is reached by about 20 km depth (Sheriff, 1980). Some idea of the Curie temperature depth for an area is thus also important.

The observed magnetic signature also depends on the geomagnetic latitude of the location of the causative body. This is defined by the magnetic inclination. At the location where the inclination is 90° the signature due to different poles overlaps and the magnetic anomaly is similar to and readily comparable with the gravity anomalies. Thus, for geomagnetic latitudes other than 90° , a transformation to that inclination is usually necessary in order to facilitate the comparison where joint interpretation of potential field data is involved. The operation is usually referred to as the reduction to the pole (Baranov, 1957). The basis for the transformation is the Poisson's theorem relating gravitational to the magnetic potential:

$$U(P) = 1 / (4G\rho) * \vec{M} \partial V / \partial \mathcal{E} (P) \quad (6.8)$$

$U(P)$: magnetic potential at point P

$V(P)$: gravitational potential at P

$\partial V / \partial \mathcal{E}$: partial derivative of V in the direction
of the magnetization vector

\vec{M} : magnetization vector

UNIVERSITY OF NAIROBI LIBRARY

G: gravitational constant

ρ : density of the causative body

Through differentiation in the direction of the normal magnetic field the following expression is obtained for the total field intensity:

$$\Delta T = -\mu_0 \frac{\partial U}{\partial S} = \mu_0 M / (4\pi G \rho) * \frac{\partial^2 V}{\partial E \partial S} \quad (6.9)$$

Through differentiation with respect to z instead of dS and dE , the field reduced to the pole (Militzer and Weber, 1984) is obtained:

$$\Delta T_{\text{pol}} = \mu_0 M \frac{\partial^2 V}{\partial (4\pi G \rho \partial^2 z)} = \Delta T_0 \frac{\partial g}{\partial (4\pi G \rho \partial z)} \quad (6.10)$$

This relationship holds only on the assumption that gravity and magnetic anomalies have the same causative bodies. Each of the bodies must have a constant density and susceptibility contrast with the surroundings.

The two other important parameters, magnetic declination and inclination (Telford et al., 1990) are easily obtainable from records of the geomagnetic observatories

6.2 Techniques used in the data analysis

The techniques used in the analysis of the magnetic data in this study are wavelength filtering, upward continuation and reduction to the pole. The main purpose of filtering in this case was to suppress undesirable effects in the effort to make the characteristics of interest more discernible. As

the wavelength filtering has already been outlined (section 4.4.2), only the latter two techniques are outlined in this section.

6.2.1 Upward continuation

Upward continuation involves the calculation of the potential field at an elevation higher than that at which the field is known (Telford et al., 1990; Degro, 1986). It is similar to wavelength filtering except that while the latter attempts to separate the regional and the residual, the former merely projects the data in such a way as to make the regional dominant. The transfer function for upward continuation is:

$$\Psi_k = e^{kz_0} \quad (6.11)$$

$$\Psi(k_x, k_y) = e^{\sqrt{k_x^2 + k_y^2} z_0} \quad (6.12)$$

where z represents the continuation plane.

The characteristics of this filter are shown in Fig 6.1 for cases where $z_{04} < z_{03} < z_{02} < z_{01} < z_{00} = 0$. In the case $z_{00} = 0$ the spectrum of the output function remains unchanged. However, with increasing heights the function shows increased low pass filter characteristics. It therefore attenuates the effects of near surface sources drastically making regional trends and lineaments more easily identifiable. A direct relationship between the continuation height and the depth of the source is however difficult to determine. Since the function approaches zero with increasing wave-number, it is necessary to introduce a taper as in the case of wavelength filtering.

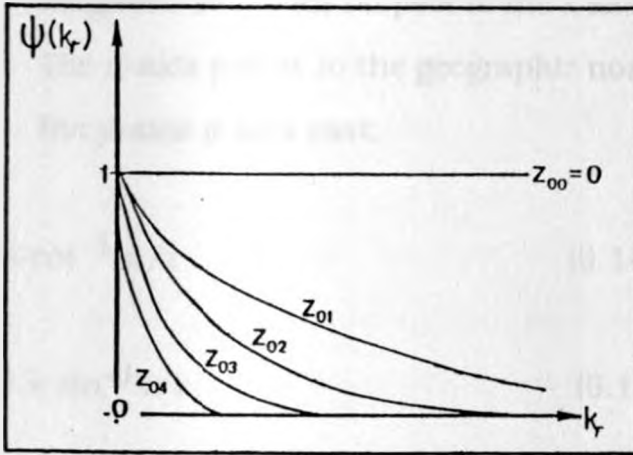


Fig. 6.1: The filter characteristics of the upward continuation filter (from Degro, 1986).

6.2.2 Reduction to the pole

The relevance of reduction to the pole has been outlined in 6.1. The reduction to the pole filter used in this study was in the frequency domain form. In its wavenumber domain form (in polar coordinates), the filter can be represented by the expression (Silva, 1986):

$$K(r, \theta) = \frac{1}{(\cos I_0 \cos(D_0 - \theta) + \sin I_0)(\cos I \cos(D - \theta) + \sin I)} \quad (6.13)$$

I, I_0 : inclinations of the magnetization and geomagnetic fields respectively.

D, D_0 : azimuths of the magnetization vector and geomagnetic field with respect to the x axis.

The x-axis points to the geographic north and the y-axis points east.

$$\theta = \cos^{-1} u/r \quad (6.14)$$

$$\text{and } \theta = \sin^{-1} v/r \quad (6.15)$$

u and v: angular wavenumber coordinates.

Analysing the expression mentioned above, it is clear that near the magnetic equator where the inclination approaches zero the weights of the filter are very high. This is also the case when the values of θ are close to $D_0 + 90^\circ$. Kis (1990) has analysed the latter case. Fig. 6.2 shows the characteristics of the transfer function for the reduction to the pole in the frequency domain for an inclination of $I=I_0=60^\circ$ and $D=D_0=0^\circ$.

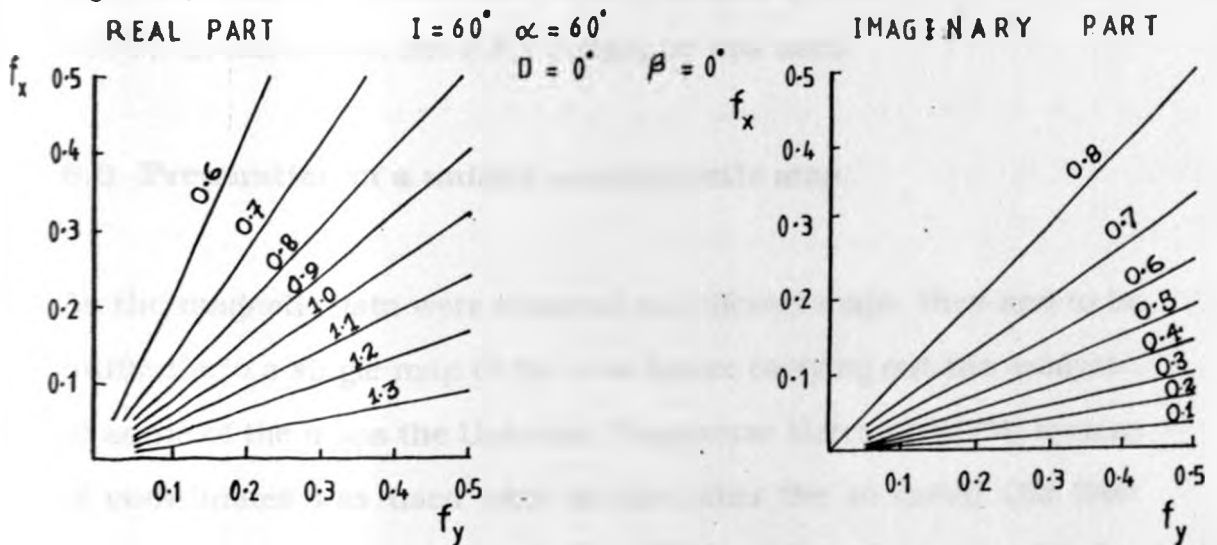


Fig. 6.2: Real and imaginary parts of the 2D transfer function of reduction to the magnetic pole for inclination $I = 60^\circ$ and declination $D = 0^\circ$ (Kis, 1990)

It is of interest to note that at the origin of the f_x - f_y plots the filter operator is undefined which means that the base level value obtained by reduction to the pole is arbitrary.

The limits of the transfer function become infinite along the f_x - and/or f_y -axes. The axes define the limits of the application of the filter. Silva (1986) pointed out that at low geomagnetic latitudes, even in the absence of noise, poor performance of the filter is to be expected due to imperfections in the data spectrum. Poor performance can be minimized by filtering out noise before reduction to the pole, by proper choice of sampling intervals and by the use of a large number of data samples. The minimum value of inclination below which instabilities make reduced-to-the-pole results uninterpretable varies with the transformation procedure used. Baranov's (1957) procedure had a limit of $I = 30^\circ$. The procedure by Baranov and Naudy (1964) had a limit of $I = 16.5^\circ$. The traditional F.F.T technique for reduction to the pole has a limit of $I = 15^\circ$ (Silva, 1986). In this study, the F.F.T technique was used.

6.3 Preparation of a unified aeromagnetic map

As the magnetic data were obtained on different maps, they had to be unified into a single map of the area before carrying out the analysis. In some of the maps the Universal Transverse Mercator (UTM) system of coordinates was used while in the other the so called Old East African (OEA) system was used. The UTM in this case has the equator as 0 km and 39°E as the longitude of origin with a grid value of

500 kmE. On the maps prepared using the OEA system, the equator has a false Northing of 4500 km and longitude $37^{\circ}30'E$ is the longitude of origin with a value of 400 kmE. Conversion of OEA to UTM did not yield a perfect match with the other UTM grids. There was an error of about 1 %.

Although the aeromagnetic data were collected at two different heights, the differences in the ground clearance between the two areas was only 200 m. Robinson and Coruh (1988) indicate a change of the main magnetic intensity with elevation of about 1.5 nT per 100 m at low geomagnetic latitudes. Using this estimate, the errors expected from merging the two data sets is likely to be small (less than 5 nT). The original data were therefore unified without effecting any continuations. The problem of continuity at the boundaries was not considered serious as an overlap of about 55 km exist between the maps. Minor artificial anomalies were however unavoidable at boundaries especially those characterized by steep gradients.

The original map was digitized using the grid of the particular map. This was done by using a digitizer selecting contour lines and picking values every 4 km. The digitizer was connected directly to an IBM PS 80 PC where the data were directly filed. In order to ascertain that there were no errors and that the digitization was correctly performed, data from each map were contoured, plotted and compared with the original map at the same scale. Finally, all the coordinates of the data were transformed to the UTM system before drawing the unified map.

6.4 Features of the magnetic maps

On the unified aeromagnetic map (Fig. 6.3), the Anza Graben appears as a zone characterized by very gentle magnetic gradients. This is clearly visible in the south but is obscured in the north by the short wavelength anomalies bearing the orientation of the Graben. The latter are easily correlated with the surface basalts (see section 2.4). The remarkable elongation of the anomalies seems to define the flow direction at the time of emplacement of the rocks. Over Anza Graben, two broad circular magnetic highs occur. The most prominent of these is centred at $38^{\circ}50'E$ and $1^{\circ}20'N$. Reeves et al. (1987) have interpreted these highs as representing anomalous sediment thicknesses at a low magnetic inclination. The close correlation on the ground between these centres with gravity lows (section 4.3) is in agreement with this view.

Across Lagh Bogal Fault (Fig. 6.3) a change of gradient occurs from gentle to the west to steep and rather erratic to the east. A good correlation between the magnetic and the gravity map (Fig. 4.3) is generally evident along this zone. However at half way distance the magnetic discontinuity assumes a north-south orientation for a distance of about 80 km. The gravity field along this section (Fig. 4.3) also shows a slight shift in the orientation towards the north. On the western flank of the structure, the boundary is less clear and there is no distinct correlation between the magnetic signature and the exposed metamorphic rocks to the west.

The anomalies at the shoulder of the Graben are easily distinguished from those associated with the basalt flows. The former tend to define

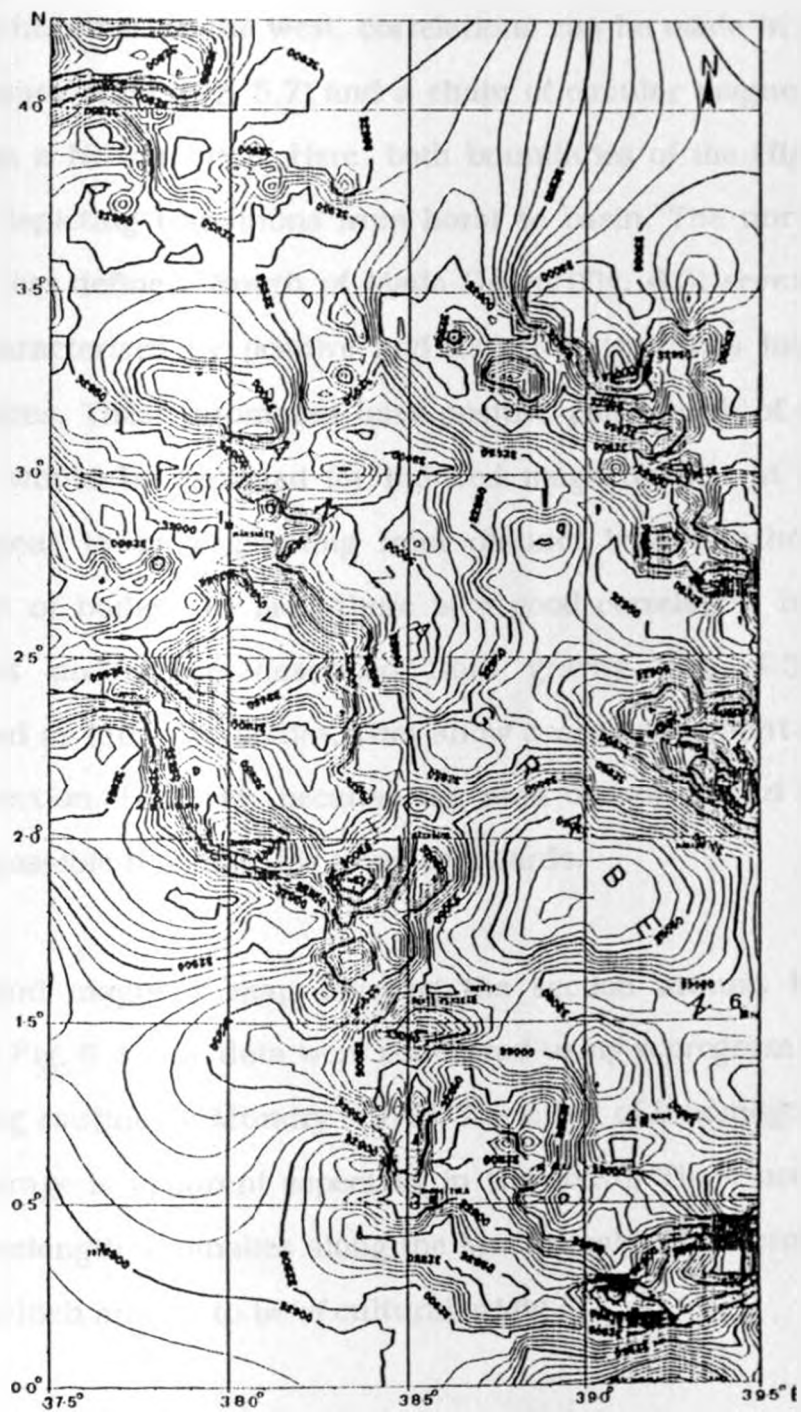


Fig 6.3 The unified aeromagnetic map of Anza Graben (contour interval: 10 nT).

lineaments of various orientations. The anomalies to the east of Lagh Bogal Fault seem to be associated with near surface rocks and are generally negative. In the west, correlations can be made in part between the Matasade High (Fig. 5.7) and a chain of circular magnetic anomalies trending in a NE direction. Here, both boundaries of the High are clearly defined, depicting transitions from horst to basin. The northern edge is however less defined. South of Mado Gashi (Fig. 6.3) several anomalies occur characterized by positive and negative signatures implying dipole type sources. These anomalies have positive poles north of the negative poles as would be expected for induced magnetization at this latitude. They appear to be originating from distinct bodies rather than from groupings of bodies. In fact, there is a good correlation between these signatures and those described from gravity (Fig. 4.3). They are interpreted as intrusive bodies. They show a weak alignment along a NEE-SWW direction. However, because the data do not extend eastwards, it was not possible to follow this trend eastwards.

The ground magnetic map covering the section around Habaswein is shown in Fig. 6.4. The data were contoured using a program based on the contouring routine by Mundry (1970). The effect of inhomogeneities in the data coverage is apparent especially in the south. There are also several short-wavelength anomalies along the Mado-Gashi-Wajir profile (Fig. 6.4), many of which appear to be of cultural origin.

Because of the overlap in some parts of ground magnetic and airborne data, it was possible not only to compare the two data sets but also to follow the anomalies eastwards beyond the termination of the

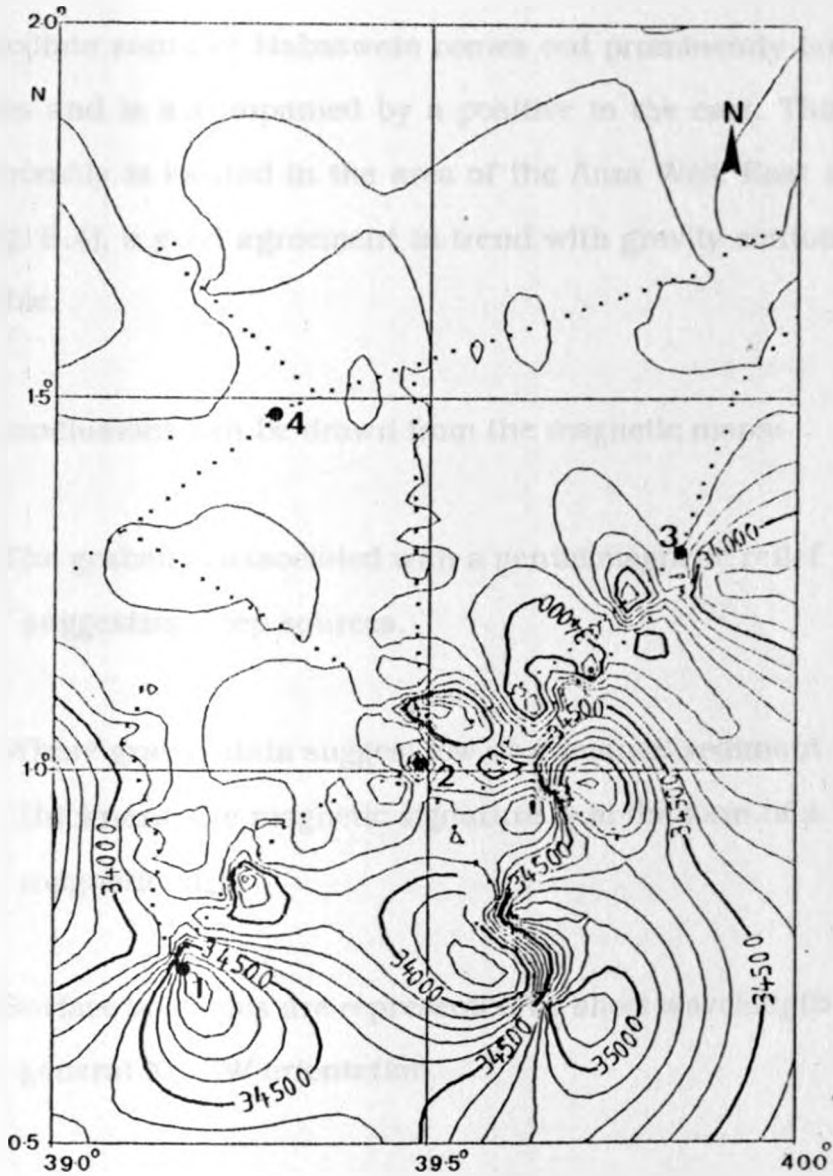


Fig. 6.4: Ground magnetic map of the southern part of Anza Graben (contour interval 100 nT) (1. Mado Gashi; 2. Habaswein; 3. Elgal; (4. Hadado).

aeromagnetic data. Thus, both maps show a gentle field to the NW of Habaswein (Fig. 6.3) and display similar contour trends. The low running NWW-SEE through Habaswein appears to be a feature of regional extent. It is partly defined by the airborne data whereas the ground data traces its continuity SEE until it terminates on a high. The high coincides with a gravity high. A negative anomaly partly defined by aeromagnetic data to

the immediate south of Habaswein comes out prominently on the ground magnetics and is accompanied by a positive to the east. This essentially dipole anomaly is located in the area of the Anza Well. East and north of Elgal (Fig. 6.4), a good agreement in trend with gravity contours (Fig. 4.2) is noticeable.

Several conclusions can be drawn from the magnetic maps:

1. The graben is associated with a gentle magnetic relief suggesting deep sources.
2. Where gravity data suggest low or abnormal sediment thickness, the magnetic signature is in the form of a magnetic high.
3. Surface volcanics are represented by short wavelength with a general NE-SW orientation.
4. Where big throws are predicted, between shoulder and basin steep anomaly gradients occur.
5. Shoulder anomalies occur as a group of lows oriented in various directions interpreted to suggest the presence of inhomogeneities or intrusives within the basement.
6. The dipole anomalies which coincide with distinct gravity highs in the south appear to represent distinct intrusive

bodies. These anomalies cluster along ENE-WSW trending lineaments.

7. It is apparent that the southern limit of the Anza Graben (as defined by this study) is characterized by the occurrence of intrusives and changes in the trends of the magnetic lineaments.

6.5 Features of the filtered aeromagnetic data

Because the area covered by the magnetic data is narrow and long, it was necessary to split the data into two sets. Each set consists of a square with dimensions 233 km * 233 km. The northern set is referred to here as the NW Anza Graben and the southern as SE Anza Graben. An overlap of 55 km which comprises 24 % was allowed between the two data sets. Data within each of these two blocks were interpolated onto a square grid at a spacing of 2.35 km. This resulted in 100 * 100 gridded data for each square. Each of these data sets were then widened on all sides to a grid of 128 * 128 thus ensuring that the format for FFT routine used was achieved and that the effect of distortion of data at the edges is minimized. The widening technique used extrapolates the values for the margins from the given field data. Each block consisted therefore of 16,384 gridded data points. Since the widening was only for the purpose of frequency domain operations, the widened margins were omitted from the final filtered maps.

6.5.1 Low pass filtered maps

Wavelength filtering of magnetic data is in practice not usually undertaken because of the uncertainties and problems associated with trying to relate the wavelength to the depth of the source. In this study, there is justification for undertaking this filtering. As described earlier, the data have several small anomalies which make it difficult to isolate the regional trends associated with the northern section of Anza Graben. This behaviour is clearly noticeable in the NW where this small wavelength anomalies correlate with the surface basalts. The low pass filtering was aimed at eliminating these effects which may be considered as originating from known sources. It was also necessary to investigate the variation of the anomalies with different cut-off wavelengths as this was deemed as a means of distinguishing between sub-regional and truly regional anomalies. The cut-off wavelengths used were 5 km, 10 km, 15 km, and 20 km. Applying a cut-off wavelength of 5 km does not alter the appearance of the field much, although it reduces the effects of the surface volcanics moderately. It is observed from filtering that a cut-off of 10 km is sufficient to suppress the effects of the surface basalts in the northern section of the area. Figs 6.5a and 6.5b show the case with a cut-off wavelength of 15 km. Both the NE and NW structural trends indicated by the geological mapping (Hackman et al., 1990) become clearly defined.

The anomalies revealed appear to delineate igneous centres in this section. Higher cut-off wavelengths merely result in increased clarity of the regional field. There is no pronounced change in the SE data when

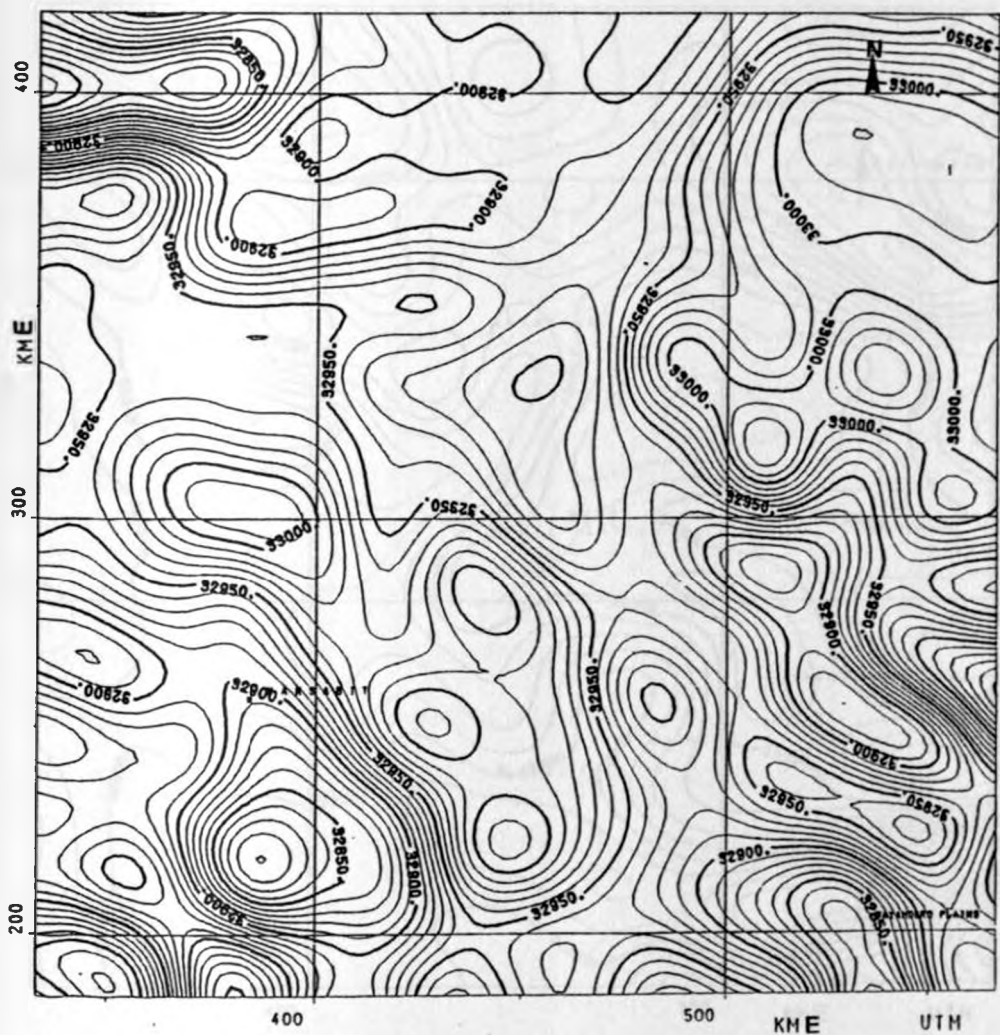


Fig. 6.5a: Filtered aeromagnetic map of NW Anza Graben (contour interval 10 nT, cut-off WL = 15 km).

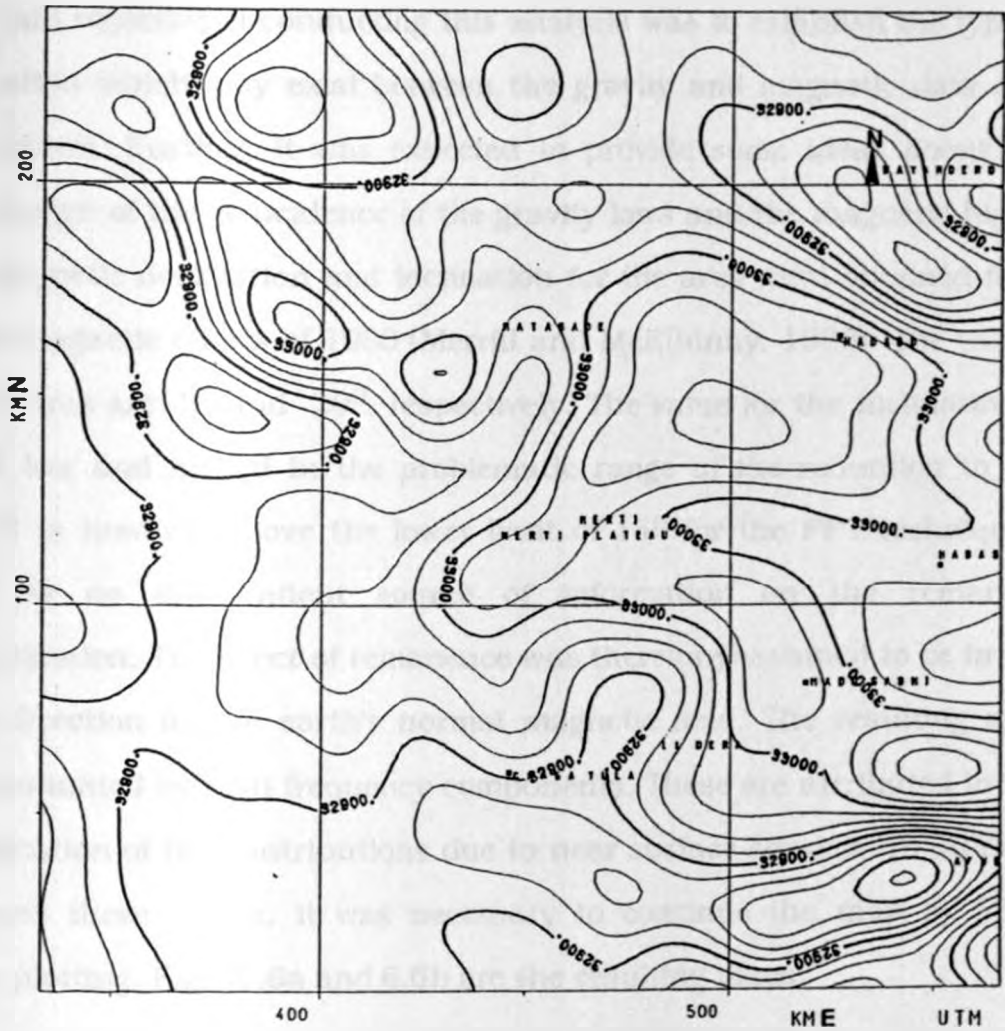


Fig. 6.5b: Filtered aeromagnetic map of SE Anza Graben (contour interval 25 nT, cut-off WL = 15 km).

the cut-off between 5 km and 20 km is applied, implying that the anomalies are largely deep-seated. This implies the absence of very shallow sources in the SE.

6.5.2 Reduced to the pole maps

The main objective of conducting this analysis was to establish the type of correlation which may exist between the gravity and magnetic data over the Graben. Further, it was expected to provide some ideas about the significance of the coincidence of the gravity lows and the magnetic highs. The magnetic declination and inclination for the area were obtained from the isomagnetic charts of 1980 (Merrill and McElhinny, 1983). The values for the area are -2° and -20° , respectively. The value for the inclination is rather low and indeed in the problematic range of the reduction to the pole. It is however above the lower limit of 15° for the FFT techniques. There is no independent source of information on the remanent magnetization. The effect of remanence was therefore assumed to be in the same direction as the earth's normal magnetic field. The resulting map was dominated by high frequency components. These are attributed to the amplification of the contributions due to near surface sources. In order to suppress these effects, it was necessary to continue the map by 5 km before plotting. Figs. 6.6a and 6.6b are the resulting maps.

The corresponding vertical gradient maps are shown in Figs. 6.7a and 6.7b. There is a moderately good agreement between the two maps. It can however be observed that a strong north-south lineation characterizes the

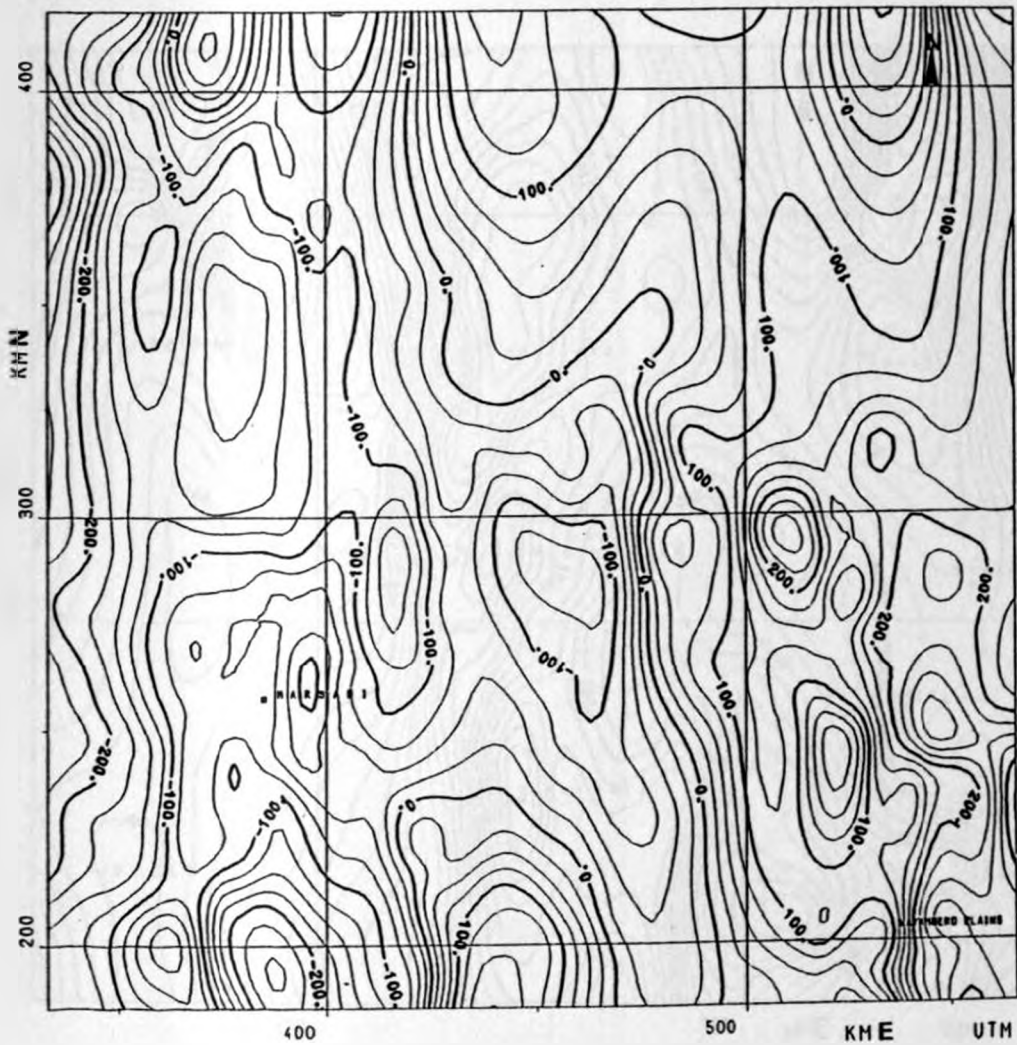


Fig. 6.6a: Pole-reduced map of the NW Anza Graben (after upward continuation of 5 km; contour interval, 25 nT, $M_I = -20^\circ$, $M_D = -2^\circ$).

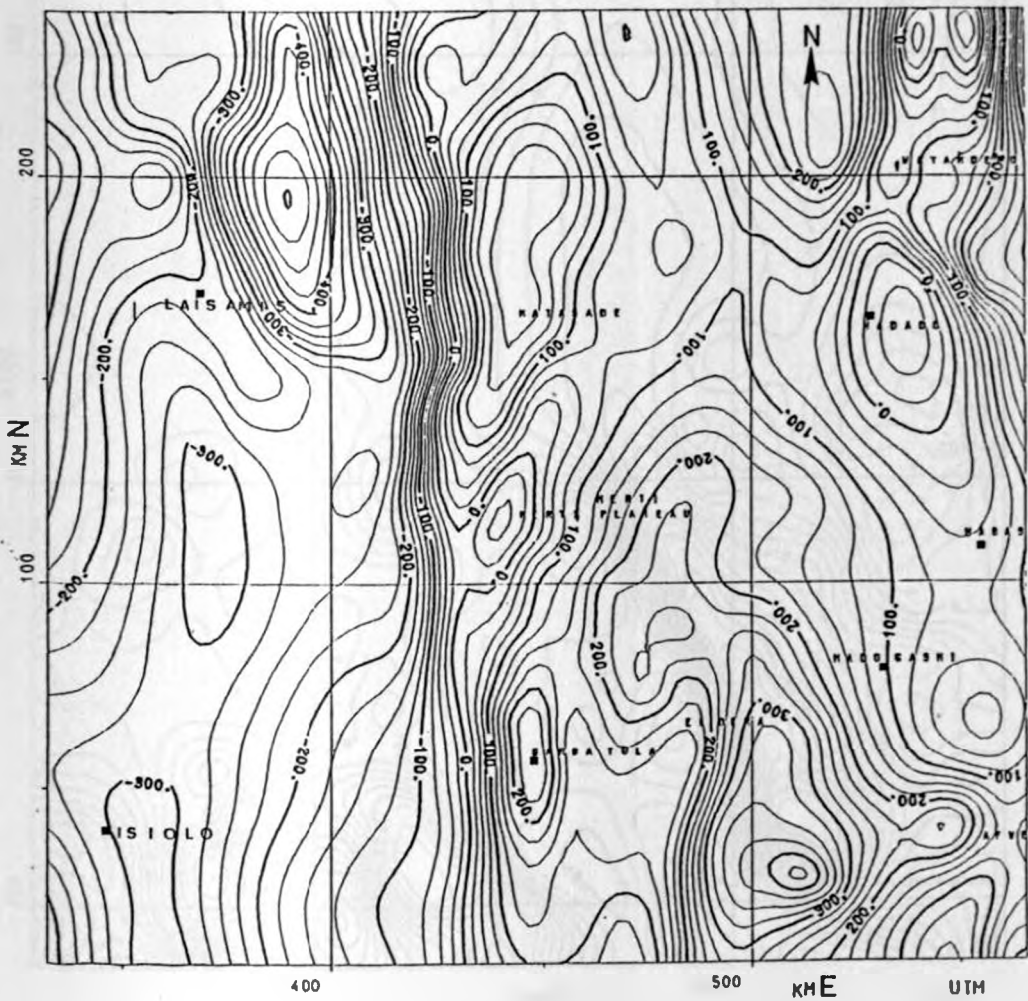


Fig. 6.6b: Pole-reduced map of the SE Anza Graben
 (after an upward continuation of 5 km
 contour interval 25 nT. MI = 20° . MD =
 -2°)

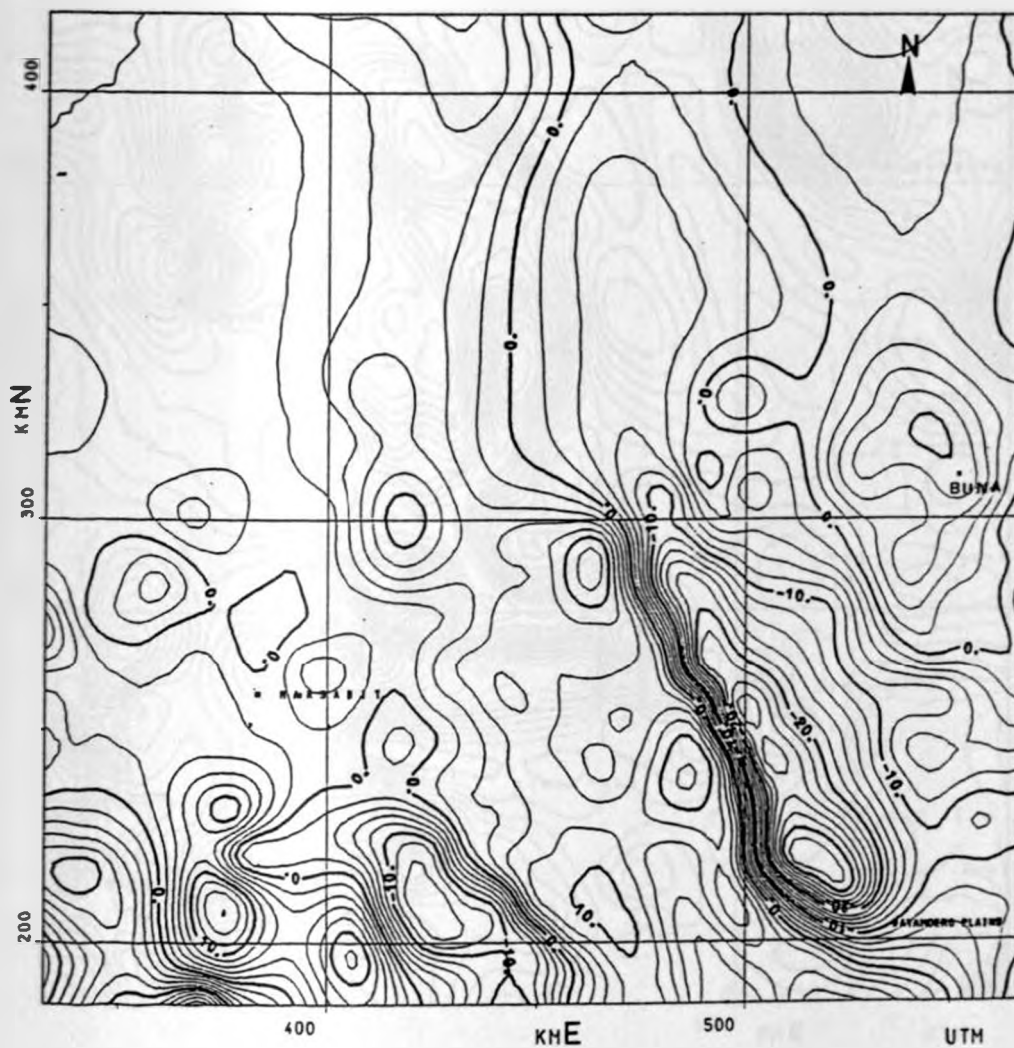


Fig. 6.7a: The vertical gradient gravity map of the NW Anza Graben at a height of 5 km (contour interval 2 E).

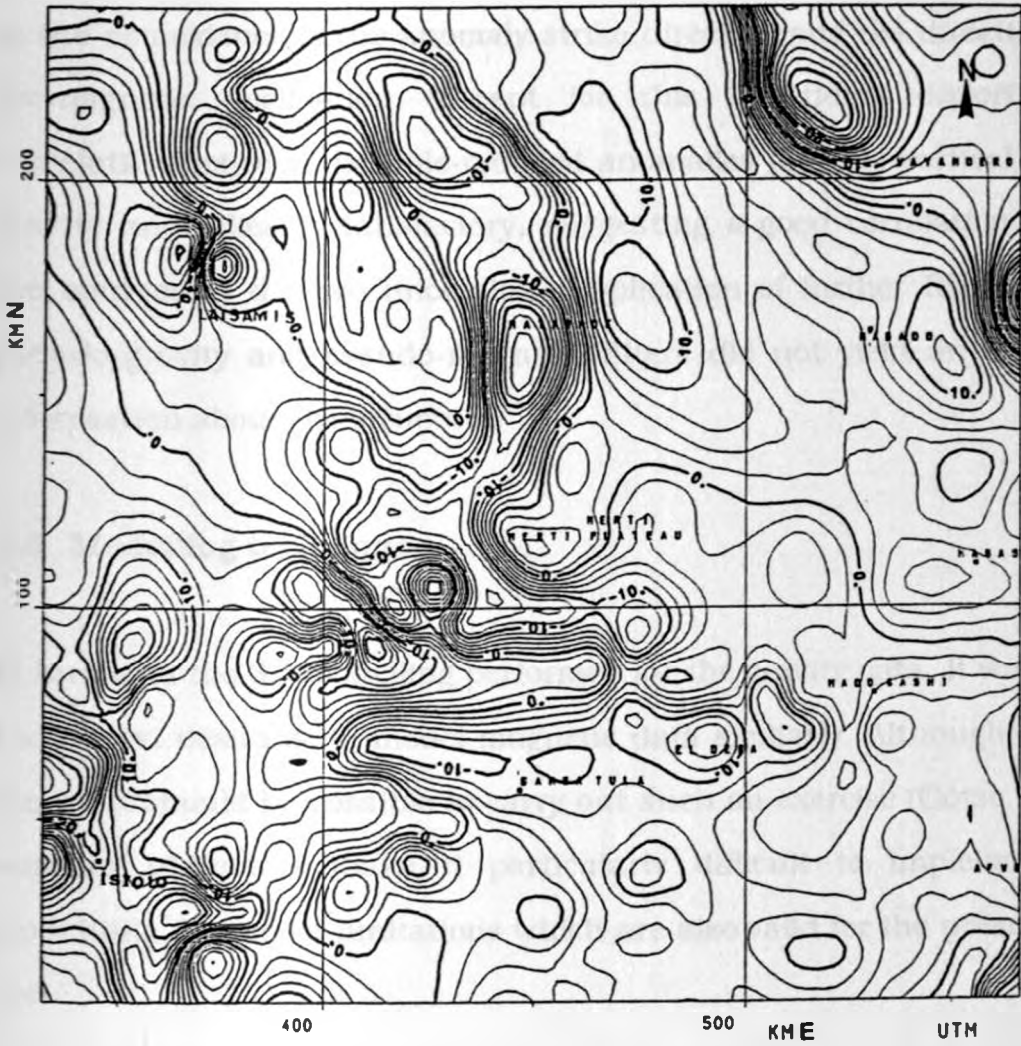


Fig. 6.7b: The vertical gradient gravity map of SE Anza Graben at a height of 5 km (contour interval, 5 E).

pole-reduced maps with nearly all closed anomalies exhibiting an elliptical shape. This strong north-south lineation is considered fictitious and attributed to filter enhancement of imperfections in the direction of the geomagnetic declination. This is mostly attributable to filter instability due to the coincidence of the anomaly strike direction and the direction of the geomagnetic declination. Except for this directional distortion, the correlation between the pole-reduced anomalies and the vertical gradient gravity anomalies is satisfactory, suggesting a good correlation between the sources of the two anomalies. Application of further filters such as pseudo-gravity and pseudo-magnetic filters did not yield any additional information about the structure.

6.6 Modelling technique

In line with the 3D modelling performed for the gravity data, it would have been most desirable to model magnetic data similarly. Although from the theory it should be possible to carry out such an exercise (Götze, 1984), a number of factors make it particularly difficult to implement such modelling. The major limitations which are also valid for the present study are:

1. the lack of control data on the magnetic variations in the area;
2. very erratic variations of the magnetic properties which are difficult to account for even in a moderate 3D model;

3. the lack of information on the heat flow level in the area and hence the Curie temperature depth.

The modelling of the magnetic data was therefore limited to 2D. A forward modelling technique by Won and Bevis (1987) was used. This is an improvement of the technique developed by Talwani et al. (1959). The routine has the advantage of using a modified formulation of the original expression in order to reduce the number of references to the trigonometric functions. Taking into account the inclination I and the strike β of the source measured anticlockwise from the magnetic north, they obtain the following expression for the horizontal and vertical components, respectively:

$$\Delta H_x = 2kH_e(\sin I \frac{\partial X}{\partial z} + \sin \beta \cos I \frac{\partial X}{\partial x}) \quad (6.16)$$

$$\Delta H_z = 2kH_e(\sin I \frac{\partial Z}{\partial z} + \sin \beta \cos I \frac{\partial Z}{\partial x}) \quad (6.17)$$

k : susceptibility

H_e : ambient scalar earth's magnetic field strength

z : vertical axis into the ground

x : axis perpendicular to the strike direction of the source

I : magnetic inclination

X and Z : line integral along the sides of the polygon

β : angle between the axis of the source and the direction of the total field magnetic field vector

With H_z and H_x known, the total field scalar anomaly H may be computed by:

$$\Delta H = \Delta H_z \sin I + \Delta H_x \sin \beta \cos I \quad (6.18)$$

The derivatives in (6.16) and (6.17) are computed from the x - and z -coordinates of the vertices and the angles made by the vertices from the horizontal axis with the observation point as the origin. In this method, the remanence is assumed to be in the same direction as the induced magnetization.

6.7 Modelling and results

The limited coverage of the magnetic data was a handicap in the effort to compare the potential fields over the entire study area. Fortunately, some of the most interesting sections of the Graben are covered by both gravity and magnetic measurements. There was a necessity to model the magnetic data over these sections in order to check their relation to the gravity models. Only the anomalies over the basin were modelled, as in this case it was possible to make assumptions about the susceptibility distribution. The sections where sediments are covered by surface volcanics were however avoided as the observed field tended to be very

noisy. The anomalies were assumed to be originating from the basement below a non-magnetic sediment infill. In order to facilitate a direct comparison of gravity and magnetic models, magnetic sections were selected so as to coincide with the gravity ones. The total field data on local coordinates were used in the modelling. Values to define the magnetic field were picked at intervals which depended on the anomaly gradient. Because the gradient is generally gentle, an average of 10 samples was sufficient to define the field along a profile. The final gravity model was used as the start model for the magnetic modelling.

No significant changes of the geometry of the start model were necessary to obtain a fit. However, it was noticed that models based on the magnetic data tended to favour thicker sediments than those from the gravity data. Nearly all profiles used were modelled with a susceptibility contrast of about 0.060 (SI). Although, this value is not constraint by field measurements, it falls within the range (0.00-0.07 SI) which is generally expected for metamorphic rocks (Telford et al., 1990). Where the interface between sediments and basement comes to the surface there is a very high sensitivity to small changes in the vertices positions of the model. Figs. 6.8a to 6.8d show models obtained along the planes 7, 11, 14 and 17.

Except for plane 7 (Fig. 6.8a), there is a clear correlation between the magnetic highs and sections of the planes modelled with maximum sediment thicknesses. The magnetic models generally suggest a deeper basin and a smoother basement surface as compared with the gravity ones. The maximum sediment thickness on the planes modelled is indicated to be over 8 km and attains a value of 15 km on plane 11. The

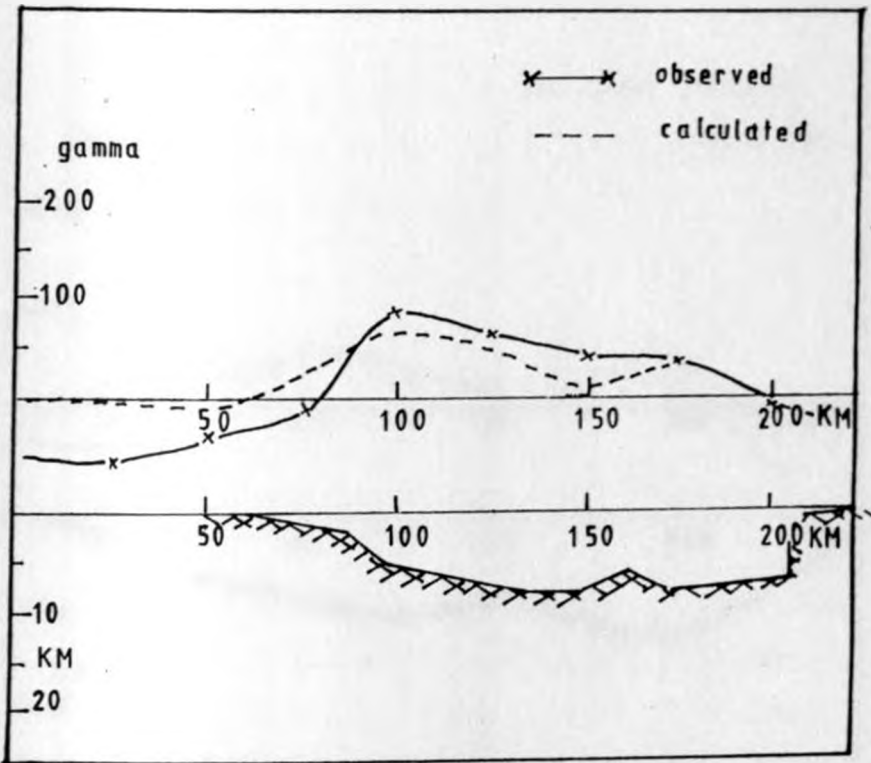


Fig. 6.8a: Magnetic profile along plane 7 (Fig. 3.1).

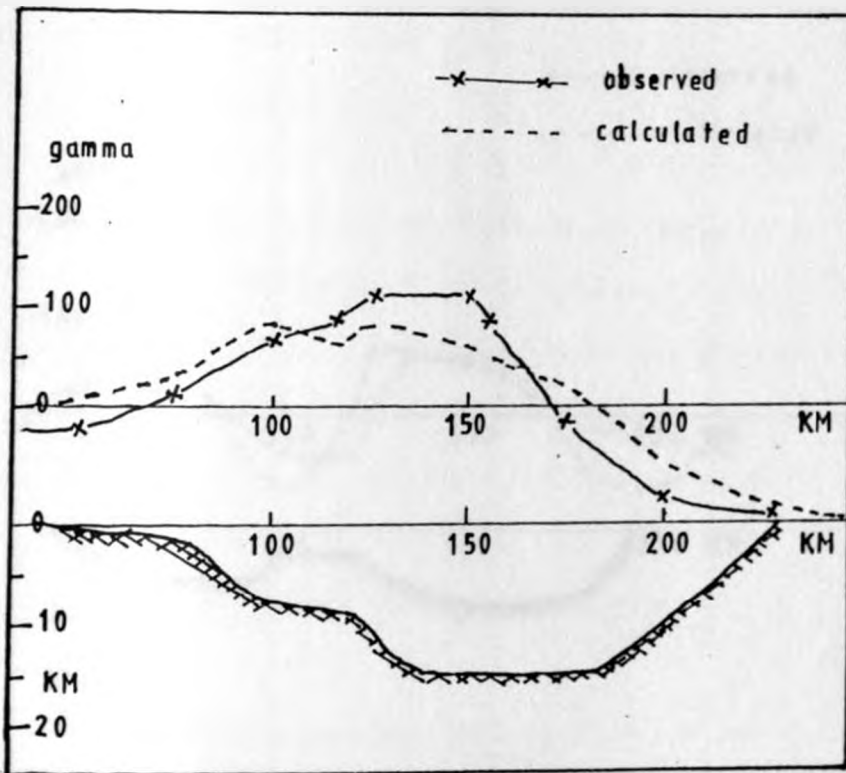


Fig. 6.8b: Magnetic profile along plane 11 (Fig. 3.1).

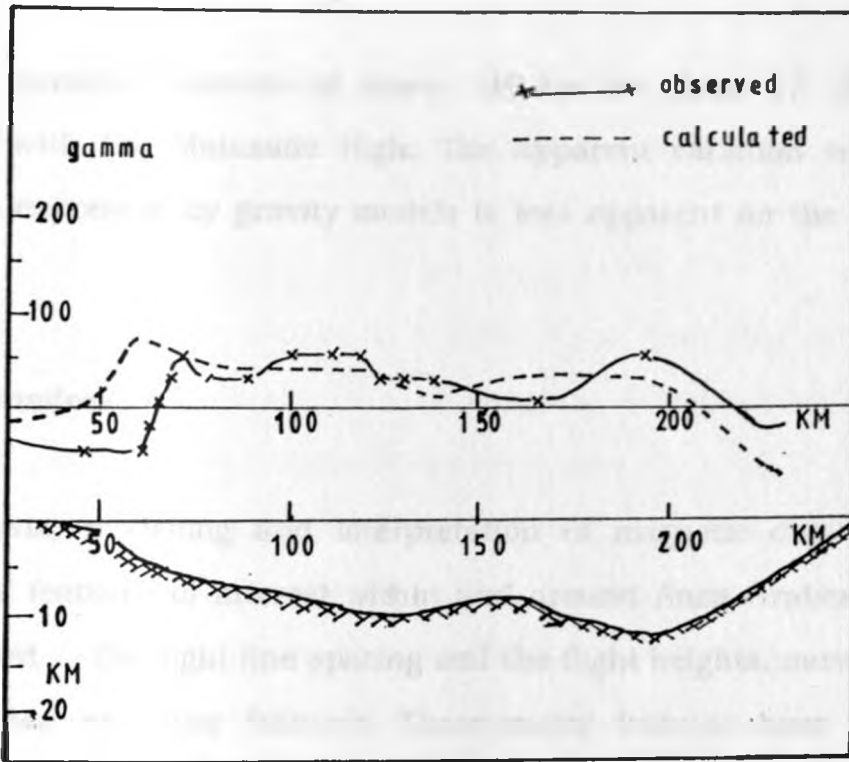


Fig. 6.8c: Magnetic profile along plane 14 (Fig. 3.1).

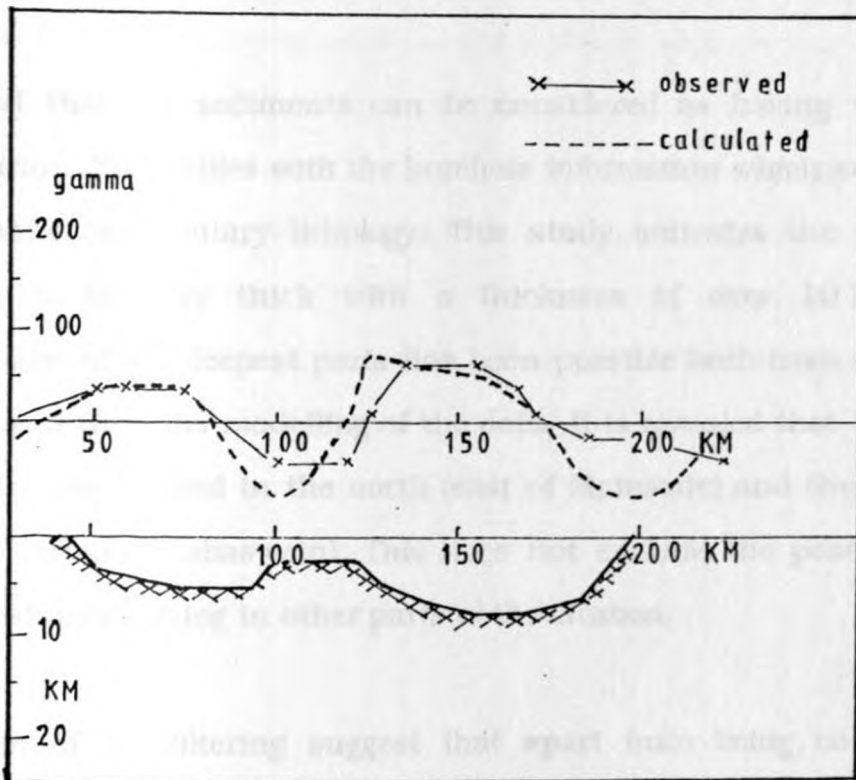


Fig. 6.8d: Magnetic profile along plane 17 (Fig. 3.1).

modelled horst-like feature at about 110 km on plane 17 (Fig. 6.8d) coincides with the Matasade High. The apparent variation in the dip directions expressed by gravity models is less apparent on the magnetic models.

6.8 Conclusions

The analysis, modelling and interpretation of magnetic data reveal a number of features of interest within and around Anza Graben. Taking into account the flight line spacing and the flight heights, most of these are identified as major features. These major features have a strong relationship to the structural and tectonic forces which have characterized the evolution of the Graben.

It is noted that the sediments can be considered as having negligible magnetization. This tallies with the borehole information which suggests a non-magnetic sedimentary lithology. This study indicates the sediment sequence to be very thick with a thickness of over 10 km. The determination of the deepest parts has been possible both from magnetic gradients and from the modelling of the data. It is revealed that two large basins exist one located in the north (east of Matasade) and the other to the south (around Habaswein). This does not exclude the possibility of smaller basins occurring in other parts of the Graben.

The results of the filtering suggest that apart from being covered by surface volcanics, the northern part of the Graben is characterized by occurrence of isolated intrusives. These could probably be the original feeder pipes for the basalts observed at the surface. These observations

are somewhat in line with views expressed by Hackman et al. (1990) that several volcanic centres exist around Marsabit related to shield volcanic events in the area.

The central part of the Graben is relatively free from shallow magnetic disturbances. This indicates the absence of volcanism or intrusive activities in this part. The southern margin is however marked by onset of dipole type anomalies, considered here to be due to isolated intrusives. These anomalies, although isolated appear to cluster along a lineament trending NEE-SWW. Their relative locations tend to suggest structural control to their emplacement. Similar anomalies can be traced further west of Garissa.

Investigations along the shoulders of the Graben indicate that they are characterized by varying basement magnetization. In particular, the half way zone on both shoulders is characterized by very strong gradients indicative of intrusives within the basement. The strong gradients strongly suggest the existence of sources within very shallow depths. These intrusives which may have resulted in the modification of the basement are probably associated with the evolution of the Graben.

CHAPTER SEVEN

GEOLOGICAL SYNTHESIS

In this chapter, all evidences obtained from the analysis, modelling and interpretation of the various data performed in this study together with evidences from earlier studies are synthesized. Attempts are made to evaluate the type of agreement between the geophysical models and the known geology. The possible evolutionary trends and tectonics which may have culminated into the present structural set-up are reconstructed. The disparities between models arising from this study and those from hypothetical models presented in the past are discussed.

7.1 Shallow structure

7.1.1 Geometry of the graben

The results of the study indicate that Anza Graben is not a simple easterly dipping trough as has been previously assumed. Instead they reveal that it is characterized by alternate symmetry with two major basins located in the area of the present study. The southern basin has a gentle northeasterly dip and is about 120 km long. The northern basin has a southwesterly dip and is about 110 km long. The northernmost 30 km of the study area covering the Marsabit region seems to mark the onset of a third basin with a northeasterly dip. In the sections marking polarity reversals no dip of the modelled floor occurs along the dip direction. The

depth of the floor also tends to be shallow. Despite the irregularities observed along the strike of the graben, a gentle northwesterly plunge is apparent. The modelled graben floor appears irregular implying a high degree of faulting. It was not however possible to determine the intensity of faulting as from the data used only those faults having a certain minimum displacement can be resolved. The model can therefore only depict major variations in the geometry of the floor. Further, the modelled graben floor is not uniquely identified. The discrepancy between gravity and magnetic modelling suggests a number of possibilities. These are:

1. The models, using the gravity data, illustrate the true crystalline basement whereas the magnetic models reveal zones within the basement.
2. The gravity models represent the depths at which contrasts between sediments and country rock become too small to be significant whereas the magnetic maps the true basement.
3. The density and susceptibility contrasts used may be incompatible and may thus give rise to the discrepancy between the models.

Additional data either of deep refraction seismics within the graben or boreholes reaching the basement are essential in order to conclusively decide between the above cases.

The margins of the graben are indistinct. This is partly because they are irregular and partly because Anza Graben is not a morphotectonic feature. The sediment and volcanic covers extend beyond the graben margins as delineated by gravity and reflection data. The eastern margin is less irregular and is fairly well delineated by the Lagh Bogal Fault. The western margin is more complicated by existence of basins joining onto Anza Graben. Where the basins occur the margins are delineated by major faulting. Elsewhere the margin is defined by a monocline which may in places involve minor faulting.

One of the basins (Kalsut) joining Anza is separated from it by the Matasade High and appears to have a very unique geometry. It is about 90 km long and only 50 km wide narrowing rapidly southwards towards a basement wall. Although the basin is narrow compared with Anza (120 km wide) it attains maximum depths which are comparable with those in the latter. The basin also shows alternate symmetry with polarity change only after about 40 km. The southernmost trough dips easterly while the northern westerly. Further north the two merge (Anza and Kalsut) giving rise to a wide basin of 200 km wide across in the Marsabit area. It is of interest to note that modelling done further north in the area to the east of Lake Turkana (Green et al.,1991) gave a southwesterly dipping basin. Their results further demonstrate the alternation in the dip of the basins along the structural lineament comprising the Anza Graben.

7.1.2 Graben fill

As known from borehole data, Anza Graben is mainly filled with sediments. A minimum sediment volume of 200,000 km³ is estimated. It

is evident from boreholes that the sedimentary sequence is inconsistent but with predominance of sandstones, siltstone, shale, and limestone. The inconsistency render lithological subdivision as a means of defining physical parameters less useful. The bulk densities of the sediment fill appear heterogeneous.

The sediments at medium depths are characterized by a gentle dip which invariably mimic the modelled dip of the graben floor. This behaviour suggests a history of continuous sag of the graben floor with sediment load. The thickness of the sediment column is variable but indicated from this study to reach 8 km in the deepest sections. This value corroborates with that obtained by Reeves et al. (1987) from 2D modelling of selected profiles. Generally the sediment thickness increases in the dip direction of the particular basin. However, in individual basins an increase in thickness in the strike direction (NW) is also apparent. This also happens to be the case in the Kaisut basin. Minor folding can be observed in some of the beds from the reflection data.

The volcanics which are significant in the northern part of the area cover an area of about 4000 km² especially around Marsabit. The Marsabit shield basalts extend beyond the margins of the graben. These are reported to be underlain by plateau basalts of thickness about 30 m (Hackmann et. al, 1990). The combined thickness of the two units does not however fill the modelled basin in this section. It is therefore expected that below the volcanics, sedimentary units occur before the modelled graben floor is reached. Both magnetic and reflection data indicate the occurrence of intrusives in the Marsabit area and also at the southern margin of Anza Graben. The lack of strong gravity anomalies over these

bodies may be indicative that they are of small sizes and with no appreciable density contrasts with the sediments.

7.1.3 Graben shoulders

The shoulders of Anza Graben show a variable depth of burial. Parts of the western shoulder are exposed while parts occur at shallow depths of up to 2 km. The whole of the eastern shoulder is buried. Depths of burial as revealed from the model studies (chapter 5) range from 0.5 km to 2 km increasing to 4 km away from the shoulder because of the tilt of the block. Each shoulder exhibits variations in properties along strike.

The eastern shoulder is characterized by strong gradient of the magnetic anomalies, high basement densities in places and a tilted top of the shoulder block. Sedimentary beds occur above the tilted block and dip perpendicular to the strike of the shoulder. The western shoulder is characterized by discontinuous magnetic anomalies with linear patterns, high basement densities and P-wave velocities in places. These observations indicate that sections of the shoulders have compositions slightly different from those of the normal basement. In particular, they suggest the presence of basic compositions within the basement which may imply modification through intrusions. The following observations however tend to support this view:

1. The basic intrusives occur as dotted outcrops where the basement is exposed along the western shoulder near Lalsamis and along the axis of the Matasade High.

2. Observations reveal linearly clustering of the aeromagnetic anomalies over intrusives marking the contact between basement and sediments in coastal Kenya (Reeves et al., 1987).

7.2 Deep structure

The present study gives some hints on the nature and physical parameters of the deep structure below Anza Graben. It is observed that there are variations in the properties of the crust in sections of the shoulders. These variations are apparent from the slightly higher P-wave velocity and bulk density values which were necessary for the modelling. Because a range of densities is possible for rocks of each seismic velocity, and vice-versa (Barton, 1986) no attempts were made to do any conversions.

The sub-Moho velocity of 8.1 km/s. suggests lack of abnormal upper mantle under Anza Graben. A hypothetical model by Bosworth (1989) depicting the mantle below Anza Graben as a cooled type is consistent with the present results. The Moho shallows in the NW direction towards Lake Turkana. The average Moho depth at the shoulder of the graben is about 38 km while within the graben it is about 35 km. The Moho depth value within the graben was obtained from gravity modelling and lacks seismic control. It however agrees well with estimates for the Moho (32 km) obtained for Marsabit based on the chemistry of the primitive magmas and the geothermobarometric results of xenoliths (Henjes-Kunst, 1989). The present study suggests a shallowing of the Moho by 5 km below Anza Graben.

Extension estimate of about 55 km results from the gravity modelling. These estimates are based on the balancing technique (Gibbs, 1984; Bosworth, 1989). The value compares well with a value of 60 km suggested by Reeves et al. (1987). The latter authors suggest that the extension could have been achieved through listric faulting. The view is supported by recent reflection data (Bosworth, 1991) which indicate a high concentration of listric faults both in the Graben and in the neighbouring Kaisut basin. No evidences for any linear pattern of intrusions within the graben have been obtained. The study of the deep structure over the entire structure is hampered by lack of control data. Detailed deep refraction work along and across the shoulder could provide such a control.

7.3 Tectonic and structural evolution models

The models worked out from this study together with existing geological and geophysical information provide an opportunity to reconstruct hypothetical evolution models to explain the present structural set up of the area. The results of this study however give hints only on the post-Early Jurassic history of the area this being the time when rifting is estimated to have began.

The tectonic evolution of Anza Graben and the basins in the vicinity is intimately related to the movements associated with the breakup of Gondwana (N.O.C.K, 1986) and the doming and subsequent development of the Kenya Rift Valley. During the Palaeozoic Era, East Africa was occupied by fold mountains being eroded (Baker et al., 1972). In Karroo

(Carboniferous-Permian) linear troughs developed striking NNE-SSW, initiated by major faulting (Kent et al., 1971; Kent, 1974). The ensuing rift is estimated to have been 200-300 km wide extending from Lake Malawi to NE Kenya (Canon et al., 1981). The Karroo now exposed in coastal Kenya and at the NE tip were deposited in this linear basin. The drainage direction during this time has been shown to have been in NNE direction (Canon et al., 1981). The deposition was entirely continental in type. It is estimated to have come to an end after a middle Jurassic faulting episode. The conditions in the Karroo appear to have been characterized by a more or less linear restricted trough of deposition and a continuous intra-continental basin. During this time the Anza area was probably part of the high platform area undergoing erosion.

Marine incursion occurred in Jurassic time with the sea invading from the NNE. This sea is considered to have been epicontinental since this was before the breakup of Gondwanaland (Canon et al., 1981). The marine conditions were established in NE Kenya and Somali in lower Jurassic (Kent, 1974) but in SE Kenya and Tanzania in middle Jurassic (Kent et al., 1971). The early upper Jurassic beds are widely developed both in Kenya and Tanzania suggesting much more extensive transgression. This episode is likely to have affected Anza area. Middle Jurassic faulting episode marked the initial movements and development of zones of weakness as suggested by N.O.C.K. (1986). Reeves et al. (1987) attribute the development of the proposed triple junction in NE Kenya to middle Jurassic.

The Garissa High which appears to have had a profound influence on the Tertiary deposition attained its maximum uplift at the end of Jurassic to

Early Cretaceous. This period corresponds to the uplift phase which affected most of the coastal Kenya region (Dixey, 1956). Initial movements causing Matasade High may have also been initiated at this time. The Garissa High may have been responsible for the cut-off of Anza from the marine influence and the establishment of deltaic conditions around Garissa. The shallow occurrence of Jurassic at Garissa could have been a result of the doming episode to which the triple junction proposed by Reeves et al. (1987) may be attributed. Upper Jurassic transgression seems to have been the last such episode before Anza area was cut off. The modelled gentle northerly plunge (Chapter 5) of the basin floor probably represent remnants of a doming episode and implies that such a doming may have affected a sizable area. This may also account for the shallowing of the Moho towards the northeast (chapter 3). If the proposed existence of the oceanic crust in Lamu Embayment (Reeves et al., 1987) is true, it should follow that a thinned crust is to be expected beyond Garissa to the south of Anza Graben. Since the crust also thins in the NW direction (see the seismic refraction model Fig. 3.8), this implies that the thickest crustal section should be expected around Garissa.

In the Cretaceous, tensional stresses in northern and NW Kenya completed the major rifting phase in Anza Graben. The alternatively dipping basins modelled in this study however suggest a number of specific phases of major faulting affecting certain sections of the structure and hence causing the variations in the geometry. The area to the SE of Garissa was a zone of deposition of marine beds but with non-marine interruptions suggesting an oscillatory fluctuation in the sea level caused by vertical tectonic movements. In Anza Graben, deposition of mainly non-marine sediments continued. The initiation of the domal movement related

to Kenya dome raised many areas rendering them more susceptible to erosion. This ensured continued deposition in the Graben from late Cretaceous to Tertiary. The period of greatest uplift in Tertiary coincided with periods of accumulation of immense thickness of sediments in the Graben. The gentle dip of the beds and the increase in thicknesses in the dip directions observed on the seismic reflection data suggests the influence of basin collapse under load and the effect of listric faulting.

Developments related to the Kenya Rift Valley affected Anza Graben in various ways. Early Tertiary extension caused Anza to experience further rifting and continued accumulation of thick sedimentary sequences (Reeves et al., 1987). There was also block faulting in the NW part resulting in the rejuvenation of structural trends oblique to the Anzan trend and active volcanicity resulting in emplacement of flood basalts and central volcanoes such as the Marsabit Shield (Hackman et al., 1990). The rejuvenation probably accounts for aligned volcanic cones and intrusives in Marsabit and Garissa areas. Deposition of sediments and volcanics caused by doming and activities related to the Kenya Rift Valley eventually obscured Anza Graben in the Quaternary.

The large extension values obtained for Anza (beta value of 1.3)(Reeves et al., 1987) and Kaisut (extension of 43-86%) (Bosworth, 1991) give some hints on the tectonic history of these basins. Several phases of major faulting are implied. The lack of intrusives at the axial region indicates that the extensions were triggered by regional stresses rather than upwelling of the mantle. However, the extension must have caused substantial crustal thinning. But only limited thinning is indicated from the modelling in this study. Bosworth (1991) predicts that this event must

have resulted in periods of significant isostatic uplift. He suggests three major rifting phases in Kalsut and four in Anza Graben between Cretaceous and Early Tertiary. The completion of these phases is suggested to have been followed by basin inversion in both Kalsut and Anza. In Kalsut the inversion episode is considered to have brought the compacted and originally deeply buried sedimentary sequence near the surface thus explaining the observed constant high velocities of the sediments in the basin (Bosworth, 1991).

In terms of tectonics, the operative major stress field during the development of Anza Graben has been indicated by several authors as NE-SW (Reeves et al., 1987; Bosworth, 1991). This is supposed to have been the same field responsible for the rifts of Sudan suggesting that the same regional tectonic forces were operative. This field changed at the beginning of the formation of the Kenya Rift Valley to E-W. (Strecker and Bosworth, 1990). During Tertiary a change to NW-SE occurred (Strecker, 1990). This stress field may account for the NNE to NE striking vents in Marsabit area and also for the intrusives interpreted around Garissa.

The proposed existence of a triple junction in NE Kenya (Reeves et al., 1987) is supported by three observations from this study. These are: a) the modelled regional plunge of the Graben floor NW-wards from the Garissa area, b) the deepening of the Moho along the western shoulder of Anza Graben in such a way as to suggest that the thickest crust may be located in the Garissa area and c) the termination of the most geophysical structural trends in the area around Garissa.

In summary, the sequence of events associated with the evolution of Anza Graben appears to have been as follows:

- 1. development of a NE-SW Karroo basin of deposition extending from Malawi to NE Kenya;**
- 2. Jurassic invasion of the basin from the north and deposition beyond the outline of the basin;**
- 3. development of weak zones in Anza area due to development of SW-NE stress fields;**
- 4. updoming of Garissa leading to the cut-off of the developing Anza Graben gentle inclination of basement floor;**
- 5. deposition of mainly continental sediments in Anza Graben; development of the various basins.**
- 6. inversion of the Anza and Kalsut basins at the early stage of the development of the Kenya Rift Valley, change of stress fields to E-W; reactivation of faults in Anza Graben, continued deposition, block faulting in the north;**
- 7. eruption of flood basalts covering most of the northern section;**
- 8. change of the stress field to NW-SE ; faulting episode on trend perpendicular to the Anzan trend resulting in**

formation of volcanic cones and shields such as Marsabit shield; possible intrusions at zones where structures cross such as in Garissa and Marsabit areas;

9. Quaternary volcanism on the high areas covering most of NW part of the graben, accumulation of sediments eroded from the basement areas completely sealing off the eastern Anza.

CHAPTER EIGHT

DISCUSSIONS AND CONCLUSIONS

Here, at the end of the studies on the Anza Graben, a comparative study on other rifts is added in order to compare the finding with the properties of other structures. Thus, it should be possible to appreciate the importance of Anza Graben as part of the East African Rift System.

Rift valleys, troughs, grabens, aulacogens are terminologies used to describe major structural breakup features of the crust (Burke, 1977). The terminologies although descriptive have a more historic as genetic significance. These features are expressions of the rifting processes. The actual order of events leading to rifting and further to the complete opening up of rifts are to date not clearly understood (Morgan and Baker, 1983). Rifts so far studied show a diversity of properties such that efforts to construct an acceptable rifting model have not been successful. It is to this date not clear whether there are standard mechanisms of rifting within which all rifts fall or whether each rift has its own style and any similarities with other rifts occur as mere coincidences. Despite the little consensus on the mechanisms of rifting, studies of the various characteristics of the rifts have made it possible to derive some crude broad based classification schemes.

A plate tectonic model classifies rifts into three main types namely the oceanic, continental active and continental passive (Sengor and Burke,

1978; Baker and Morgan, 1981; Morgan and Baker, 1983). Oceanic rifts are successful rifts which have passed through all stages of development resulting in the formation of oceanic basins. Continental active rifts are those which show all characteristics of developing into oceanic rifts in future. These characteristics include high heat flow, volcanism, high seismicity and a fast rate of separation of the crust. The Kenya Rift Valley is considered as a good example of this type of rift (Girdler et al., 1969; Fairhead, 1976). Continental passive rifts are those that began to open but for some reason the process aborted and the rift remained as an inactive feature. Such rifts are also referred to as failed rifts. They are characterized by lack of seismicity, lack of volcanic association and thick sediment fill. The failure of such rifts is usually attributed to failure in the movement of plates due to stress changes. Anza Graben and Benue Trough are considered to belong to this category (Reeves et al., 1987).

Attempts have also been made to classify rifts on the basis of age. The main contention under this scheme is that at distinct ages, the stress field that caused rifting operated over large areas causing rifts having related well defined directional trends to form. Under this classification, a number of distinct rifting episodes can be recognized. The applicability of this scheme has been demonstrated in a study (Lamblase, 1989) on African rifts of the Phanerozoic era. The scheme is most useful in regions which have experienced similar stress fields.

In the following sections the important characteristics of some known rifts are briefly summarized to facilitate easy comparison of parameters with those of Anza Graben. Three young rifts namely Kenya Rift Valley (Kenya), Rhine Graben (Germany), and Baikal Rift (Russia) and three old rifts

namely the South Sudan rifts (Sudan), the Benue Trough (Nigeria) and the Godavari Rift (India) are chosen for the comparative study.

8.1 Comparison of some rifts with Anza Graben

8.1.1 Kenya Rift Valley

The Kenya Rift Valley is a Tertiary rift. It trends almost N-S through central Kenya and has an average width of 50 to 60 km. In the Lake Turkana area (fig. 1) it is crossed by trends related to the continuity of the Anzan trend. In this region it loses clarity and is characterised by block faulting and tilting of blocks. Bosworth et al. (1987) proposed a model in which the rift is made up of a series of connecting half grabens characterized by alternate symmetry. The basement shallows in accommodation zones to about 2 km (Smith pers. comm., 1991). The total volume of volcanics associated with the Kenya Rift Valley have been estimated at 100,000 km³ (Logatchev et al., 1983) to 150,000 km³ (Baker et al., 1972). Although sediments also occur they are irregularly distributed and appear to have been less significant than volcanics in the rift development. They are estimated to constitute less than 25 % of the rift fill (Smith, pers. comm., 1991). The maximum subsidence of the graben basement has been estimated to reach 4 km (Fairhead, 1976). The typical fill is estimated to be in the range 2 to 4 km.

Although the gravity field varies along the strike, typically it is characterized by a negative Bouguer anomaly. On the negative Bouguer anomaly is superimposed a positive axial anomaly which has been attributed to axial dyke injection extending for about 100 km (Griffiths et

al., 1971). The negative anomaly on the other hand is superimposed on a broad positive which has been attributed to upwelling of the asthenosphere. The negative is attributed partly to low density asthenosphere beneath the rift and partly to low density sediments in the rift. The aspects of the structure revealed by the KRISP data (KRISP Working Party, 1991) were discussed in chapter 3.

The evolution of the Kenya Rift Valley is attributed to initial doming of the so called Kenya dome which is clearly delineated by gravity (Swain, 1979) and other geological data. The domal uplift is estimated to have began in Miocene before the rift development (Logatchev et al., 1983). Structural development and volcanic activity are considered

to have alternated and the area of activity to have shifted with age from the shoulders to the central axis. The rift is considered to have formed by imposition of new structural lines across pre-existing fabric but as having taken advantage of pre-existing structures where the latter happen to be favourably located (Baker et al., 1972).

8.1.2 The rifts of Southern and Central Sudan

A number of parallel NW-SE trending rifts occur in southern and central Sudan. These have been assigned the names Atbara, Blue Nile, White Nile, Abu Gabra Muslad and Bahr el Arab rifts (Browne et al., 1985; Jorgensen and Bosworth, 1989; Bosworth, 1991). They are estimated to be of late Cretaceous to Tertiary but as having developed before the main phase of rifting in East Africa (Baker et al., 1972). The Abu Gabra Muglad and Bahr al Arab rifts are collectively referred to as the Southern Sudan rifts. All the

rifts of Sudan are sediment filled. A sediment thickness of up to 14 km have been reported with Cretaceous alone attaining a value of 6 km in the deepest troughs (Schull, 1988). Over 5 km of Tertiary sediments is estimated from seismic data.

The Abu Gabra Rift which constitutes the main basin of the southern Sudan rifts bears a NW-SE trend. It is about 150 km wide and is filled by Cretaceous and Tertiary sediments but has little volcanic association. Locally, sediment thickness of up to 4500 m are considered to exist. Gravity modelling (Jorgensen and Bosworth 1989) favour thinning of the crust. Gravity models have been worked out with a crustal thickness of 30 km. A density contrast of 600 kg/m^3 was used between the mantle and country rock. The sediments filling the basin were assigned a contrast of -400 kg/m^3 . Using these models, a crustal extension of up to 48 km has been estimated (Browne and Fairhead, 1983). The broad positive associated with the rift is interpreted in terms of a thinned crust.

The White Nile has the same trend as the Abu Gabra rift but is located to the NE of it. It is characterized by a series of linked gravity minima approximately 40 km wide and having amplitude 20.0-30.0 mGal (Browne et al, 1985). A broad positive Bouguer anomaly of about 15 mGal occur in the southern part and has been interpreted in terms of a thinned crust beneath the rift. The White Nile rift has been modelled with sediment densities increasing from 2100 to 2500 kg/m^3 with depth and country rock density of 2700 kg/m^3 (Jorgensen and Bosworth, 1989). The modelling indicated maximum basin depth of about 4200 m.

In the case of the Blue Nile Rift located some 300 km NE of White Nile, the models favour densities in the range 2200-2400 kg/m³. The maximum sediment thickness is about 2000 m. Post-rift sediments in the basin have been shown by palynological studies (Aboul Ela and Mabrouk, 1978) to be upper Cretaceous in age.

The Atbara Rift which lies some 300 km further NE is about 300 km long and 65 km wide. Density values used in Atbara rift lie in the range 2100-2300 kg/m³. The maximum depth estimates is 3100 km.

Except for the Blue Nile and Atbara rifts which are short, the rest of the rifts are systems of connecting rifts with a total length of about 1000 km. Both gravity and seismic data demonstrate that the asymmetry half graben geometry is characteristic of Sudan rifts. Most basins are composed of series of individual sub-basins about 30-50 km in length. The major phase of rifting in southern and central Sudan is considered to have been in Cretaceous. All the rifts have similar tectonic characteristics in that they follow similar trends and terminate in line at the northern end. The termination is considered to coincide with a structural lineament (Browne et al., 1985). The Sudanese rifts are considered to be different from the Kenya Rift Valley in that they took the path of extension and crustal subsidence while the latter suffered mainly uplift with little extension. (Browne et al, 1985). The overall extension province is 1000 km long and at least 800 km wide. Three phases of rifting are recognized in Sudan (Schull, 1988).

8.1.3 The Benue Trough

The Benue Trough is believed to be an intercontinental rift (Burke and Whiteman, 1973). It has a width ranging from 120-200 km and extends for about 800 km from Niger delta in the south to the southern edges of Lake Chad basin in the north. It has been estimated to be of Cretaceous age. It is structurally linked to the Cretaceous rifts of Sudan through a complex pattern of Cretaceous troughs (Ajakaiye et al., 1991). The basin is filled with predominantly marine sediments and some continental volcanics. The total sediment fill was estimated to be 6000 m from gravity modelling (Browne and Fairhead, 1983). Seismic reflection data however yields estimates of up to 8 km (Avbovbo et al., 1986).

The gravity field is characterized by a broad positive regional anomaly over the whole trough attributed to a Moho uplift. Imposed on the high is an axial positive of width about 100 km which has been interpreted variously as due to a basic body of density 2900 kg/m^3 (Adighije, 1981) and also as due to a basement horst at the axis (Fairhead and Okereke, 1987; Benkhellil et al., 1988). Negative anomalies which are especially prominent in the upper parts are attributed to sediment fill. In the middle and lower Benue occur flanking negative anomalies considered as having been caused by post deformation sediments of up to 5000 m thickness. Adighije (1981) used a number of profiles to conduct gravity modelling across the trough. The ensuring gravity models favour raised Moho with sub-Moho densities of 3270 kg/m^3 and basement of 2700 kg/m^3 . The sediments were assumed to be relatively light with densities in the range 2200-2650 kg/m^3 . He modelled the axial positive anomaly as originating from an intrusive body possibly of gabbroic composition of density 2900 kg/m^3 .

with average width of 30 km extending upward to about 20 km. He attributed the large intrusive to an abortive attempt to open Benue Trough into a proto-ocean in the late Cretaceous.

Ajakiaye et al. (1991) have attempted to correlate major magnetic features in the area of the trough with the known tectonic and geologic features. Their work reveals good correlation between magnetic features and structures. Their models of magnetic data reveal that igneous intrusions exist on both flanks of the trough adjacent to the sediment basement contact corresponding to the negative magnetic anomalies along the flanks of the trough. They show that these anomalies can also be modelled with positive density contrasts. They attribute the negative magnetic anomaly to a fracture zone and argue that it may explain the abnormally wide basin. They consider the magnetic bodies modelled to be basic to intermediate deep seated intrusions.

The trough is believed to have originated as a tensional graben system during Cretaceous and to have experienced a period of compressional deformation at the end of Cretaceous. This resulted in folding of sediments parallel to the axis of the trough. The trough is estimated to have suffered an extension of about 95 km (Fairhead and Green, 1989).

8.1.4 The Baikal Rift

The Baikal Rift of eastern Siberia (25-30 MY) trends NE-SW and has a length extent of about 1000 km (Logatchev et al., 1983). It consists of several depressions whose depths vary along the strike. Geophysical data (Zorin, 1981) indicate that the thickness of sediments reaches 6 km in the

south Baikal basin, 4 km in the northern and 2-3 km in the other depressions. The depressions range in length from 100 km to 350 km and have a width of 35-50 km. The various depressions are separated by mountainous regions. Volcanics do not play an important role as they do not exceed 6000 km^3 in volume (Logatchev et al., 1983). On the other hand, the volume of continental sediments is estimated at close to 100000 km^3 (Zorin, 1971). The amount of crustal extension associated with the rifting is estimated at about 15 to 25 km (Logatchev et al., 1983).

The rift is characterized by a broad negative anomaly and a very gentle positive. The zone of uplift extends for 1500 km and locally widens to 300 km and narrows to less than 200 km. The mantle has been found to be anomalous (Zorin, 1981) characterized by a decrease in seismic velocity from the range 8.1-8.2 to the range 7.7-7.8 km/s. The Moho is at 35 km while under the shoulders the crust thickens to 42-46 km.

8.1.5 The Rhine Graben

The Rhine Graben of SW Germany is a Tertiary rift (38-45 Ma) (Seidler and Jakoby, 1981). It trends NE-SW and has a strike length of about 310 km and width 40 km. The maximum fault throws are estimated to be about 1-3 km with maximum sediment thickness of about 3 km. The graben is associated with a negative Bouguer anomaly of about -35 mGal amplitude (Seidler and Jakoby, 1981).

The map of the crust mantle boundary (Edel et al., 1975) shows that the Moho is shallowest within the graben with a minimum depth of 24 km.

The Moho dips asymmetrically towards the east and the west to attain a depth of 28 km and 30 km respectively under the flanks.

The lower crust is at depth of 18 km within the graben but only 14 km in the shoulder region (Edel et al., 1975). It has been shown (Gajewski and Prodehl, 1987) to be laminated. The top of this laminated zone has been suggested to mark the boundary between the upper and the lower crust. It has a P-wave velocity of 6.5 km/s. or greater (Fuchs et al., 1987).

The graben is considered to be an active rift (Gajewski et al., 1987). It has a seismic and geodetic split rate of 0.05-0.5 mm/year (Ahorner, 1975). Heat flow values are high with an average of 73 Wm^3 (Hurtig and Oelsner, 1977).

8.1.6 The Godavari rift of India

The Godavari Rift of India (Qureshy et al., 1968) is about 50 km wide and has a strike length of 800 km. It is not a continuous rift but consists of several grabens in line. The rift is believed to be upper Cretaceous in age. It is associated with a gravity low of the order of 50 mGal. The valley floor is estimated to lie at a depth ranging from 3-4 km. The gravity low has a NW-SE trend. Highs flanking the lows are attributed to uplift of the shoulders. Gravity modelling with a contrast of -400 kg/m^3 between rift sediments of density about 2300 kg/m^3 and the surrounding Archean rocks of density 2700 kg/m^3 yielded a minimum thickness of 3-5 km. Several models of 2D suggest that the eastern side of the rift is steeper than the western. A northeasterly tilt of the beds is also noted. Gravity data also indicate existence of several grabens rather than one long

graben. Godavari Rift is suggested to occupy a zone of weakness inherited from Archean orogenesis. The basin is devoid of igneous activities.

8.2 Some deductions from the comparative study

In comparison with the grabens outlined above, Anza Graben shows three major characteristics which can be considered as unique. These are the enormous sediment fill, the unusually wide size and the anomalous crust at the shoulders.

The thickness values indicated from the modelling are only comparable with those for the Benue Trough and the rifts of southern Sudan. This enormous sediment fill is probably reflection of the influence of development of the neighbouring Kenya Rift Valley on the sedimentation and tectonic history Anza Graben.

The width of the graben is almost twice the average for most rifts. It implies high values of extension. The width value is again of the order reported only in the case of Benue Trough. This extension is considered to have been accommodated through listric faulting (Bosworth, 1991).

The anomalous behaviour in the shallow sections of the shoulders cannot be considered typical of rifts. This behaviour is probably associated with the evolution of some rifts. Similar models of rifts requiring denser materials at the shoulders have been reported in the cases of the Benue Trough (Ajakaiye et al., 1991) and the Cambidano Graben of Italy (Balla et al., 1990; Balla et al., 1991). In both cases, the anomalous materials have been interpreted as intrusives of basic and hence dense materials.

Anza Graben differs from the young grabens such as Kenya Rift Valley, Rhine Graben and Baikal Rift in that it is devoid of high heat flow, high seismicity, pronounced volcanic association, and abnormal mantle. Similarities occur only in the typical asymmetrical structure giving rise to half grabens.

It differs from other old grabens in a number of ways. Unlike the Benue Trough it has no central linear horst and there is no evidence that the extension was accompanied by strike slip movement as in the latter case (Benkheilil, 1989). The main difference with the Sudan rifts lies in the size of the area over which the extension occurred. Whereas in the case of

Sudan rifts the extension was distributed over a number of parallel rifts, in Anza Graben it occurred over one solid structure. Except for the differences in the magnitude of the various parameters, a number of similarities can be observed between the characteristics of Anza Graben and the Godavari Rift of India.

8.3 Conclusions

The present study reveals a few facts about the structure of Anza Graben. Although the different methods used in this study gave results with a certain amount of ambiguity, the results thereof helped in the definition of models which agree with the basic information supplied by the different methods as well as by geological knowledge.

The results confirm that Anza Graben has an unusually thick sediment fill attaining values of over 8 km. These results corroborate with those of Reeves et al. (1987) and indicate that Anza Graben may rank among the few very deep grabens known. The excessive sediment fill cannot however be regarded as indicative of the normal rift development but as having been strongly influenced by the doming associated with the development of the Kenya Rift Valley. The almost complete absence of syne-rifting igneous rocks suggest that lateral extension was to a great extent accommodated by listric faulting than by injection of dykes within the graben.

Like many other known rifts, Anza Graben exhibits alternate symmetry. The main graben is characterized by large half grabens while the neighbouring Kaisut basin by smaller ones. The maximum depths attained are however comparable in the two cases.

The entire structural floor appears gently tilted in the strike direction (NW). This inclination although gentle may be of significance as it is of a regional magnitude.

The structures under sections of the shoulders of the Graben are rather unique in that they appear to have slightly high densities and (in the case of the western shoulder) high P wave velocities are required for the modelling. This setup suggests existence of denser rocks in the shallow crust in sections of the shoulders. This behaviour cannot be said to be typical of rifts although it has been observed on a few other rifts. It is probably related to the evolution of some rifts.

The southern edge of Anza Graben appears to be an area of a complex structural set-up. In this section two structural trends converge. It is characterized by uplift and probably occurrence of several intrusive bodies at depth. This structure appears to have also influenced the development of Anza Graben especially the sedimentation regime.

The study has given some insight into the nature of both the shallow and the deep structure in the region. The aspects of the structure requiring further work have been discussed. The main priorities for the future in this regard will be (a) the extension of refraction profiles to cover the axis of the Graben as well as its eastern shoulder and (b) the drilling of more deep boreholes within the graben.

REFERENCES

- Aboul, E., and Mabrouk, B., 1978. Palynological studies of some Nubian sandstone samples in Ed Dueim area. Sudan: *Revista Espanola de Micropaleontologia* 10, No. 3: 395 - 406.
- Adighije, C.I., 1981. A gravity interpretation of the Benue Trough, Nigeria. *Tectonophysics* 79: 100 - 128.
- Ahorner, L., 1975. Present day stress field and seismo- tectonic block movement along fault zones in Central Europe. *Tectonophysics* 29: 233 - 249.
- Ajakalaye, D.E., Hall, D.H., Ashlekaa, J.A., and Udensi, E.E., 1991. Magnetic anomalies in the Nigerian continental mass based on aeromagnetic surveys. *Tectonophysics* 192: 211 - 230.
- Akamaluk, T., 1989. The gravity field and crustal structure of East Africa. Ph.D. Thesis. University of Hamburg. Issue 93. 212pp.
- Artemyer, E.M., and Artyushkov, E.V., 1971. Structure and isostasy of the Baikal Rift and mechanism of rifting. *J. Geophys. Res.* 76: 1197 - 1211.
- Avbovbo, A.A., Ayoola, E.O., and Osahon, G.A., 1986. Depositional and structural styles in Chad Basin, North Eastern Nigeria. *Amer. Ass. Pet. Geol. Bull.* 12: 1787 - 1798.

Ayer, F.M., 1952. Geology of the Wajir - Mandera District, North Eastern Kenya. Report No. 22. Geol. Surv. Kenya. Unpubl.

Baker, B.H., and Morgan, P., 1981. Continental Rifting: Progress and outlook. EOS, Trans. Am. Geophys. Union. 62.

Baker, B.H., and Saggerson, E.P., 1958. Geology of El-Wak Aus Mandula Area, Mandera District. Report No. 44. Geol Surv. Kenya.(Unpubl).

Baker, B.H. and Wohlenberg J., 1971. Structure and evolution of the Kenya Rift Valley. Nature, 229: 538 - 542.

Baker, B.H., Mohr, P.A., and Williams, L.J., 1972. Geology of East African Rift System of Africa. Soc. Am., Special Paper, No. 136.

Balla, R., Fals, S., Klingele, E., Marson, I., and Porcu, A., 1990. Aeromagnetic constraints for the geostructural interpretation of the southern part of the Campidano Graben (Italy) (Unpubl).

Balla, R., Illiceto, V., Loddo, M., and Santarato, G., 1991. Modelling of the Campidano Graben (Sardinia, Italy) by combined geophysical data. Geoexploration 28: 43 - 54.

Baranov, V., 1957. A new method for interpretation of aero- magnetic maps: pseudogravimetric anomalies. Geophysics vol. 22: 203-226.

- Baranov, V., Naudy, H., 1964. Numerical calculations of the formula of reduction to the magnetic pole. *Geophysics* vol. 29: 67 - 79.
- Barton, P.J., 1986. The relationship between seismic velocity and density in the continental crust - a useful constraint ? *Geophys. J. astr. Soc.* 87: 195 - 208.
- Benkhellil, J., 1989. The origin of Cretaceous Benue Trough, Nigeria. *Journal of African Earth Sciences.* vol. 8. No. 2/3/4 252 - 282.
- Benkhellil, J., Dainelli P., Ponaard, J.F., Popoff, M., and Saugy., L. 1988. The Benue Trough: Wrench fault related basins on the border of the Equatorial Atlantic In: Triassic - Jurassic rifting and the opening of the Atlantic Ocean. Ed. W. Manspeizer. Elsevier. Publ. Dev. in *Geotectonics* 22: 787 - 819.
- Black, D.I., and Scollar, I., 1969. Spatial filtering in wave -vector domain. *Geophysics* vol. 34: 916 - 923.
- Bonjer, P.K., Fuchs, K., and Wohlenberg, J., 1970. Crustal structure of the East African Rift System from spectral response ratios of long period body waves. *Z. Geophysik.*, 36: 287 - 297.
- Books, K.G., 1962. Remanent magnetization as a contributor to some aeromagnetic anomalies. *Geophysics* vol. 27: 359 - 375.
- Bosworth, W., 1987. Off-axis volcanism in the Gregory rift, east Africa: implications for models of continental rifting. *Geology* 15: 397 - 400.

- Bosworth, W., 1989. Basin and range style tectonics in East Africa. *Journal of African Earth Sciences*, vol. 8 Nos. 2/3/4 191 - 201.
- Bosworth, W., 1991. Mesozoic and Early Tertiary rift tectonics in East Africa. (Unpubl).
- Browne, S.E., and Fairhead, J.D., 1983. Gravity study of the central African Rift System: a model of continental disruption. 1. The Ngaoundere and Abu Gabra Rifts. *Tectonophysics* 94: 187 - 203.
- Browne, S.E., Fairhead, J.D. and Mohamed, L., 1985. Gravity study of the White Nile Rift, Sudan and its regional tectonic setting. *Tectonophysics* 113: 123 - 137.
- Burke, K., 1977. Aulacogens and continental breakup. In: *Annual Review of earth and Planetary Sciences* Ed. Donath F.A. vol. 5.
- Burke, K., and Whiteman, A.J., 1973. Implication of continental drift on the earth sciences. In: D.A. Tarling and S.K. Runcon (Eds.), *Academic Press, London*. 735 - 755.
- Burkhardt, H., and Veis, R., 1975. Explosions in shallow water for deep seismic sounding experiments. *J. Geophysics* 41: 463 -474.
- Canon, R.T., Simiyu Siambi, W.M.N., and Karanja F.M., 1981. The Proto - Indian Ocean and a probable Palaeozoic/ Mesozoic tridial rift system in East Africa. *Earth and Planetary Science Letters* vol. 52: 419 - 426.

- Caswell, P.V., 1956. The Geology of the Kilifi Mazeras Area. Report No.34 Geol. Surv. Kenya. Unpubl.
- Caswell, P.V., and Baker, B.H., 1953. The Geology of Mombasa - Kwale area. Geol. Surv. Kenya. Report No. 24 69pp. (Unpub)
- Cerveny, V., 1985. Gaussian beam synthetic seismograms. J. Geophys. 58: 44 - 72
- Cerveny, V., 1989. Synthetic body wave seismograms for laterally varying media containing thin transition layers. Geophys. J. Int. 99: 331 - 349.
- Cerveny, V., Molotkov, I.A., and Psencik, I., 1977. Ray method in seismology, 214pp., University of Karlova, Prague.
- Clark, D., 1944. Plane and Geodetic Surveying. vol. 2, 3rd. Ed. Constable, London.
- Coolcy, J.W., Lewis, P.A.W., and Welch, P.D., 1967. Historical notes on the Fast Fourier Transforms. Proc. I.E.E.E., v. 55: 1675 - 1677.
- Degro, T., 1986. Zur Interpretation gravimetrischer und magnetischer Feldgrößen mit Hilfe von Übertragungsfunktionen. Dissertation T.U Clausthal, 187S, Clausthal Zellerfeld.

- Deters, F.J., 1990. Vergleichsrechnungen mit drei dimensional gravimetrischen "Inversion" Verfahren - am Beispiel des Anza-Grabens (Kenia). Diploma Arbeit TU Clausthal. 98 S.
- Dindi, E.W., 1983. A gravity survey of the Jombo hill Area South Coast, Kenya. M.Sc. Thesis. 102 pp. University of Nairobi.
- Dindi, E.W., 1986. A gravity model for the Jombo hill, Alkaline Complex, south coast Kenya. African Journal of Geosciences. Special Issue on 1st ANST Meeting in Dakar Senegal.
- Dindi, E.W., and Swain, C.J., 1988. Joint three - dimensional inversion of gravity and magnetic data from Jombo Hill alkaline complex, Kenya. Journal of Geological Society, London, vol. 145, 493 - 504.
- Dixey, F., 1956. The East African Rift System: Colon. Geol. Miner. Res. Bull. Supp. 1.
- Dunkelman, T.J., Rosendahl., B.R., and Karson., J.A., 1989. Structure and stratigraphy of the Turkana rift from seismic reflection data. Journal of African Earth Sciences vol. 8 No. 2/3/4 489 - 510.
- Edel, J.B., Fuchs, K., Gelbke, C., and Prodehl, C., 1975. Deep structure of the southern Rhinegraben area from seismic refraction investigations. J. Geophys. 41: 333 - 356.

- Fairhead, J.D., 1976. The structure of the lithosphere beneath the eastern rift, East Africa deduced from gravity studies. *Tectonophysics* 30: 269 - 298.
- Fairhead, J.D. and Green, C.M., 1989. Controls on rifting in Africa and the regional tectonic model for the Nigeria and East Niger rift basins. *Journal of African Earth Sciences*. vol. 8 Nos. 2/3/4 231 - 249.
- Fairhead, J.D., and Okereke, C.S., 1987. A regional gravity study of the West African rift system in Nigeria and Cameroon and its tectonic interpretation. In: Ramberg, I.B, Milanovsky E.E. and Ovale G. (Eds). *Continental Rifts. Principal and Regional characteristics*. *Tectonophysics* 143: 141 - 159.
- Fuchs, K., Bonjer, K.P., Gajewski, D., Lüschen, E., Prodehl, C., Sandmeier, K.J., Wenzel, F., and Wilhelm, H., 1987. Crustal evolution of Rhinegraben area. I. Exploring the lower crust in the Rhinegraben rift by unified geophysical experiments. *Tectonophysics* 141: 261 - 275.
- Gajewski, D., Holbrook, W.S., and Prodehl, C., 1987. Three dimensional crustal model of southwest Germany from seismic refraction data. *Tectonophysics* 142: 49 - 70.
- Gajewski, D., and Prodehl, C., 1987. Seismic refraction investigation of the Black Forest. *Tectonophysics* 142: 27 - 48

- Gibbs, A.D., 1984. Structural evolution of extensional basin margins. Geol. Soc. London 141: 609 - 620.
- Giese, P., 1976. General Remarks on Travel Time Data and the principle of correlation. In: Giese, P. Prodehl, C. Stein, A (Eds). Exploration Seismology in Central Europe. Data and results. Springer, Berlin, Heidelberg, New York 429pp.
- Girdler, R.W., Fairhead, J.D., Searle, R.C., and Sowerbutts, W.T.C., 1969. Evolution of rifting in Africa. Nature 224: 1178 - 1182.
- Götze, H.J., 1984. Über den Einsatz interaktiver Computer graphik im Rahmen 3-dimensionaler Interpretations-techniken in Gravimetrie und magnetik. Habilitation- schrift, TU Clausthal 236S. Clausthal Zellerfeld.
- Götze, H.J., and Lahmeyer, B., 1988. Application of three dimensional interactive modeling in gravity and magnetics. Geophysics vol. 53: 1096 - 1108.
- Grant, F.S and West, G.F., 1965. Interpretation theory in Applied Geophysics. New York, Mcgraw Hill Book Co. 583pp.
- Green, L.C., Richards, D.R. and Johnson R.A., 1991. Crustal structure and tectonic evolution of the Anza rift, northern Kenya. Tectonophysics 197: 203-211.

- Green, R., 1960. Remanent magnetization and the interpretation of magnetic anomalies. *Geophysical Prospecting* 8: 98 - 110.
- Griffins, D.H., King, R.F., Khan, M.A. and Blundell, D.J., 1971. Seismic refraction line in the Gregory Rift. *Nature Phys. Sci.* 229: 69 - 75.
- Hackman, B.D., Charsley, T.J., Key, R.M., and Wilkinson, A.F., 1990. The development of the East African Rift System in north - central Kenya. *Tectonophysics* 184, 189 - 211.
- Henjes-Kunst, F., 1989. Mantle xenoliths in Quaternary basalts from East Africa: evidence of old lithospheric structures in a young continental rift ? *Terra abstracts* 1, S 275.
- Henry, W.J., Mechie J., Maguire P.K.H., Khan M.A., Prodehl C., Keller G.R., and Patel J.P. 1990. A seismic investigation of the Kenya Rift Valley. *Geophys. J. Int.* 100: 107-130.
- Hinze, W.J., Ed. 1985. *The Utility of Regional Gravity and Magnetic Anomaly maps.* Society of exploration Geophysicists. Tulsa. 454pp.
- Hurting, E., and Oelsner, C.H.R., 1976. Heat flow temperature distribution and geothermal models Europe: Some tectonic implications. *Tectonophysics* 41: 147 - 156.
- Jorgensen, G.J., and Bosworth, W., 1989. Gravity modelling in the Central African Rift System, Sudan: rift geometries and tectonic significance. *Journal of African Earth Sciences.* vol. 8. No. 2/3/4 283 - 306.

- Jung, K., 1961. *Schwerkraftverfahren in der angewandten Geophysik* 348S. Akademische Verlagsgesellschaft Gees and Portig K.G., Leipzig.
- Kanasewich, E.R., 1975. *Time sequence Analysis in Geophysics*. University of Alberta Press.
- Kenya - Austria Mineral Exploration Project., 1977. *The Geology of Mombasa Kwale Area*. Mines and Geological Department. Nairobi Kenya.(Unpubl).
- Kent, P.E., 1974. Continental margin of east Africa: A region of Vertical Movements. In: *Geology of Continental Margins*. Eds. Burk, C.A., and Drake, C.L., 313 - 320.
- Kent, P.E., Hunt, J.A., and Johnstone, D.W., 1971. *The Geology and Geophysics of coastal Tanzania* 101pp. Institute of Geol Sci. Geoph. Paper 6 HMSO London.
- Kertz, W., 1970. *Statistik geophysikalischer Beobachtungsreihen-Skriptum des Institut für Geophysik der TU Braunschweig*, 178S Braunschweig.
- Key, R.M., Rop, K., and Rundle, C.C., 1987. *Geology of Marsabit area*. Mines and geological Dept. Report No. 108. Nairobi. (Unpubl).
- Kis, K., 1990. Transfer properties of reduction of magnetic anomalies to the pole and to the equator. *Geophysics* vol. 55: 1141 - 1147.

- KRISP Working Party., 1991. Large-scale variation in lithospheric structure along and across the Kenya rift. Nature vol. 354.**
- Lamblase, J.J., 1989. The Framework of African Rifting during the Phanerozoic. Journal of African Earth Sciences. Vol. 8 No. 2/3/4 183 - 190.**
- Litinsky, V.A., 1989. Concept of effective density: Key to gravity depth determination for sedimentary basins. Geophysics vol. 54: 1474 - 1482.**
- Logatchev, N.A, Zorin, Y.A., and Rogozhina, V.A., 1983. Baikal rift: active or passive? Comparison of the Baikal and the Kenya rift zone. In: Morgan P. and Baker B.H. (Eds), Processes of Continental Rifting. Tectonophysics, 94: 223 - 240.**
- Marple, S.L., 1987. Digital spectral analysis with applications. Prentice Hall Signal Processing series. New Jersey. 492pp.**
- Maxant, J., 1980. Variation of density with rock type, depth and formation in the western Canada Basin from density logs. Geophysics. vol. 45: 1061 - 1076.**
- McQuillin, R., Bacon, M. and Barclay, W., 1984. An introduction to seismic interpretation. Graham and Trotman Ltd. 287pp.**
- Merrill, R.T., and McElhinny, M.W. 1983. The Earth's magnetic field. International Geophysics series 32. Academic Press Inc. 401.pp.**

- Milltzer, H., and Weber, F., 1984. Gravimetrie und Magnetik. Angewandte Geophysik Ed. 1 Springer Verlag 3535 Wien-N.Y.
- Miller, J.M., 1952. The Geology of Marakani Mackinnon Road Area. Rept. No. 20 Geol. Survey of Kenya. (Unpubl).
- Mines and Geological Department, Ministry of Environmental and Natural Resources., 1967. Geological map of Kenya. (Unpubl).
- Mochizuki, E., 1987. Ray tracing of body waves in anisotropic medium. Geophys. J.R. astro. Soc. 627 - 634.
- Morgan, P., and Baker, B.H., 1983. Processes of Continental Rifting. Special Issue of Tectonophysics vol. 94 No. 1 - 4.
- Morley, C.K., Wescott, W.A., Stone, D.M., Harper, R.M., Wigger, S.T., and Karanja, F.M., 1991. Tectonic evolution of the northern Kenya Rift. (Unpubl).
- Mundry, E., 1970. Zur automatischen Herstellung von Isolinenplänen.. Beih. geol. Jb. 98: 77 - 93.
- Mutunguti, F.N., 1988. Kerogen Analyses of sediments in the Lamu Embayment, Kenya. M.Sc. Thesis. University of Nairobi. 84pp.
- National Oil Corporation of Kenya (N.O.C.K.), 1982. A paper Petroleum Exploration Promotion. (Unpubl).

National Oil Corporation of Kenya (N.O.C.K.), 1986. The Kenya Rift Study .
Unpubl. 324pp.

National Oil Corporation of Kenya (N.O.C.K.), 1987. Geological Map,
Geostructural Map and Bouguer gravity map of Kenya. Nairobi,
Kenya.

Nyambok, I.O., 1985. Evolution of the East African rift system with special
emphasis on the central rift of Kenya: A new model. Kenya Journal of
Science and Technology. Series A, 6, (2): 83-90.

Oxburgh, R.E., 1978. Rifting in East Africa and large scale tectonic
process. In: Geological background to fossil man. Bishop, W W., ed.,
Edinburg, Scottish Academic Press. 7 - 18.

Patrut, I., 1977. The Oil Prospects of the Eastern Kenyan Sedimentary
Basins. Ministry of Mines and Geology .Institute of Research for Oil
and Gas Bucharest - Rumania .(Unpubl).

Petroleum Exploration Promotion Project. Ministry of Energy and Regional
Development., Kenya. 1983. Aeromagnetic Survey Maps. (Unpubl).

Pointing, A.J., Maguire, P.K.H., Khan, M.A., Francis, D.J., Swain, C.J.,
Shah, E.R., and Griffiths, D.H., 1985. Seismicity of the northern part
of Kenya Rift Valley. Journal of Geodynamics 3: 23 - 37.

- Gureshy, M.N., Brahman, N.K., Garde, S.C., and Mathur, B.K., 1968. Gravity Anomalies and the Godavari Rift, India. *Geol. Soc. Am. Bull.* 79: 1221 - 1230.
- Rabinowitz, P.D., Coffin, M.F., Falvey, D., 1982. Salt Diapirs Bordering the continental margin of northern Kenya and southern Somalia. *Science* 215: 663 - 665.
- Rabinowitz, M.F., Coffin, M.F., and Falvey, D., 1983. The separation of Madagascar and Africa. *Science*: 220, 67 - 69.
- Reeves, C.J., Karanja, F.M., and Macleod, I.N., 1987. Geophysical evidence for a failed Jurassic rift and triple junction in Kenya. *Earth and Planetary Science Letters* 81: 299 - 311.
- Richardson, R.M and MacInnes, S.C., 1989. The Inversion of gravity data into three dimensional polyhedral models. *J. Geoph. Res.* 94: 7555 - 7562.
- Robertson Research International Ltd., 1986. Source rock potential of Kenya. Report on Geochemical data. 60pp. (Unpubl).
- Robinson, S.E., and Coruh, C., 1988. Basic Exploration Geophysics. John Wiley. 562pp.
- Saggerson, E.P., and Müller, J.M., 1957. Geology of Takabba - Wegudud Area Mandera District. Report No. 40 Geol. Surv. Kenya. (Unpubl).

- Sanders, L.D., 1956. The Geology of the Mid-Galana Area. Report No. 46 Geol. Surv. Kenya. (Unpubl).
- Schull, T.J., 1988. Rift Basins of Interior Sudan : Petroleum Exploration and Discovery. A.A.P.G. v. 72 No. 10: 1128 - 1142.
- Searle, R.C., 1969. Barometric hyposometry and geophysical study of the part of the Gregory Rift Valley in Kenya. Ph.D. Thesis. University of Newcastle upon Tyne.
- Seidler, E., and Jakoby, W.R., 1981. Parameterized rift development and upper mantle anomalies. Tectonophysics 73: 53 - 68.
- Sengor, A.M.G., and Burke, K., 1978. Relative timing of rifting and volcanism on Earth and its tectonic implications. Geoph. Res. Lett., 5.
- Sheriff, R.E., 1980. Encyclopedic dictionary of Exploration Geophysics. Society of Exploration Geophysicists. 266pp.
- Silva, J.B.C., 1986. Reduction to the pole as an inverse problem and its application to low latitude anomalies. Geophysics vol. 51: 369 - 382.
- Simiyu, S.M., 1989. Geophysical studies in Lamu Embayment to determine its structure and stratigraphy. M.Sc. Thesis. University of Nairobi. 164pp.

- Strecker, M.R., 1990. Das zentrale und südliche Kenia-Rift unter besonderer Berücksichtigung der Neotektonischen Entwicklung. Habilitationsschrift, Karlsruhe. 182S.
- Strecker, S., and Bosworth, W., 1991. Quaternary Stress - Field Change in the Gregory Rift Kenya. vol. 72 No. 3
- Swain, C.J., 1979. Gravity and seismic measurements in Kenya. Ph.D. Thesis . University of Leicester.
- Swain, C.J., and Khan, M.A., 1977. A catalogue of gravity measurements in Kenya. Geology Dept. University of Leicester.
- Talwani, M., Worzel, J.L., and Landman, M., 1959. Rapid gravity computations for two dimensional bodies with application to the Mendocino submarine fracture zone. J. Geophys. Res. 64: 49 -59.
- Telford, W.M., Geldart, L.P., and Sheriff, R.E., 1990. Applied Geophysics. Syndicate Press Cambridge. 860pp.
- Thompson, A.C., 1954. Geology of the Malindi Area. Report No. 36. Geol. Surv. Kenya.(Unpubl).
- Tole, P. M., 1990. Present day ore deposition in the geothermal systems of Kenya-1. The Mwananyamala hot springs north east of Jombo Hill, Coast Province. Geothermics vol. 19 No. 2: 233 - 239.
- Torge, W., 1988. Gravimetry. Walter de Gruyter. Berlin. 465pp.

Tsuboi, C., 1983. Gravity. George Allen and Unwin. London. 254pp.

Wagener, M., and Götze, H.J., 1989. Regional three dimensional gravity investigations in the Black Forest, Southwest Germany. Tectonophysics 157: 13- 23.

Walsh, J., 1972. Geology of the Moyale Area. Report No. 89. Geol. Surv. Kenya. Unpubl.

Williams, L.A.J., 1958. Geology of Hadu - Fundi Area, North of Malindi. Report. No. 52. Geol. Surv. Kenya.

Williamson, P.G., and Savage, R.J.G., 1986. Early rift sedimentation in the Turkana basin northern Kenya: Sedimentation in the African Rifts. Frostick, L.E., Renant, R.W., Reid, I. and Tiercelin J.J. Eds. Geol.Soc. London., Spec. Publication 25., Blackwell Sci. Publ., London. U.K.

Won, I.J., and Bevis, M., 1987. Computing the gravitational and magnetic anomalies due to a polygon: Algorithms and Fortran subroutines. vol.52 No. 2: 232 - 238.

Zorin, Y.A., 1971. Recent structure and isostasy of the Baikal rift zone and adjacent regions. Nauka Moscow 168pp.

Zorin, Y.A., 1981. The Baikal Rift: An example of intrusion of asthenosphere material into the lithosphere as the cause of disruption of lithospheric plates. Tectonophysics 73: 91 - 104. In J.H. Illies Ed. Mechanics of Graben Formation.

APPENDIX

SHORT NOTES ON THE PROGRAM PACKAGES USED

BEAM87

BEAM87 Program Package enables travel times, synthetic seismograms and many other parameters of crustal models to be computed.

The INPUT data consist of the model parameters which include the vertices of the layer boundaries, the numbers of layers, the velocity distribution, the position and type of source, the receiver positions, and the frequency ranges.

The OUTPUT can be optionally selected (see Fig. A). This includes the ray paths, travel times, amplitudes, frequency response, synthetic seismograms and particle motion plots.

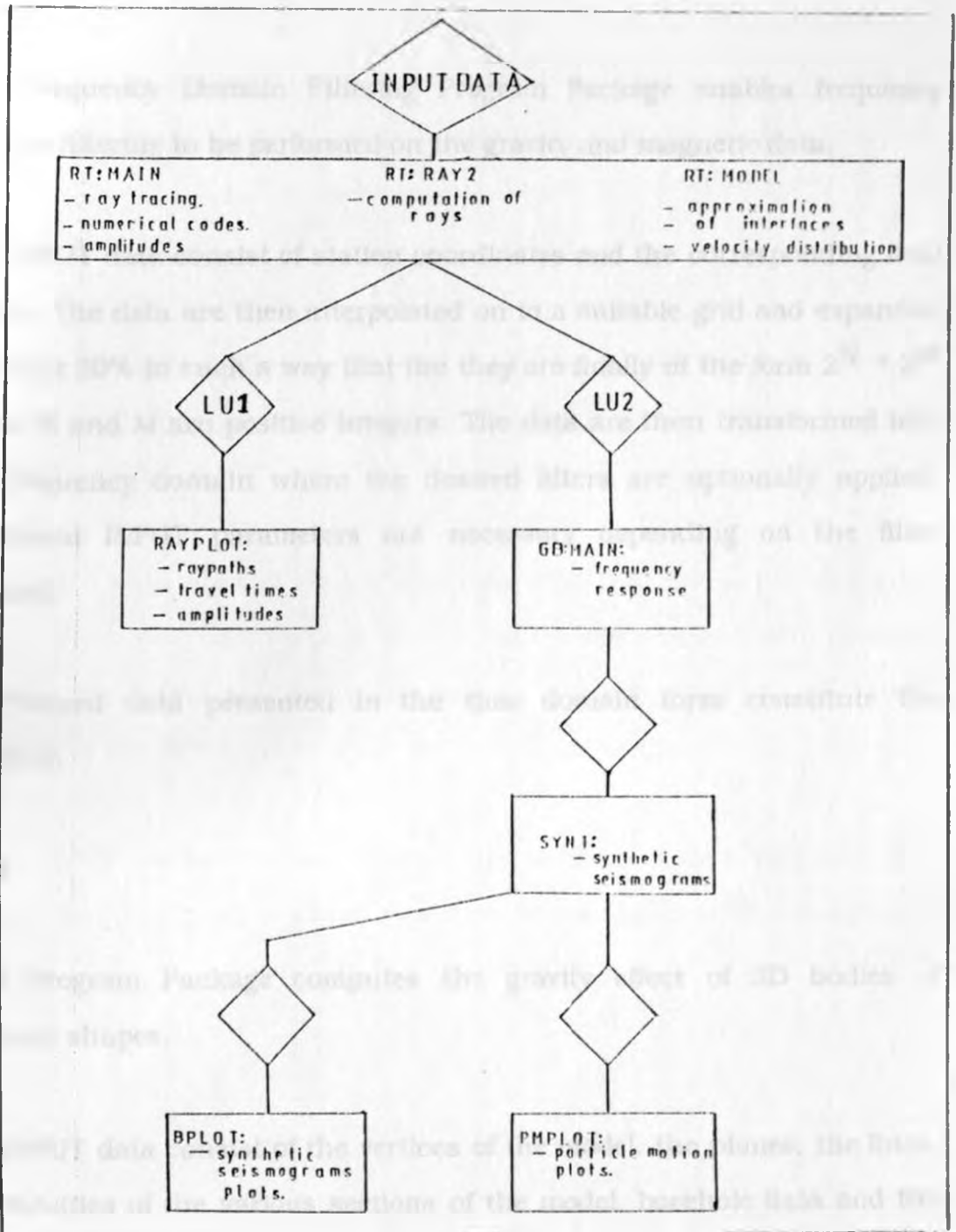


Fig. A: Flow chart for the ray tracing package BEAM87

The Frequency Domain Filtering Program Package

The Frequency Domain Filtering Program Package enables frequency domain filtering to be performed on the gravity and magnetic data.

The INPUT data consist of station coordinates and the corresponding field values. The data are then interpolated on to a suitable grid and expanded by about 20% in such a way that they are finally of the form $2^N \times 2^M$ where N and M are positive integers. The data are then transformed into the frequency domain where the desired filters are optionally applied. Additional INPUT parameters are necessary depending on the filter selected.

The filtered data presented in the time domain form constitute the OUTPUT.

IGAS

IGAS Program Package computes the gravity effect of 3D bodies of arbitrary shapes.

The INPUT data consist of the vertices of the model, the planes, the lines, the densities of the various sections of the model, borehole data and the observed gravity field.

The OUTPUT consists of the gravity effect of the model and the residuals left after fitting the model to the observed data. Refinement of the model is done interactively. Inversion of densities is also performed by the program.

MAG2D

MAG2D Program performs forward modelling of the magnetic data. It computes the vertical, horizontal and the total magnetic field due to a 2D magnetic body.

The INPUT data consist of the observed total field at points along the profile of interest, the vertices of the model, the susceptibility contrast between the model and the surroundings and the magnetic inclination and declination of the area.

The OUTPUT consists of the vertical, horizontal and total magnetic field values along the profiles which can then be compared with the observed values.